INTERNATIONAL ATOMIC ENERGY AGENCY
UNITED NATIONS EDUCATIONAL, SCIENTIFIC AND CULTURAL ORGANIZATION
INTERNATIONAL CENTRE FOR THEORETICAL PHYSICS
I.C.T.P., P.O. BOX 586, 34100 TRIESTE, ITALY. CABLE: CENTRATOM TRIESTE

SMR/459- 16

SPRING COLLEGE IN CONDENSED MATTER
ON
'PHYSICS OF LOW-DIMENSIONAL STRUCTURES'
(23 April - 15 June 1990)

ELECTRON TRANSPORT IN SMALL SYSTEMS

Markus BUTTIKER
IBM Thomas J. Watson Research Center
P.O. Box 218
Yorktown Heights, NY 10598
U.S.A.

New Techniques and Ideas in Quantum Measurement Theory
Reprinted from Vol. 480
ANNALS OF THE NEW YORK ACADEMY OF SCIENCES

ELECTRON TRANSPORT IN SMALL SYSTEMS

MARKUS BUTTIKER

Flux-Sensitive Effects in Normal Metal Loops

MARKUS BÜTTIKER

IBM Thomas J. Watson Research Center
Yorktown Heights, New York 10598

INTRODUCTION

In this paper, we are concerned with coherent quantum mechanical electron transport in disordered normal metal structures and the role of inelastic events in bringing about electrical resistance. The wave nature of electrons plays an important role whether we study transport through a periodic lattice, which is governed by Bloch electrons, or whether we consider transport in disordered systems where we deal with localized wave functions. However, a striking manifestation of coherent transport can be expected when we form the conductor into a loop (or other multiply connected geometry) and study the sensitivity of the conductor to the flux through the hole. In the absence of inelastic scattering events, such a loop exhibits coherent transport phenomena that we tend to associate only with superconductors. The key phenomena (on which we expand in this paper) is that such structures support circulating, persistent currents.[1,2] It is of interest, then, to understand the effect of inelastic relaxation on these coherent transport phenomena and to study the transition from coherent to lossy and resistive behavior.

The study of electron transport is a central topic of solid-state physics. Much of this discussion has been carried out within the general framework of the linear response theory as advanced by Kubo[3] and Greenwood.[4] In this approach, transport coefficients are expressed in terms of time-dependent equilibrium correlation functions. We, however, pursue a different approach (one that has been put forward by Landauer[5]) that expresses transport coefficients in terms of stationary scattering properties of the sample. We start this paper with a brief discussion of Landauer's approach to resistance, and discuss the connection between inelastic events and resistance. This is followed by a discussion of the normal metal structures shown in FIGURE 1. We first treat a closed loop without inelastic events (FIGURE 1a), but with disorder, and then point out the existence of persistent currents.[1] The onset of resistance in such a loop[2,6,7] will be discussed using the model[7] of FIGURE 1b. The geometry of FIGURE 1c allows the study of the Aharonov-Bohm effect in normal metal loops. Reference 8, using weak localization theory, predicted Aharonov-Bohm resistance oscillations with period, $hc/2e$, and higher harmonics. Oscillations with this period have been seen in a number of ingenious experiments.[9,10] On the other hand, references 11–13, invoking the Landauer formula, predicted resistance oscillations with a fundamental period, hc/e. These predictions are not contradictory, but apply to physically distinct situations. Experiments have now demonstrated oscillations with period, hc/e, in a striking and clear fashion in single normal metal loops,[14–16] in semiconductors,[17] and in short series of loops.[18] For an extended discussion of the experiments of references 14 and 15, we refer the reader to reference 19.

RESISTANCE AND IRREVERSIBILITY

Landauer studied the resistance of an obstacle in an otherwise perfect wire.[5,20] The perfect wire connects to reservoirs, as shown in FIGURE 2. A complete spatial separation between elastic scattering and inelastic scattering is assumed. Scattering at the obstacle is elastic; inelastic processes occur only in the reservoirs. The reservoirs

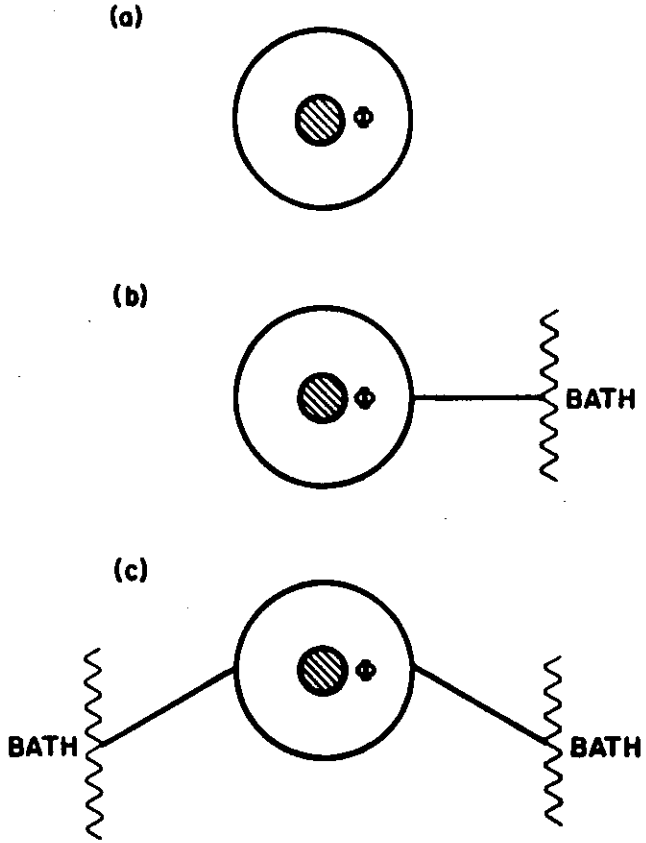

FIGURE 1. Normal metal loops penetrated by a flux, Φ. (a) Closed loop; (b) loop connected to a single lead and (c) to two leads. The reservoirs act as a source and a sink of carriers and of energy.

have the property that they absorb all carriers traveling toward them and that they reemit carriers with a phase and energy that is unrelated to that of the absorbed carriers. A current is imposed if the reservoirs have differing chemical potentials. The resistance is determined by studying the currents and the densities associated with the wave functions at the Fermi energy. In a one-dimensional wire, the obstacle is

characterized by the transmission probability, $T(E)$, for carriers to traverse the sample. For zero temperature, Landauer finds a resistance,[5,20]

$$\mathcal{R} = \left(\frac{2\pi\hbar}{e^2}\right)\left(\frac{1 - T(E_F)}{T(E_F)}\right), \tag{1}$$

where E_F is the Fermi energy. Equation 1 can also be applied to calculate the resistance of a series of obstacles if the transmission through such a sequence is coherent and can be characterized by a transmission probability.[20] This has been used to find the dependence of the conductance of a one-dimensional disordered wire on the length of the wire,[20] and has also been used to develop the modern scaling theory for one-dimensional conductance.[21]

Equation 1 depends only on the elastic, static scattering properties of the sample. This might give the impression that it is the elastic scattering at the barrier that leads to resistance. However, reference 1 emphasizes that this is not correct. The scattering at the barrier at the Fermi energy is described by four wave functions; in addition to the two wave functions describing waves of unit amplitude incident on the sample from the

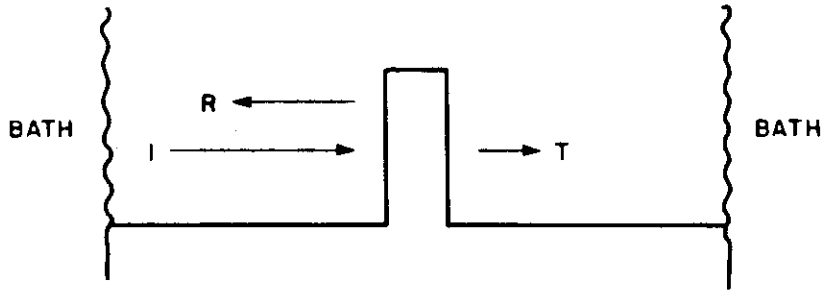

FIGURE 2. Barrier connected to ideal leads connected to reservoirs.

left or from the right, there are the complex conjugate (time-reversed) wave functions that describe waves of intensities, T and $R = 1 - T$, incident from both reservoirs. However, these later two wave functions, which require coherent incident streams from both reservoirs, are not realized in the arrangement of FIGURE 2 because the reservoirs cause phase randomization. It is the elimination of these two wave functions that gives rise to a positive resistance. Thus, the phase-randomizing reservoirs in FIGURE 2 are essential to obtain a positive resistance.[1]

It is worth noting that if the reservoirs, which we can picture as large blocks of normal metal, are replaced by superconductors, then the resulting SNS-microbridge exhibits no resistance if the inelastic scattering length is large compared to the length of the metal wire.[22,23]

We should emphasize that the system discussed here has very particular properties not commonly associated with discussions of resistance. The Joule heat due to the resistance (equation 1) is produced only in the reservoirs and not in the sample. While real systems do not, of course, exhibit the clear-cut separation of elastic and inelastic scattering assumed here, the spatial separation of elastic scattering and inelastic

relaxation is, nevertheless, a real physical feature of systems that exhibit an inelastic scattering length that is large compared to the dimension of the obstacle.[24] It is this spatial separation that leads to an apparent deviation from the Onsager relations.[25] The measurements on Au loops and wires in references 14 and 15, as well as in earlier experiments,[26] indeed exhibit a pronounced asymmetry in the conductance if the magnetic field is reversed.

THE CLOSED NORMAL METAL LOOP

The connection between resistance and irreversibility discussed above raises the question asked in reference 1: What happens if we eliminate the reservoirs that introduce irreversible effects into our system? We can eliminate the reservoirs by forming the ideal wires that connect to the obstacle into a loop. To study transport, we apply a magnetic flux, Φ. For simplicity, we assume that the flux is entirely confined to the hole of the loop (see FIGURE 1a). This system is now completely described by a Hamiltonian with a vector potential, A, and a nonuniform potential, $V(x)$, due to the obstacle in the loop. Here, x is the coordinate along the loop. If we assume that the loop is circular, then the component of the vector potential along x is related to the flux, Φ, by $A = \Phi/L$, where L is the circumference of the loop. The motion of electrons in the loop is, therefore, governed by the Hamiltonian,

$$H = \frac{1}{2m}[p - (e\Phi/cL)]^2 + V(x). \tag{2}$$

As pointed out in reference 1, electrons circuiting the loop in the presence of a flux, Φ, behave like electrons traversing an infinite periodic structure with a potential, $V(x + L) = V(x)$; that is, a lattice with a unit cell equal to the circumference of the loop. The electronic states of such a lattice are Bloch functions, $\psi_{n,k} = e^{ikx}u_{n,k}(x)$, $u_{n,k}(x + L) = u_{n,k}(x)$, with energy, $E_n(k)$. The Schrödinger equation of the periodic lattice can be mapped onto equation 2, and this yields $k = -k_0\Phi/\Phi_0$, where $k_0 = 2\pi/L$ is the width of the Brillouin zone of the periodic lattice and $\Phi_0 = hc/e$ is the single-charge flux quantum. The eigenfunctions of equation 2 are the $u_{n,k}(x)$ with k determined by the flux. The energy spectrum of equation 2 (shown in FIGURE 3) is given by the bands, $E_n(k)$. The eigenstates of the normal metal loop are thus given by a ladder of Bloch states with k selected by the flux. We have, at most, one electron per band (two if we take spin into account). The mapping discussed above now allows us to apply the usual solid-state schemes to calculate the quantities that we are interested in. Consider first a constant flux, Φ. The current in the loop is given by

$$I(k) = -\frac{e}{L}\sum_{n=1}^{N} v_n(k), \tag{3}$$

where n labels all occupied states up to the Fermi energy. The velocities in successive bands alternate, but, typically, higher lying bands have a larger velocity. Thus, typically, the current in equation 3 is determined by the highest occupied state. From this, we obtain a persistent current that is a periodic function of k and therefore of the flux, with a period, Φ_0. The current vanishes at the center of the Brillouin zone ($k = 0$) and at the boundary of the Brillouin zone ($k = \pm k_0/2$).

For weak disorder along the loop, the bands, $E_n(k)$, closely follow a free electron spectrum, $E \simeq k^2$. In this case, the persistent current given by equation 3 has a magnitude, $I \simeq ev_F/L$. For a metal with a lattice constant of $a \simeq 2 \cdot 10^{-8}$ cm forming a loop consisting of 10^4 atoms, this yields a current, $I \simeq 10^{-7}$ A. With increasing disorder in the loop, the bands, $E_n(k)$, become flatter, and the velocities in equation 3 become smaller. Consequently, with increasing disorder, the persistent current decreases.

Next, consider a flux that increases linearly in time, $\Phi = -cFt$, where F is the field induced in the loop. Using Bloch's law, $\hbar dk/dt = -eF$, yields a lattice vector that increases linearly with time, $k = -\omega t/L$. Here, $\omega = eU/\hbar$ (with $U = FL$) is a Josephson frequency with a single charge. Due to the induced electric field, F, the carriers in the loop are pushed in synchronism through the Brillouin zone. If k varies

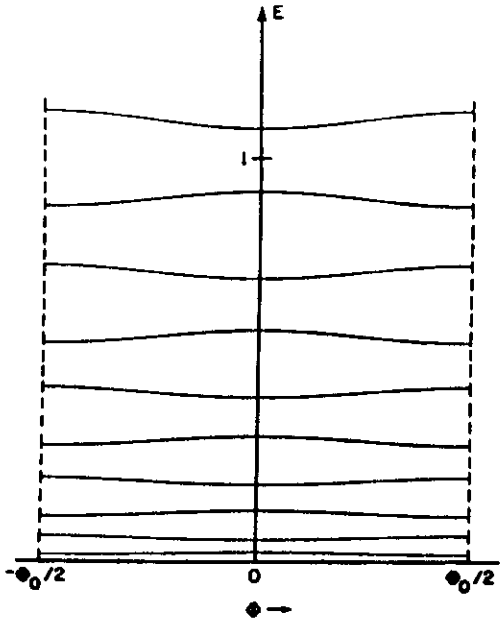

FIGURE 3. Energy spectrum of the closed loop of FIGURE 1a as a function of flux, Φ. The energy scale is $10^3 E_0$, with $E_0 = \hbar^2/2mL^2$. L is the circumference of the loop.

slowly enough, the gaps in FIGURE 3 confine the carriers to the bands, and Zener tunneling can be neglected. In the presence of a linearly increasing flux, we have, therefore, an oscillatory, Josephson-like current that is periodic in time with a period, $2\pi/\omega$. The time-averaged Josephson current, $I(k_n \omega t)$, vanishes because $\int dk v_n(k) = 0$ when integrated over the whole Brillouin zone. Therefore, there is no Joule heat associated with this current. Bloch[37] shows that persistent currents and Josephson currents always occur together; we cannot have one without the other.

We have neglected transitions into higher lying unoccupied states. This requires that the energy, $\hbar\omega$, is small compared to the gaps in FIGURE 3. For a loop of 10^4 atoms, the gaps are of the order of $E_F/N \sim 10^{-4}$ eV for $E_F \sim 1$ eV, which correspond to frequencies of the order of 10^{12} Hz. Even for frequencies that are high enough to induce

transitions to higher unoccupied states, we expect this Hamiltonian system to exhib complete phase coherence and to be completely reversible.[38] This system stores energ and has no mechanism to dissipate it.

Subsequently, we illustrate our results for the example of a loop with a single poin scatterer characterized by an energy-independent transmission probability, T. FIGUR 3 shows the energy spectrum for such a loop with $T = 0.1$. The energy levels[39] are give by $E_n = E_0[\phi_n^2 + 2(-1)^n \phi_n \sqrt{T} \cos(2\pi\Phi/\Phi_0)]$, where $E_0 = \hbar^2/2mL^2$ and $\phi_n = (2n - 1)(\pi/2)$.

ONSET OF RESISTANCE

The effect of inelastic events on the coherent phenomena discussed in the previou section has been the subject of two recent publications. Landauer and Büttiker[6] hav considered a closed loop in which the electronic degrees of freedom are weakly couple to nonelectronic degrees of freedom. This work has been reviewed and extended i reference 2. Here, we expand on a model introduced in reference 7. Reference considered the normal metal structure shown in FIGURE 1b. A current lead i connected to the loop and permits exchange of carriers between the loop and th reservoir. In contrast to the closed loop studied in reference 6, the number of carriers i the loop of FIGURE 1b is not a constant of motion. The model of reference 7 invokes th same spatial separation of elastic and inelastic scattering as we used in the discussion o the resistance of an obstacle in a wire (see FIGURE 2). Scattering in the loop and th lead is elastic. Inelastic scattering occurs only in the reservoir. The reservoir continu ously injects carriers into the lead. These carriers travel towards the junction with th lead and the loop. At the junction, the carriers are either reflected and travel back t the reservoir, or they enter the loop. Eventually, a carrier in the loop will escape into th lead and reach the reservoir. In the reservoir, the carriers are scattered inelastically and reemitted into the lead with a phase and energy that is unrelated to the value of these quantities upon incidence. We have, thus, a model that describes an irreversible system, yet all the calculations can still be done by solving an elastic scattering problem. A particular example of such a loop was treated in reference 7. Here, we go on to give a simple discussion of the properties of this system without repeating these calculations.

We first describe the junction between the lead and the loop in more detail.[12] Suppose a carrier circling in the loop and approaching the junction has a probability, ϵ, to escape from the loop into the lead. A carrier approaching the junction from the lead has then a probability, $1 - 2\epsilon$, to be reflected at the junction and a probability, 2ϵ, to enter the loop. In the case, $\epsilon = 0$, the loop and the lead are disconnected. Carriers can neither enter nor escape from the loop. The electron levels in the loop, therefore, are the same as in the closed loop; that is, we have an energy spectrum as shown in FIGURE 3. If we allow ϵ to be nonzero, but small, the loop and the lead are only weakly coupled. The effect of weak coupling is to broaden the energy levels. The electron states in the loop acquire a finite lifetime. The level broadening is determined by the rate of escape of a carrier from the loop into the lead, and is proportional to an attempt frequency times the probability, ϵ, to tunnel from the loop into the lead. Thus, each state, E_n, in the loop is characterized by a lifetime, τ_n, that is proportional to ϵ^{-1}.

Let us assume a temperature such that kT exceeds the width of the levels, $\hbar/\tau_n$. Because the reservoir injects carriers into the lead according to the Fermi distribution, the levels in the loop are, in equilibrium, occupied with a probability, $f_n = f[E_n(k)]$. (If kT is smaller than the width of the energy level, we cannot characterize the occupation of the state by a single occupation probability, but have to take into account the variation of the occupation probability within a single broadened energy level.[7]) Suppose that the system has, through the action of some force, been driven away from equilibrium. If the actual occupation probability, ρ_n, is less than the equilibrium occupation probability, f_n, then carriers from the lead penetrating into the loop will drive the occupation probability toward the equilibrium value. If the occupation probability exceeds f_n, then carriers leak out of the state into the lead and into the reservoir. Thus, the temporal change of the actual occupation probability, ρ_n, is proportional to the imbalance between the actual occupation probability and the equilibrium occupation probability. The rate of change is determined by the lifetime of the state. Therefore, the time dependence of the occupation probabilities in this system is simply

$$\partial\rho_n/\partial t = -\frac{1}{\tau_n}(\rho_n - f_n). \tag{4}$$

The circulating current in the loop is now given by

$$I = -\frac{e}{L}\sum_n \rho_n v_n. \tag{5}$$

For a time-independent flux, $\rho_n = f_n$, and equation 5 gives the temperature-dependent persistent current of the weakly coupled loop. For the model discussed in reference 7, we found that this current decreases monotonically with increasing temperature and that the fundamental period remains Φ_0.

Consider next the case where the flux increases linearly in time, $d\Phi/dt = -cU$. According to Bloch's law, $k = -\omega t/L$, where $\omega = eU/\hbar$. Now, the equilibrium occupation probabilities are time-dependent, $f_n(t) = f(E_n[k(t)])$, and through equation 4, they give rise to time-dependent occupation probabilities, ρ_n. For simplicity, we take from now on the lifetime, τ_n, to be independent of flux and, thus, independent of time. We can then proceed as in reference 6 and expand E_n and f_n in Fourier series:

$$E_n(k) = \sum_{m=0}^{\infty} \Delta_{nm} \cos m\omega t, \tag{6}$$

$$f_n(k) = \sum_{m=0}^{\infty} g_{nm} \cos m\omega t. \tag{7}$$

Substituting f_n into equation 4, we solve for $\rho_n(t)$. Using this result to evaluate equation 5, and taking into account that $v_n = \hbar^{-1}dE_n/dk$, yields a time-averaged current,

$$\langle I \rangle = (e^2/L^2)\sum_n (\tau_n/m_n^*)U. \tag{8}$$

The bracket denotes a time average over a period of $2\pi/\omega$. Here, we have introduced

the effective mass weighted by the actual distribution function,

$$\frac{1}{m_n^*} = \frac{1}{k_0}\int \frac{dk\, d^2E_n}{\hbar^2 dk^2}\rho_n = -\frac{L^2}{2\hbar^2}\sum_m \frac{m^2\Delta_{nm}g_{nm}}{1 + m^2\omega^2\tau_n^2}. \tag{9}$$

Note that the effective mass as defined in equation 9 depends on the temperature and is a function of the induced voltage, U. Equation 8 is a dc current accompanying the Josephson current. The dc current voltage characteristic is shown in FIGURE 4 (using the spectrum shown in FIGURE 3). At $U = 0$, for a constant flux, we have a branch due to the persistent currents; that is, equation 5 with $\rho_n = f_n$. We move up and down this branch as a function of flux, typically reaching the maximum current when $\Phi = \Phi_0/4$ and reaching the minimum when $\Phi = -\Phi_0/4$. Equation 8 gives the second branch shown in FIGURE 4, which exists for nonzero voltage, $U = \hbar\omega/e$. We have evaluated

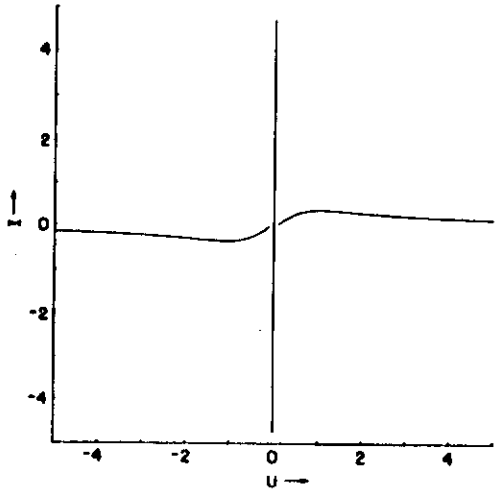

FIGURE 4. The dc current voltage characteristic of a normal metal loop with inelastic scattering for the model of FIGURE 1b and the spectrum shown in FIGURE 3 ($kT = 40E_0$). Current is in units of $e\hbar/mL^2$, and voltage is in units of $\hbar/e\tau$.

this branch for the loop of FIGURE 3 coupled with the junction invoked in references 7 and 12 to an ideal lead. We find[29] a lifetime, $\tau_n = \hbar/(\epsilon E_0\phi_n)$, where $E_0 = \hbar^2/2mL^2$ and $\phi_n = (2n - 1)(\pi/2)$. The Fermi energy has been taken halfway between the tenth and eleventh energy level (for $\Phi = 0$). The temperature is $kT = 40E_0$, which is of the order of the width of the energy bands adjacent to the Fermi energy. Equation 8 exhibits a maximum at a voltage, $U = \hbar\omega/e = \hbar/e\tau$, where τ is a typical relaxation time; in our example, it is given by $\tau = \hbar/(10\pi\epsilon E_0)$.

The dc current (equation 8) vanishes for $\tau = 0$ and $\tau = \infty$, and peaks in between. There are other related problems in which the low-frequency transport peaks at an intermediate relaxation rate. Thermally activated escape from a metastable state is an example.[30] Another example comes from one-dimensional localization. In the absence of inelastic scattering, the carriers are confined to localized states. In the presence of intense inelastic scattering, current flow is impeded by inelastic scattering. A

maximum current flow occurs for an intermediate scattering rate.[31,32] Furthermore, it is worth pointing out that transport in a single narrow conduction band, such as in a superlattice,[33] gives rise to a dc current that depends on the voltage and the scattering rate as a single term of equation 8. In this latter case, electron-electron interactions render the branch of the dc-characteristic, where dI/dV is negative, unstable against the formation of dipole domains.[34]

Of special interest is the slope of the dc current near the origin, which yields the dc conductance of the loop,

$$G_J = \langle I \rangle / U = e\langle I \rangle / \hbar\omega = (e^2/L^2) \sum_n (\tau_n / m_n^*). \tag{10}$$

The index, J, here emphasizes that this conductance characterizes a current accompanying Josephson oscillations. The effective mass in equation 10 is the zero frequency limit of equation 9; that is, the effective mass that is obtained by replacing the actual distribution function, ρ_n, by the equilibrium distribution function, f_n. Note that the effective mass, as defined in equation 9, is infinite if the level is completely filled ($f_n = 1$) or completely empty ($f_n = 0$). The conductance, G_J, diverges as τ_n tends to infinity, thus indicating that we are approaching a state without resistance. It should, however, be emphasized that the range over which $G_J U$ agrees well with equation 8 becomes smaller as the lifetime increases. For $U > \hbar/e\tau$, the effective mass (equation 9) diverges as τ tends to infinity. This implies that linear response is valid only for voltages, $U = \hbar\omega/e$, that are smaller than $\hbar/e\tau$.

It is interesting to compare this result with that of Greenwood (equation 30 of reference 4). Greenwood is interested in the resistance of a wire, not of a loop. However, he imposes periodic boundary conditions and applies a linearly increasing flux. His system is equivalent to a loop. In the presence of a constant induced voltage, he also finds a contribution to the current given by equation 5 (that is, an alternating Josephson-like current), and names it a "ripple current." However, because he considers only electronic degrees of freedom, and because he lets the density matrix evolve accordingly, the Josephson current is zero when averaged over a period, $2\pi/\omega$. Despite the fact that no dissipative mechanism is invoked, he finds a conductance and, thus, resistance. In Greenwood's calculation, the occupation probabilities change because of field-induced transitions into higher levels. One might think that such transitions (or, equivalently, Zener tunneling) provide a dissipative mechanism, and this seems to be the view of Lenstra and van Haeringen.[35] However, in a Hamiltonian system, such transitions are coherent and represent energy storage. By a suitable procedure, the system can be brought back into the original state as pointed out by Landauer.[28] Our key point is that inelastic phase-randomizing events are needed to obtain resistance.

We can elucidate the physics further by considering the response of the loop to an oscillating flux superimposed on a static flux, $\Phi = \Phi_1 + \Phi_2 \cos \Omega t$. We assume Φ_2 to be small compared to the flux quantum, Φ_0. Such a flux induces a time-dependent voltage, and via Bloch's law, this gives rise to a time-dependent k vector, where $k = k_1 + k_2 \cos \Omega t$, with $k_1 = k_0\Phi_1/\Phi_0$ and $k_2 = k_0\Phi_2/\Phi_0$. We now determine ρ_n to first order in k_2 using equation 4, and calculate the current to this order using equation 5. We then determine the Joule heat, $\langle I(t)U(t) \rangle$, averaged over a period, $2\pi/\Omega$. Dividing this by the time-averaged induced voltage, $\langle U^2 \rangle$, yields an ac conductance,

$$\alpha(\Omega, \Phi_1) = \frac{e^2}{L^2} \sum_n \frac{\tau_n v_n^2}{1 + \tau_n^2 \Omega^2} \left(-\frac{df}{dE} \right) \Bigg|_{E=E_n}. \tag{11}$$

Again, we find that the zero-frequency conductance diverges as the lifetime of the states tends to infinity. FIGURE 5 shows the zero-frequency limit of equation 11 for the spectrum of FIGURE 3 for two different temperatures. If the temperature is small compared to the bandwidth of the energy levels adjacent to the Fermi energy, α exhibits a double peak either at the center of the Brillouin zone or at the boundary of the Brillouin zone, depending on where the gap, $E_{n+1}(\Phi) - E_n(\Phi)$, is minimal. As the temperature rises and kT exceeds the width of the energy levels, the flux dependence is determined by the square of the velocity in equation 11. The square of the velocity exhibits a strong second harmonic, and as shown in FIGURE 5, the periodicity of the ac conductance changes from hc/e to $hc/2e$ as the temperature increases. This crossover

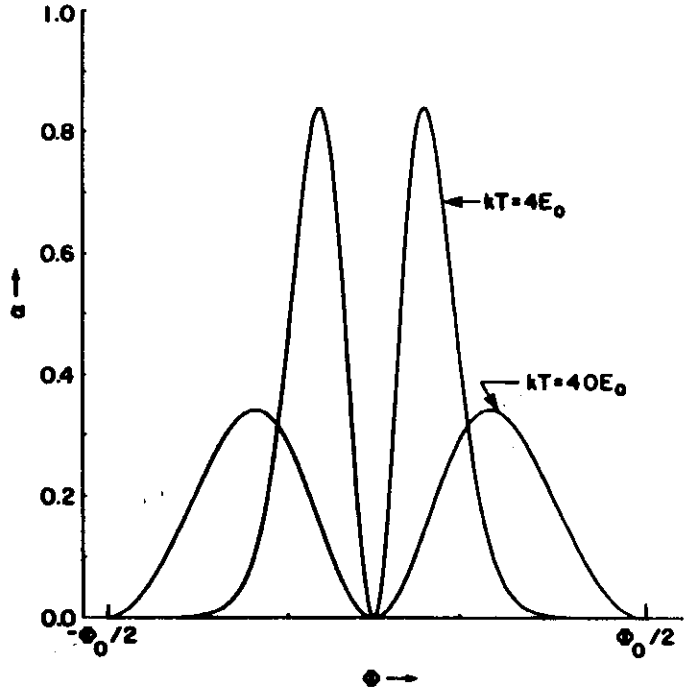

FIGURE 5. Zero-frequency limit of the ac conductance (equation 11) for two different temperatures, $kT = 4E_0$ and $kT = 40E_0$. Conductance is in units of $e^2/\hbar\epsilon$. The ϵ measures the coupling strength between the loop and the lead.

is the main subject of a paper by Imry and Shiren.[36] The main part of their investigation is based on the Greenwood formula. Dissipation is introduced into the loop, using a scheme of Czycholl and Kramer,[37] which was also invoked by Thouless and Kirkpatrick.[31] Because the Greenwood result (equation 30 of reference 4) does not contain the current (equation 5), this approach yields a result that is different from equation 11. In this approach, it is the field-induced transitions from one level, E_n, to another level, E_m, that give rise to the absorption of power. Because such field-induced transitions do not take place until the applied field is almost in resonance with the energy difference, $E_n - E_m$, these transitions give only a small contribution to the power absorption at low frequencies that is proportional to $1/\tau$. In contrast, the contribution given by equation 11 due to motion along the bands is proportional to τ. Field-induced transitions[36] between levels give rise to a conductance that peaks at $\Phi = 0$ or at $\Phi = \Phi_0/2$, which is in contrast to our result[2,7] that yields maxima away from the center or the boundary of the "Brillouin zone."

We can highlight the difference between the processes contained in the Greenwood formula and that of equation 11 by considering the ac conductance as a function of frequency for a fixed temperature and flux, Φ_1. Field-induced transitions give rise to peaks in the ac conductance at the frequencies, $(E_n - E_m)/\hbar$, where $n \neq m$. Centered at zero frequency, $\Omega = 0$, there is an additional peak, given by equation 11, that is not contained in the Greenwood formula. This zero-frequency peak is due to the motion of the carriers along the energy levels.

In the approach of reference 7, both the motion of the carriers along the bands, as well as the field-induced transitions, are taken into account. The derivation of the low-frequency result (equation 11) from the general result of reference 7 is the subject of reference 36. We stress here the similarity of the results (equations 9–11) to those obtained in references 2 and 6. However, the model in FIGURE 1b is an open system. Both in the presence of a linearly increasing flux and in the presence of an oscillating flux, we have an oscillating current in the lead connecting the loop and the reservoir.[7] In many ways, the open system is simpler than the closed loop. In the closed loop, it is the total energy of a configuration that determines the probability of the system to be in an excited state. (For a closed loop, these probabilities are not Fermi functions.[2,6]) In the loop connected to a reservoir (discussed here), we deal with single particle excitations and, consequently, with Fermi occupation probabilities.

The low frequency limit of the ac conductance as given by equation 11 is not the same as the dc conductance accompanying the Josephson current (equation 10). This is in contrast to what we are used to when considering the conductance of large systems (i.e., systems with a dense level of energy states). As pointed out in reference 2, however, the two are related. It turns out that the ac conductance integrated over the whole "Brillouin zone" is equal to the dc conductance (equation 10):

$$G_J = (1/\Phi_0) \int_{-\Phi_0/2}^{\Phi_0/2} d\Phi \alpha(\Phi, 0). \tag{12}$$

This relation between the two conductances is valid even when we consider the flux dependence of the lifetime. In this case, it is $d/dk(\tau_n v_n)$ that has to be weighted with the distribution function, f_n. Finally, we emphasize that the small signal conductance, α, and G_J bear no direct relationship to the recent experiments of references 9 and 14

on cylinders and loops with two attached leads. The two-terminal conductance that is relevant for these experiments is the subject of the next chapter.

AHARONOV-BOHM EFFECT

Consider now the loop shown in FIGURE 1c that is connected to two current leads. If the two reservoirs are at the same chemical potential and if the leads are weakly coupled to the loop, then this structure behaves the same way as the loop with a single lead.[2] (Because carriers in the loop now have two ports to escape from the loop, the broadening of the energy levels is enhanced compared to the loop connected to a single lead.) The interesting new features that can be studied in the geometry of FIGURE 1c arise if we consider transport through the loop. If the leads coupled to the loop are assumed to be perfect, we are back to the situation considered in FIGURE 2; however, instead of a barrier, the obstacle is now a loop penetrated by a flux. We can, therefore, ask what the resistance of this obstacle is, invoking equation 1. To do so, we have to determine the transmission probability for carriers incident in one lead to traverse the loop and exit through the other lead. Such a calculation for a one-dimensional loop was carried out by Gefen *et al.*[11] Because of the enclosed flux and because the waves are coherent through the loop despite elastic scattering (disorder), the transmission probability depends on the flux. Therefore, using equation 1, the resistance is a function of the flux, Φ. Reference 11 finds that $\mathcal{R}(\Phi)$ is periodic in the flux with a fundamental period, Φ_0.

Reference 11 investigated the case of strong coupling between the loop and the leads. It is, however, instructive to consider the limit of weak coupling.[12] Weak coupling means that carriers in the loop have only a small probability to escape into the leads. As indicated above, the density of states in the loop is then sharply peaked at or near the energies of the closed loop. This has the consequence that the transmission probability as a function of energy can be represented by a series of Breit-Wigner resonances,[12]

$$T(E, \Phi) = \sum_n T_{res,n} \frac{(\hbar/2\tau_n)^2}{[E - E_n(\Phi)]^2 + (\hbar/2\tau_n)^2}, \tag{13}$$

where $E_n(\Phi)$ is the energy spectrum shown in FIGURE 3, and $T_{res,n}$ is the value of the transmission probability at resonance. To evaluate the resistance at zero temperature, we have to take the transmission probability at the Fermi energy, E_F. Then, only the bands immediately adjacent to the Fermi energy matter. Suppose the Fermi energy is between two bands, N and $N + 1$. If the energy difference between these two bands is minimal at $\Phi = 0$, the transmission probability, T, is maximal for $\Phi = 0$ and is minimal at $\Phi_0/2$. If the energy difference between the two levels is maximal at $\Phi = 0$, the transmission probability is minimal at $\Phi = 0$ and maximal at $\Phi_0/2$. If the Fermi energy intersects an energy level, then the transmission probability is maximal at the flux, $\pm \Phi_1$, for which $E_n(\Phi_1) = E_F$. In this case, the transmission probability reaches only a local minimum (or maximum) at $\Phi = 0$ and $\Phi_0/2$.

To compare the conductance of the loop of FIGURE 1c with our results for the loop connected to a single lead, we also consider the case where $kT > \hbar/\tau$. In this limit, we

find

$$G \simeq \frac{e^2}{2\pi\hbar}\int dE\left(-\frac{df}{dE}\right)T(E,\Phi) \simeq \frac{e^2}{4}\sum_n \frac{1}{\tau_n}\left(-\frac{df}{dE}\right)\Big|_{E=E_n}. \qquad (14)$$

Note that the two-terminal conductance, G (equation 14), is inversely proportional to the lifetime of the electron states of the loop. In contrast, the conductance of the dc current accompanying the Josephsen current, G_J (equation 10), and the ac conductance, α (equation 11), are proportional to τ. The conductance of carriers through the loop, G, is smaller when the leads are coupled to the loop more weakly. On the other

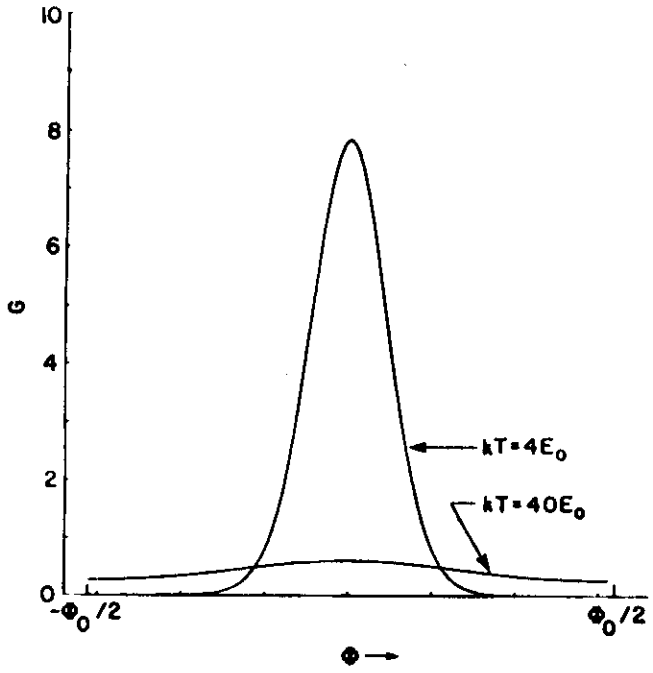

FIGURE 6. Two-terminal conductance of a normal metal loop (see FIGURE 1c) for two different temperatures, $kT = 4E_0$ and $kT = 40E_0$. Conductance is in units of $e^2\epsilon/\hbar$.

hand, the conductance associated with the motion of the carriers around the loop is *better* when the coupling of the loop to the leads is weaker. The conductance, G, (equation 14), is shown in FIGURE 6 for the same loop (spectrum) as was used in FIGURES 3–5. In the second expression of equation 6, we have also assumed that $T_{out,n}$ is independent of the flux and of order unity. For $kT > \hbar/\tau$, G is sensitive to the flux only through the dependence of the occupation probabilities on the energies, $E_n(\Phi)$. The conductance thus becomes insensitive to the flux if kT exceeds the width of the energy

bands, $E_n(\Phi)$. The tight-binding spectrum that we have used here does not give rise to a transition from a conductance that is periodic with hc/e at low temperatures to a conductance that is periodic with period, $hc/2e$, at higher temperatures. Detailed studies of the temperature dependence of the two-terminal conductance are given in references 38 and 39.

Several papers[38–40] have treated ensemble averages of the two-terminal conductance and have shown that ensemble averaging leads to a conductance that is periodic with $hc/2e$. These results are relevant if we consider a one-dimensional array of loops in series. We assume that the phase breaking length is of the order of a circumference of a loop, but consecutive loops in the array are far enough apart so that there is no coherence between the loops. To find the total resistance of the array, we can then add the resistances of the single loops. (Strictly speaking, this is not correct because we also obtain a contribution to the total resistance due to the inelastic events that randomize the phase between consecutive loops.[32]) The resistance of a single loop is characterized by a transmission probability, $T(E_F, \Phi)$. As discussed above, the behavior of the transmission probability depends on the location of the Fermi energy with respect to the energy levels in the specific loop. The phase of the hc/e oscillations is either 0 or π. For some of the loops in the array, the Fermi energy, E_F, lies within a band, and $T(E_F, \Phi)$ reaches a maximum away from the symmetry points. In this case, the Fourier transform of $T(E_F, \Phi)$ has a substantial $hc/2e$ component. The phase of this $hc/2e$ oscillation is also not fixed, but, predominantly, it is such that the conductance is minimal for zero flux. Thus, if we add the single-loop resistances of an array consisting of N loops, we find the following results: Because each loop contributes an hc/e oscillation with a phase that is either zero or π, the amplitude of the resistance oscillations with period, hc/e, increases like $\sqrt{N}$. The flux-insensitive part of the resistance and the contribution to the resistance with period, $hc/2e$, increase proportional to N. Thus, the ratio of the hc/e amplitude and the total resistance decreases like $1/\sqrt{N}$ for a large number of loops. Therefore, in a large array of loops, the hc/e period is averaged to zero, and only a periodicity of $hc/2e$ and higher harmonics can be seen. The dependence on N of the Fourier amplitudes of the resistance oscillations of a series of loops has also recently been observed.[18]

The predictions of hc/e oscillations in references 11–13 and the prediction of $hc/2e$ oscillations in reference 8 are thus both correct, but they apply to distinct physical situations. Reference 8 employed a formalism that took an ensemble average at the outset.[38] In contrast, references 1 and 11–13 did not invoke ensemble averaging, but studied the properties of a specific sample. Whether a single sample effectively incorporates averaging[38,39] depends on the temperature and the size of the sample with respect to the inelastic scattering length.

In this paper, we have discussed persistent currents and Josephson-like currents in the metal structures of FIGURE 1. Persistent currents survive even a limited amount of inelastic events. In the presence of inelastic scattering, the time-dependent coherent phenomena are accompanied by resistive currents. We have distinguished three conductances (equations 10, 11, and 14) that are associated with current flow around the loop or through the loop. The experimental success with the Aharonov-Bohm effect in single loops raises the prospects that, in the future, other coherent phenomena in such small systems (such as the persistent currents and the low-frequency resistance phenomena discussed in the bulk of this paper) will be observed.

ACKNOWLEDGMENTS

Discussions with R. Landauer and Y. Imry have been important for this work. I thank R. Webb, S. Washburn, C. Umbach, C. van Haesendonck, and R. Laibowitz for many discussions of the experimental results, and for their interest in the work presented here.

REFERENCES

1. BÜTTIKER, M., Y. IMRY & R. LANDAUER. 1983. Josephson behavior in small normal one-dimensional rings. Phys. Lett. **96A**: 365.
2. BÜTTIKER, M. 1985. Quantum oscillations in normal metal loops. *In* SQUID '85. Proceedings of the Third International Conference on Superconducting Quantum Interference Devices, Berlin (West), June 23, 1985. H. D. Hahlbohm & H. Lübbig, Eds.: 529–560. de Gruyter. Berlin/New York.
3. KUBO, R. 1957. Statistical-mechanical theory of irreversible processes. J. Phys. Soc. Jpn. **12**: 570–586.
4. GREENWOOD, D. A. 1956. The Boltzmann equation in the theory of electrical conduction in metals. Proc. Phys. Soc. **71**: 585–596.
5. LANDAUER, R. 1957. Spatial variation of currents and fields due to localized scatters in metallic conduction. IBM J. Res. Dev. **1**: 223–231.
6. LANDAUER, R. & M. BÜTTIKER. 1985. Resistance of small metallic loops. Phys. Rev. Lett. **54**: 2049–2052.
7. BÜTTIKER, M. 1985. Small normal-metal loop coupled to an electron reservoir. Phys. Rev. **B32**: 1846–1849.
8. ALTSHULER, B. L., A. G. ARONOV & B. Z. SPIVAK. 1981. The Aharonov-Bohm effect in disordered conductors. Sov. Phys. JETP Lett. **33**: 94–97.
9. SHARVIN, D. YU. & YU. V. SHARVIN. 1981. Magnetic-flux quantization in a cylindrical film of a normal metal. JETP Lett. **34**: 272–275.
10. DOLAN, G. J. & D. J. BISHOP. The nonlocal character of the conductance in the weakly localized limit. This volume; GIJS, M., C. VAN HAESENDONCK & Y. BRUYNSERAEDE. 1984. Resistance oscillations and electron localization in cylindrical Mg films. Phys. Rev. Lett. **52**: 2069–2072; PANNETIER, B., J. CHAUSSY, R. RAMMAL & P. GANDIT. 1984. Magnetic flux quantization in the weak-localization regime of a nonsuperconducting metal. Phys. Rev. Lett. **53**: 718–721; GORDON. J. M. 1984. Quantum phase sensitivity to macroscopic boundaries: Al cylinders and wires. Phys. Rev. **B30**: 6770–6773.
11. GEFEN, Y., Y. IMRY & M. YA. AZBEL. 1984. Quantum oscillations and the Aharonov-Bohm effect for parallel resistors. Phys. Rev. Lett. **52**: 129–132.
12. BÜTTIKER, M., Y. IMRY & M. YA. AZBEL. 1984. Quantum oscillations in one-dimensional normal-metal rings. Phys. Rev. **A30**: 1982–1989.
13. BÜTTIKER, M., Y. IMRY, R. LANDAUER & S. PINHAS. 1985. Generalized many-channel conductance formula with application to small rings. Phys. Rev. **B31**: 6207–6215; STONE, A. D. 1985. Magnetoresistance fluctuations in mesoscopic wires and rings. Phys. Rev. Lett. **54**: 2692.
14. WEBB, R. A., S. WASHBURN, C. UMBACH & R. A. LAIBOWITZ. 1985. Observation of h/e Aharonov-Bohm oscillations in normal metal rings. Phys. Rev. Lett. **54**: 2696–2699.
15. WASHBURN, S., C. P. UMBACH, R. B. LAIBOWITZ & R. A. WEBB. 1985. Temperature dependence of the normal-metal Aharonov-Bohm effect. Phys. Rev. **32**: 4789–4792.
16. CHANDRASEKHAR, V., M. J. ROOKS, S. WIND & D. E. PROBER. 1985. Observation of Aharonov-Bohm electron interference effects with periods h/e and $h/2e$ in individual micron-size, normal metal rings. Phys. Rev. Lett. **55**: 1610–1613.
17. DATTA, S., M. R. MELLOCH, S. BANDYOPADHYAY, R. NOREN, M. VAZIRI, M. MILLER & R. REIFENBERGER. 1985. Novel interference effects between parallel quantum wells. Phys. Rev. Lett. **55**: 2344–2347.
18. UMBACH, C. P., C. VAN HAESENDONCK, R. B. LAIBOWITZ, S. WASHBURN & R. A. WEBB. 1986. Direct observation of the self-averaging of the Aharonov-Bohm effect in normal metals. Phys. Rev. Lett. **56**: 386–389.
19. WEBB, R. A., S. WASHBURN, C. P. UMBACH & R. B. LAIBOWITZ. 1985. In search of magnetic flux quantization in normal metal rings. *In* SQUID '85. Proceedings of the Third International Conference on Superconducting Quantum Interference Devices. H. D. Hahlbohm & H. Lübbig, Eds.: 561–584. de Gruyter. Berlin.
20. LANDAUER, R. 1970. Electrical resistance of disordered one-dimensional lattices. Philos. Mag. **21**: 863–867.
21. ANDERSON, P. W., D. J. THOULESS, E. ABRAHAMS & D. S. FISHER. 1980. New method for a scaling theory of localization. Phys. Rev. **B22**: 3519–3526.
22. BARDEEN, J. & J. L. JOHNSON. 1972. Josephson current flow in pure superconducting–normal-superconducting junctions. Phys. Rev. **B5**: 72–78.
23. BÜTTIKER, M. & T. M. KLAPWIJK. 1986. Flux sensitivity of a piecewise normal and superconducting metal loop. Phys. Rev. **B33**: 5114–5117.
24. LANDAUER, R. 1978. Electrical conductivity in inhomogeneous media. *In* Electrical Transport and Optical Properties in Inhomogeneous Media. J. C. Garland & D. B. Tanner, Eds.: 2–45. AIP. New York.
25. BÜTTIKER, M. & Y. IMRY. 1985. Magnetic field asymmetry in the multichannel Landauer formula. J. Phys. **C18**: L467–472; SIVAN, U. & Y. IMRY. 1986. Multichannel Landauer formula for thermoelectric transport with application to thermopower near the mobility edge. Phys. Rev. **33**: 551–558.
26. UMBACH, C. P., S. WASHBURN, R. B. LAIBOWITZ & R. A. WEBB. 1984. Magnetoresistance of small, quasi-one-dimensional, normal-metal rings and lines. Phys. Rev. **B30**: 4048–4051.
27. BLOCH, F. 1968. Simple interpretation of the Josephson effect. Phys. Rev. Lett. **21**: 1241–1243.
28. LANDAUER, R. 1986. Zener tunneling and dissipation in small metal loops. Phys. Rev. **B33**: 6497–6499.
29. BÜTTIKER, M. Onset of resistance in small normal metal loops. Preprint.
30. BÜTTIKER, M., E. P. HARRIS & R. LANDAUER. 1983. Thermal activation in extremely underdamped Josephson-junction circuits. Phys. Rev. **B28**: 1268–1275.
31. THOULESS, D. J. & S. KIRKPATRICK. 1981. Conductivity of the disordered linear chain. J. Phys. **C14**: 235–244.
32. BÜTTIKER, M. 1986. Role of quantum coherence in series resistors. Phys. Rev. **B33**: 3020–3026.
33. ESAKI, L. & R. TSU. 1970. Superlattice and negative differential conductivity in semiconductors. IBM J. Res. Dev. **14**: 61–65.
34. BÜTTIKER, M. & H. THOMAS. 1979. Bifurcation and stability of dynamical structures at a current instability. Z. Phys. **B34**: 301–311.
35. LENSTRA, D. & W. VAN HAERINGEN. 1985. On the theory of conductance in a one-dimensional statically disordered system. Physica **128B**: 26–38.
36. IMRY, Y. & N. S. SHIREN. 1986. Energy averaging and the flux-periodic phenomena in small normal metal rings. Phys. Rev. **B33**: 7992–7997.
37. CZYCHOLL, G. & B. KRAMER. 1979. Nonvanishing zero temperature static conductivity in one-dimensional disordered systems. Solid State Commun. **32**: 945–951.
38. MURAT, M., Y. GEFEN & Y. IMRY. 1986. Ensemble and temperature averaging of quantum oscillations in normal metal rings. Phys. Rev. **B34**: 659–668.
39. STONE, A. D. & Y. IMRY. 1986. Ensemble and temperature averaging of quantum oscillations in normal metal rings. Phys. Rev. Lett. **56**: 189–192.
40. LI, Q. & C. M. SOUKOULIS. 1986. Quantum oscillations in one-dimensional metal rings: average over disorder. Phys. Rev. **B33**: 7318–7321.

Symmetry of electrical conduction

by M. Büttiker

The resistance of a conductor measured in a four-probe setup is invariant if the exchange of the voltage and current sources is accompanied by a magnetic field reversal. We present a derivation of this theorem. The reciprocity of the resistances is linked directly to the microscopic reciprocity of the S-matrix, which describes reflection at the sample and transmission through the sample. We demonstrate that this symmetry holds for a conductor with an arbitrary number of leads. Since leads act like inelastic scatterers, consideration of a many-probe conductor also implies that the reciprocity of resistances is valid in the presence of inelastic scattering. Various conductance formulae are discussed in the light of the reciprocity theorem. Finally, we discuss some implications of our results for the nature of a voltage measurement and point to the difference between chemical potentials and the local electric potential.

1. Introduction

Symmetries are of paramount importance, since they force certain constraints on the laws of physics. Once established, symmetries can provide sample tests of experimental accuracy and greatly reduce the amount of data which has to be taken. In this paper we are concerned with the reciprocity theorem for electrical conductors. This theorem applies to conductors which are connected to several contacts. In a four-probe experimental setup, two of these contacts are used to supply and draw current from the sample, and the potential difference is measured between another pair of probes. The reciprocity theorem, in the absence of a magnetic field, states that the resistance measured in a particular configuration of current and voltage leads is equal to the resistance in the configuration where the current and voltage leads have been exchanged,

$$\mathcal{R}_{mn,kl} = \mathcal{R}_{kl,mn}. \tag{1}$$

Here the first pair of indices represents the contacts used to supply and draw current, and the second pair of indices represents the probes used to measure the potential difference. Reciprocity of current sources and voltage sources has long been understood. Searle [1], in his 1911 article, presents a derivation of Equation (1) which he attributes to Heaviside. A more recent discussion is given by van der Pauw [2].The reciprocity theorem is rarely mentioned in modern textbooks, which instead emphasize the Onsager–Casimir symmetry relations of the *local* conductivity tensor [3, 4],

$$\sigma_{\alpha\beta}(H) = \sigma_{\beta\alpha}(-H). \tag{2}$$

Here the indices refer to coordinates and not, as in Equation (1), to the contacts. The extension of Equation (1) to the case of a magnetic field, surprisingly, is of more recent origin. In the presence of a magnetic field the exchange of the current and voltage leads has to be accompanied by a reversal of the magnetic field,

$$\mathcal{R}_{12,34}(H) = \mathcal{R}_{34,12}(-H). \tag{3}$$

The reciprocity theorem, Equation (3), is related to the

Onsager–Casimir symmetry relations, Equation (2); Spal [5] and Sample et al. [6] give a derivation of Equation (3) which rests on the validity of the local symmetry relations, Equation (2). Thus, by using Equation (2) one can arrive at Equation (3). On the other hand, verification of Equation (3) in a particular four-probe geometry does not imply the validity of Equation (2). In fact, according to Casimir [4], a whole series of four-probe measurements with differing geometrical arrangement of the contacts must yield equivalent results for Equation (2) to be valid. It is clear, therefore, that conductors might exist which do not obey the local Onsager–Casimir symmetry relations, Equation (2), but which nevertheless obey the *global* symmetry, Equation (3). Hence, it is desirable to derive Equation (3) directly without invoking Equation (2). A direct derivation of the reciprocity theorem, Equation (3), was given by the author in [7] and is reviewed and extended in this paper.

Our interest in these symmetries stems from a concern for electron conduction in tiny disordered conductors. We refer the reader to some review papers and papers with a large number of citations on this topic [8–16]. Interesting effects in such small conductors arise from the quantum-mechanical nature of electron transport. If the wave-like nature of the carriers plays a role, the relation between the current and the electric field cannot be local. The symmetry properties of the magnetoresistance have been of interest to us for some time. Early experiments [9, 17] in quest of h/e oscillations in disordered normal loops [18–23] revealed a magnetoresistance which was not symmetric with regard to field reversal. In view of the prevailing (and mistaken) expectation at that time that these experiments were designed to measure a longitudinal conductance, this was noticeable and triggered our attention. A possible explanation of this asymmetry was offered by the observation [24] that a conductance formula due to Azbel [21, 25] is also not symmetric under field reversal. However, as it turned out, the asymmetry given by this conductance formula is, for metallic conductors in the diffusive regime, too small to account for the experimentally observed effect. Others argued that the asymmetry was not an intrinsic property but could be due to magnetic impurities [26]. It was in conjunction with an additional experiment, carried out by Benoit et al. [27], specifically designed to clarify the nature of the asymmetry, that we derived a resistance formula [7] for quantum coherent electron transport which also obeys the reciprocity symmetry given by Equation (3). The resistances obtained in [7] are related to the probabilities of carriers for transmission through the sample and reflection at the sample. The possibility of relating the resistance of a sample directly to transmission and reflection probabilities was pointed out by Landauer [28, 29]. The sample is viewed as a target at which carriers are reflected or transmitted. In contrast to the Greenwood–Kubo formulation, the resistance is related to *static* scattering properties of the sample. The point of view advanced in [28] and [29] has received increasing attention since the beginning of this decade [21, 24, 25, 30–35]. However, despite the fact that four-terminal conductors have been studied [32], and other results [21, 25] have been interpreted as four-terminal resistances [34, 35], a resistance formula with the symmetry of Equation (3) was lacking. The derivation of Equation (3) given in [7] assumed a disordered sample which scatters carriers only elastically. Inelastic scattering is assumed to be spatially separated [28, 29] from the conductor, and occurs only in the reservoirs (see Figure 1, shown later). Instead of a uniform magnetic field which penetrates the conductor and reaches the carriers, a field is introduced via an Aharonov–Bohm flux through a hole in the conductor. The reciprocity theorem was derived by first demonstrating the global Onsager–Casimir symmetry relations for the conductances relating the currents in the leads to the chemical potentials of the reservoirs. Reference [7] relates the reciprocity relations of the resistances directly to the reciprocity of the scattering matrix, the S-matrix, describing transmission and reflection of carriers at the sample. A basic feature of the resistance formula derived in [7] is the equivalent quantum-mechanical treatment of the contacts which are used to carry current to and from the sample and those which are used to measure voltages. Previous works on conductance formulae have made a number of either implicit or explicit assumptions on what constitutes a voltage measurement. Our work implies that these assumptions have to be revised, and in Sections 3 and 5 we briefly return to this subject.

In submicron structures, at very low temperatures, the magnetoresistance is sensitive to the specific configuration of the impurities and inhomogeneities. Thus, the experiment of Benoit et al. [27] must be regarded as a particularly sensitive test of the symmetries predicted by Equation (3). Even in larger samples the symmetries predicted by Equation (3) have been tested only recently. In connection with the von Klitzing effect, the reciprocity relations have been experimentally confirmed by Sample et al. [6]. High-field magnetoresistance measurements on single-metal samples of a shape with low symmetry have been carried out by Soethout et al. [36], who find generally good agreement with Equation (3) except for small discrepancies which they attribute to the possibility of structural changes induced by Hall currents. In view of these experiments, it is clear that the reciprocity theorem is a fundamental physical law.

In this paper we extend the derivation of Equation (3) given in [7]. We show that the validity of Equation (3) is independent of the number of leads attached to the sample. Since leads leading away from a conductor to a reservoir, in which carriers suffer phase-randomizing events, act like inelastic scatterers [37–40], this demonstrates that, as expected, the symmetries of Equation (3) apply to conductors which are large compared to an inelastic length.

This then also removes the need to keep the reservoirs (the measuring pads) close to the sample. Since the reciprocity theorem is fundamental, it is worthwhile discussing the symmetry of other expressions derived for the conductance. We analyze the four-terminal interpretation of the Landauer formula [28, 29], which yields a resistance proportional to $R/(1-R)$, and the many-channel generalization of this expression [21, 25, 34] in the light of the reciprocity theorem. We point to certain interference terms which are neglected in these conductance formulae.

Recent experiments by Benoit et al. [41] and Skocpol et al. [42] further demonstrate that the probes are an integral part of the conductor. In these experiments the voltage difference is measured on leads which are separated by less than a phase-breaking length. To understand these experiments, it is essential to take into account that carriers can make large excursions into the voltage probe and experience inelastic events in such a probe [40]. A diagrammatic discussion of these phenomena has been put forth by Maekawa et al. [43], Kane et al. [44, 45], and Hershfield and Ambegaokar [46]. References [44] and [45] investigate the connection of the results of [7], expressing resistances in terms of transmission probabilities, with the Greenwood–Kubo linear response formalism. An alternative way to calculate transmission probabilities is by direct computation [47, 48], and for multiport conductors this has been achieved by Baranger et al. [49, 50]. We do not address the statistical aspects of voltage fluctuations; instead, we focus on the implications of [7] for the definition of resistance and voltage measurement.

Before concluding this section we mention, for completeness, a further generalization of the reciprocity theorem. Deviations from Equation (3) can occur if the sample admits a magnetic moment M. In such a case, as pointed out by Strikhman and Thomas [51], the conductivity tensor obeys $\sigma_{\alpha\beta}(H, M) = \sigma_{\beta\alpha}(-H, -M)$. Correspondingly, the reciprocity theorem for a conductor with a magnetization M can be stated as

$$\mathcal{R}_{mn,kl}(H, M) = \mathcal{R}_{kl,mn}(-H, -M); \tag{4}$$

i.e., the exchange of leads must be accompanied by a reversal of the magnetic field H *and* the magnetization M.

2. Multiprobe conductance formula

Consider the conductor shown in **Figure 1**. A field dependence is introduced by studying the response of the conductor to an Aharonov–Bohm flux through the hole [18–21]. In a uniform magnetic field, there are, in addition to the resistance oscillations with fundamental period [18–23] $\Phi_0 = hc/e$, also aperiodic resistance variations as a function of the magnetic field [9, 17, 48]. While we focus on the Aharonov–Bohm oscillations, our conclusions apply equally to the aperiodic resistance variations [40–46, 48–50]. In the presence of a uniform magnetic field, a two-

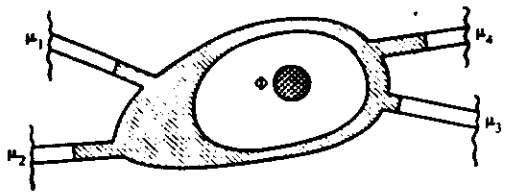

Figure 1

Disordered normal conductor with four terminals connected via perfect leads (unshaded) to four reservoirs at chemical potentials μ_1, μ_2, μ_3, and μ_4. An Aharonov–Bohm flux Φ is applied through the hole of the sample. From [7], reprinted with permission.

dimensional disordered conductor can be considered as a network of microscopic loops of size a with a flux $\Phi = Ha^2 \ll \Phi_0 = hc/e$ threading each loop. The leads in Figure 1 are connected to reservoirs which are at chemical potentials μ_1, μ_2, μ_3, μ_4, respectively. The reservoirs serve both as a source and as a sink of carriers and of energy and have the following properties: At zero temperature they feed the leads with carriers up to the energy μ_i. Every carrier coming from the lead and reaching the reservoir is absorbed by the reservoir irrespective of the phase and energy of the incident carrier. Technically, it is convenient to introduce a piece of perfect wire (unshaded part of the leads in Figure 1), free of elastic scattering, between the disordered terminals and the reservoirs. First we assume that these perfect leads are strictly one-dimensional quantum channels; i.e., there are only two states at the Fermi energy, one with positive velocity (taken to be the direction away from the reservoir) and one with negative velocity. The multichannel case is discussed later. Scattering in the sample is elastic; inelastic events occur only in the reservoirs. The elastic scattering properties of the sample are described by an S-matrix, which relates the amplitudes α_i', $i = 1, \cdots, 4$, of the outgoing currents to the amplitudes α_i of the incident currents,

$$\alpha_i' = \sum_{j=1}^{j=4} s_{ij}\alpha_j.$$

Since current is conserved, the S-matrix is unitary, $S^\dagger = S^{-1}$. Here † denotes Hermitian conjugation. Time reversal implies $S^*(-\Phi) = S^{-1}(\Phi)$. Here the star denotes complex conjugation. Hence, the S-matrix obeys the *reciprocity relations* $s_{ij}(\Phi) = s_{ji}(-\Phi)$. The transmission amplitude $s_{ij}(\Phi)$ for a carrier incident in contact j to reach contact i in the presence of a flux Φ is the same as that of a carrier incident in contact i to reach contact j if the flux has been

reversed. Below we use the reciprocity of the S-matrix to derive the reciprocity theorem for the electrical resistance. We only invoke the probabilities $T_{ij} = |s_{ij}|^2$, $i \neq j$ for transmission of carriers incident in lead j to reach lead i and the probabilities $R_{ii} = |s_{ii}|^2$ for carriers incident in lead i to be reflected into lead i. The reciprocity symmetry of the S-matrix implies that

$$R_{ii}(\Phi) = R_{ii}(-\Phi), \quad T_{ij}(\Phi) = T_{ji}(-\Phi). \tag{5}$$

We now use these probabilities to determine the currents in the leads. Let the difference between the highest potential and the lowest potential be so small that the energy dependence of the transmission and reflection probabilities in this range can be neglected. It is convenient to introduce a fifth chemical potential μ_0 which is smaller than or equal to the lowest of the four potentials μ_i. Below μ_0 the states with negative and positive velocity are filled, and zero net current flows in each of the leads. We only need to consider the energy range $\Delta\mu_i = \mu_i - \mu_0$ above μ_0. The reservoir i injects a current $ev_i(dn_i/dE)\Delta\mu_i$ into the lead i. Here v_i is the velocity at the Fermi energy in lead i, and $dn_i/dE = 1/2\pi\hbar v_i$ is the density of states for carriers with negative or with positive velocity at the Fermi energy. Thus the current injected by reservoir i is $(e/h)\Delta\mu_i$. Consider the current in lead 1. A current $(e/h)(1 - R_{11})\Delta\mu_1$ is reflected back to reservoir 1. Carriers which are injected by reservoir 2 into lead 2 reduce the current in lead 1 by $-(e/h)T_{12}\Delta\mu_2$. Similarly, from the current fed into leads 3 and 4 we obtain in lead 1 a current $-(e/h)(T_{13}\Delta\mu_3 + T_{14}\Delta\mu_4)$. Collecting these results and applying similar considerations to determine the currents in the other leads yields

$$I_i = (e/h)\left[(1 - R_{ii})\mu_i - \sum_{j \neq i} T_{ij}\mu_j\right]. \tag{6}$$

Note that these currents are independent of the reference potential μ_0, since the coefficients multiplying the potentials add to zero. If we write Equation (6) in matrix form, both the rows and the columns of this transmission/reflection matrix add to zero (current conservation).

Let us generalize these results and assume that the perfect leads have many states at the Fermi energy. In leads with a cross section we have to consider both the motion of carriers across the lead and the motion along the lead. Motion in the transverse direction is quantized and characterized by a set of discrete energies, E_n, $n = 1, 2, \cdots$. To this energy we have to add the kinetic energy for motion along the direction of the lead, $\hbar^2k^2/2m$, such that $E_F = \hbar^2k_n^2/2m + E_n$. For each energy E_n, which is smaller than E_F, we obtain two states at the Fermi energy (quantum channel). Each lead is thus characterized by a number N_i of quantum channels. The scattering matrix now contains

$$\left(\sum_{i=1}^{i=4} N_i\right)^2$$

elements denoted by $s_{ij,mn}$. Such an element gives the transmission amplitude for a carrier incident in channel n in lead j to reach channel m in lead i. The reciprocity of the S-matrix is now stated as $s_{ij,mn}(\Phi) = s_{ji,nm}(-\Phi)$. The probability for a carrier incident in channel n in lead i to be reflected into the same lead into channel m is denoted by $R_{ii,mn} = |s_{ii,mn}|^2$, and the probability for a carrier incident in lead j in channel n to be transmitted into lead i into channel m is $T_{ij,mn} = |s_{ij,mn}|^2$. Following [21], we assume that the reservoir feeds all channels equally up to the chemical potential μ_j. Furthermore, as in [21], we assume that the current injected into a channel is incoherent with the current in other channels. The current injected into each channel is then $(e/h)\Delta\mu_j$ independent of the velocity and the density of states of this channel. The current in lead i due to carriers injected in lead j is

$$I_{ij} = -(e/h)\sum_{mn} T_{ij,mn}\Delta\mu_j.$$

Therefore, if we introduce the traces

$$R_{ii} = \sum_{mn} R_{ii,mn}, \qquad T_{ij} = \sum_{mn} T_{ij,mn},$$

which have the symmetry properties given in Equation (5), we find for the currents flowing from the reservoirs toward the conductor,

$$I_i = (e/h)\left[(N_i - R_{ii})\mu_i - \sum_{j \neq i} T_{ij}\mu_j\right]. \tag{7}$$

Here N_i is the number of channels in lead i. Recently, alternative derivations of Equation (7) have also been obtained [43–45]. Equations (6) and (7) provide the starting point for our subsequent discussion, giving the currents as response to the chemical potential differences between the reservoirs. Since the coefficients in Equation (7) obey Equation (5), they have the symmetry typical for linear response problems [4, 5]. The transmission probabilities in Equation (7) multiplied by e^2/h are the conductances which would be measured if the currents and potentials were measured simultaneously at all the probes. That, however, is not what is typically done in the experiments.

To derive the experimentally measured quantities, we proceed as in [7]. First let us connect Equation (7) to the (global) Onsager–Casimir symmetry relations. Casimir [4] considers a four-probe conductor (see Figure 1) where a current I_1 is fed into lead 1 and is taken out in lead 3, and a current I_2 is fed into lead 2 and leaves the sample through lead 4. Thus, we have to solve Equation (7) with the condition that $I_1 = -I_3$ and $I_2 = -I_4$. The result of such a calculation expresses the two currents as a function of differences of voltages $V_i = \mu_i/e$,

$$I_1 = \alpha_{11}(V_1 - V_3) - \alpha_{12}(V_2 - V_4), \tag{8}$$

$$I_2 = -\alpha_{21}(V_1 - V_3) + \alpha_{22}(V_2 - V_4). \tag{9}$$

The conductance matrix α_{ij} is expressed in terms of transmission probabilities in Appendix A. The diagonal elements are symmetric in the flux $\alpha_{11}(\Phi) = \alpha_{11}(-\Phi)$, $\alpha_{22}(\Phi) = \alpha_{22}(-\Phi)$, and the off-diagonal elements satisfy $\alpha_{12}(\Phi) = \alpha_{21}(-\Phi)$.

There are two additional ways of feeding two currents into the conductor of Figure 1. For each of these possibilities the currents and chemical potentials are as in Equations (8) and (9), related by a conductance matrix β_{ij} and γ_{ij}. The β and γ conductances have the same symmetry as the α conductances, but are generally not equal to these. The α, β, and γ conductances obey the *global* Onsager–Casimir symmetry relations referred to in the Introduction. These global symmetries for the conductances are more fundamental than the symmetry of the local conductivity tensor, Equation (2). The global symmetries hold even in situations where Equation (2) is not valid.

Now we can derive the resistance from Equations (8) and (9). In a four-probe setup only two of the chemical potentials are measured. Suppose the current flows from lead 1 to lead 3. The potentials measured are $\mu_2 = eV_2$ and $\mu_4 = eV_4$ under the condition that the current in leads 2 and 4 is zero. Taking $I_2 = 0$ in Equation (9) yields $V_2 - V_4 = (\alpha_{21}/\alpha_{22})(V_1 - V_3)$, and by using this in Equation (8) the current I_1 can be expressed as a function of $V_1 - V_3$. Thus, in this configuration the measured resistance is

$$\mathcal{R}_{13,24} = (V_2 - V_4)/I_1 = \frac{\alpha_{21}}{(\alpha_{11}\alpha_{22} - \alpha_{12}\alpha_{21})}. \tag{10}$$

Since α_{21} is in general not symmetric, the resistance $\mathcal{R}_{13,24}$ is also not symmetric. This result, however, is completely compatible with the (global) Onsager–Casimir symmetry relations. The point is that we are measuring an off-diagonal Onsager coefficient and not a diagonal element. It is V_2 and V_4 which determine the voltage drop across the sample, and not V_1 and V_3. Now we switch the current and the voltage leads but keep the flux fixed. This means that I_1 in Equation (7) is zero. This yields a resistance

$$\mathcal{R}_{24,13} = \alpha_{12}/(\alpha_{11}\alpha_{22} - \alpha_{12}\alpha_{21}). \tag{11}$$

The sum of these resistances, $\mathcal{S}_\alpha = (\mathcal{R}_{13,24} + \mathcal{R}_{24,13})/2$, is symmetric, due to the Onsager–Casimir relation $\alpha_{21}(\Phi) = \alpha_{12}(-\Phi)$.

For a given flux we find in general six resistances,

$$\mathcal{R}_{mn,kl} = (h/e^2)(T_{km}T_{ln} - T_{kn}T_{lm})/D, \tag{12}$$

which differ in magnitude. $D = (h/e^2)^2(\alpha_{11}\alpha_{22} - \alpha_{12}\alpha_{21})/S$ is a subdeterminant of the matrix defined by Equation (7). S is defined in Appendix A. All subdeterminants D of this matrix are equal and symmetric in the flux due to current observation. D is independent of the indices mn, kl. The resistances given by Equation (12) obey $\mathcal{R}_{mn,kl} = -\mathcal{R}_{mn,lk} = -\mathcal{R}_{nm,kl}$, and, more fundamentally, the reciprocity relation (3). The six resistances, which differ in magnitude, can be grouped into three pairs, each pair associated with one of the possibilities for feeding two currents into the four-probe conductor as discussed above. Thus, in addition to $\mathcal{S}_\alpha$ we also have the combinations $\mathcal{S}_\beta = (\mathcal{R}_{14,32} + \mathcal{R}_{32,14})/2$ and $\mathcal{S}_\gamma = (\mathcal{R}_{12,43} + \mathcal{R}_{43,12})/2$, which are symmetric in the flux. Taking into account the symmetries of the transmission probabilities, Equation (5), we can now extend a relation, known in the classical case in the absence of a field [2], to our phase-coherence problem in the presence of a flux, and show that

$$\mathcal{S}_\alpha + \mathcal{S}_\beta + \mathcal{S}_\gamma = 0. \tag{13}$$

The key result of this paper is Equation (12). An interesting property of Equation (12) is that the resistance measured in a four-probe setup is not necessarily positive. Resistances which change sign as the sample is rotated in the external magnetic field have indeed been measured by Soethout et al. [36], and were understood to be a property of a four-terminal measurement. Resistances which change sign as the magnetic field is increased have been observed in submicron structures by Timp et al. [52], but are interpreted as a "dynamic" phenomenon. Negative resistances are possible in a four-terminal resistance measurement. The resistance measured is not the total resistance of the sample, which is, of course, positive. Indeed, the total joule heat W produced by the conductor is

$$W = \frac{1}{e}\sum_i I_i\Delta\mu_i = \frac{1}{2h}\sum_{i<j}(T_{ij} + T_{ji})(\mu_i - \mu_j)^2. \tag{14}$$

To derive Equation (13) we have used Equation (7). Thus W is positive and is determined by the part of the transmission coefficients T_{ij} which is symmetric with regard to flux reversal.

3. Special limits of Equations (7) and (12)

In this section we discuss the application of the approach outlined above to a number of special cases.

- *Two-terminal conductance*

Current conservation in a two-port conductor requires $N_1 = R_{11} + T_{12}$ and $N_1 = R_{22} + T_{21}$, where N_1 and N_2 are the numbers of channels to the left and right. Using these relations, we see that the symmetry of the reflection coefficients implies $T_{12}(\Phi) = T_{12}(-\Phi)$ and $T_{21}(\Phi) = T_{21}(-\Phi)$. From this and Equation (5), we find that $T = T_{12} = T_{21}$. The transmission coefficient of a two-port conductor is thus symmetric,

$$T(\Phi) = T(-\Phi). \tag{15}$$

Equation (6) or Equation (7) with $i = 1, 2$ and $T = T_{12} = T_{21}$ yields a two-terminal conductance,

$$\mathcal{G} = eI/(\mu_1 - \mu_2) = (e^2/h)T. \tag{16}$$

Therefore, Equation (15) implies that the two-terminal

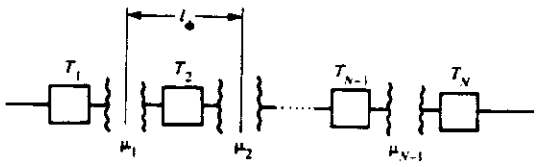

Model of a long wire: The phase is randomized in the reservoirs which are an inelastic length l_ϕ apart. From [38], reprinted with permission.

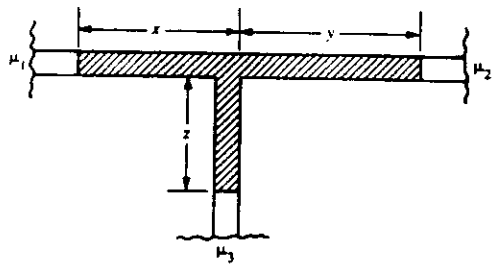

Three-probe conductor. The extra lead (z segment) connected to a reservoir can be viewed as a model of an inelastic scatterer or, alternatively, as a voltage probe. From [40], reprinted with permission.

conductance is symmetric with regard to flux or magnetic field reversal. All experiments known to us which are genuine two-probe experiments obey this symmetry.

Equation (16) was obtained in [30] in the limit of a large number of channels. The connection of Equation (16) with the Greenwood-Kubo formulation has been explored by Fisher and Lee [33]. This two-terminal formula has recently been used to discuss conductance fluctuations [48, 53–55] (variations of the conductance from sample to sample due to the microscopic disorder configuration in macroscopically identical conductors). On the basis of Equation (16), these fluctuations have been found to be universal in the (metallic) diffusive limit, i.e., to be independent of the degree of disorder and only weakly dependent on the geometrical shape of the conductor. The "universality" critically hinges on the simple relation between transmission and conductance given by Equation (16), and breaks down if more sophisticated expressions for the conductance (or resistance) such as Equation (12) are invoked [40–46, 49–50].

To describe the conductance of a piece of wire much longer than the phase-breaking length l_ϕ, with the help of Equation (16), we imagine the wire divided into segments of length l_ϕ. Inelastic scattering cannot be neglected and is concentrated into reservoirs spaced a distance l_ϕ apart, as shown in Figure 2. This procedure, of course, is an approximation to reality, since inelastic scattering occurs uniformly in the bulk. Reference [38] uses this approach to show that the resistance of a one-dimensional conductor as a function of increasing inelastic scattering passes through a minimum. Furthermore, such a simple model allows an easy prediction of the size of conductance fluctuations or voltage fluctuations for voltage probes which are separated by a distance that is large compared to the phase-breaking length [12, 15]. Figure 2 represents a physical picture only if the portions of the conductor adjacent to the segment under study do act like reservoirs. This is not obvious. In the adjacent segments, in narrow wires, the current is, of course, not zero as it is in a reservoir. For small currents, as long as the currents and voltages are related linearly, that seems unimportant. Other features, such as the amplitude of the Aharonov–Bohm oscillations, depend on the fact that inelastic scattering occurs continuously throughout the conductor [56]. Therefore, there is a need for a conductance formula which takes into account the fact that most carriers traversing a segment of length l_ϕ have suffered at least one phase-randomizing event [38].

• *The three-port conductor*

A number of important insights can be gained by considering a conductor with three probes [1, 38]. It is considerably simpler to discuss such a conductor than the four-probe conductor described in [7] and Section 2. Consider the conductor shown in Figure 3, and let us focus on the situation where probe 3 is used to measure the chemical potential μ_3. From Equation (6) or Equation (7) with $i = 1, 2, 3$, we find the chemical potential in lead 3 by taking $I_3 = 0$,

$$\mu_3 = \frac{T_{31}\mu_1 + T_{32}\mu_2}{T_{31} + T_{32}}. \tag{17}$$

Note that for $\mu_1 > \mu_2$ the chemical potential μ_3 is always between the two chemical potentials which drive the current through the conductor, $\mu_1 \geq \mu_3 \geq \mu_2$. Furthermore, $\mu_3(\Phi)$ is neither symmetric nor antisymmetric with regard to flux reversal. We can now use probe 3 to measure the potential differences $\mu_1 - \mu_3$ and $\mu_3 - \mu_2$ and can calculate the resistances

$$R_{12,13} = (\mu_1 - \mu_3)/eI = \left(\frac{h}{e^2}\right)\frac{T_{32}}{D}, \tag{18}$$

$$\mathcal{R}_{12,32} = (\mu_3 - \mu_2)/eI = \left(\frac{h}{e^2}\right)\frac{T_{31}}{D}, \tag{19}$$

with

$$D = T_{21}T_{31} + T_{21}T_{32} + T_{31}T_{23}. \tag{20}$$

D is a subdeterminant of the matrix defined by Equation (6) or Equation (7), and is invariant under flux reversal. Thus the two resistances given by Equations (18) and (19) are determined by the symmetry of T_{32} and T_{31}; i.e., these resistances are neither symmetric nor asymmetric under flux reversal. However, the combined resistance (the two-terminal resistance)

$$\mathcal{R}_{12,12} = (\mu_1 - \mu_2)/eI = \left(\frac{h}{e^2}\right)\frac{T_{31} + T_{32}}{D} \tag{21}$$

is symmetric. Thus, with regard to the two-terminal conductance, the fact that we have an additional lead does not change the symmetry. That important feature of our formulation of resistances is taken up again in Section 4.

The two-terminal conductance in the presence of an additional lead $\mathcal{G} = (\mathcal{R}_{12,12})^{-1}$ differs now from Equation (16); it is given by

$$\mathcal{G} = \left(\frac{e^2}{h}\right)(T_{el} + T_{in}), \tag{22}$$

where the elastic transmission probability describing the transmission of carriers which emanate from port 1 and end up in port 2 without ever entering reservoir 3 is given by

$$T_{el} = T_{21}. \tag{23}$$

The inelastic transmission probability T_{in} describes carriers which emanate from port 1, reach reservoir 3 (where their energy and phase are randomized), and from reservoir 3, in an additional step, reach reservoir 2. Comparing Equation (22) with Equation (21) yields

$$T_{in} = \frac{T_{31}T_{23}}{T_{31} + T_{32}}. \tag{24}$$

Thus, the additional lead connected to an electron reservoir acts like an inelastic scatterer. Equation (22) allows us to describe the continuous transition from completely coherent transmission through the conductor to completely incoherent or sequential transmission. In the limiting case of completely coherent transmission, carriers are not allowed to enter reservoir 3. Consequently, $T_{13} = T_{32} = 0$, and the two-terminal conductance is given by Equation (16); i.e., $T_{el} = T$ and $T_{in} = 0$. In the limit of completely incoherent transmission, $T_{21} = T_{el} = 0$. In this case Equation (21) yields

$$\mathcal{R}_{12,12} = \mathcal{G}_{12,12}^{-1} = \frac{h}{e^2}\left(\frac{1}{T_{31}} + \frac{1}{T_{23}}\right). \tag{25}$$

To obtain the latter result we have made use of the fact that for $T_{12} = 0$ we have $T_{23}(\Phi) = T_{23}(-\Phi)$. Equation (25) is

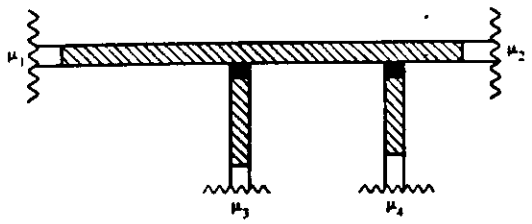

Four-terminal conductor with tunneling barrier junctions (dark areas) for two of the probes.

nothing but the classical addition of series resistors. Equations (15)–(25) extend results presented in [38–40] for a sample without flux to the more general case of a three-probe conductor subject to a flux.

Adding a lead away from a conductor and connecting it to a reservoir gives us a simple way of introducing inelastic scattering into the conduction process. This method was used in [37] to study the effect of phase-randomizing events on the persistent current in a small normal loop and to investigate the dissipative response to a small oscillating flux superimposed on a static flux. Reference [38] investigates the transmission as a function of increasing inelastic scattering through a series of closely spaced barriers; and the effect of phase-randomizing events on resonant transmission through a double barrier is discussed in [39]. Thus, additional leads allow a double interpretation: They can be thought of as voltage probes, and they can be introduced as inelastic scatterers. Sample-specific fluctuations of voltage, resistance, and conductance in a three-probe conductor are the subject of [40, 45, 50].

• *Point contacts*

Further progress in lithography will make it possible to produce samples with leads made from different materials. An interesting possibility is the fabrication of barriers which separate the conductor and the leads.* This produces current leads [14, 20] and/or voltage leads which are weakly coupled [37–39] to the conductor.

Let us consider the conductor shown in Figure 4. Current is fed in at probe 1 and taken out at probe 2. Probes 3 and 4 serve to measure the voltage and are weakly coupled via tunneling barriers to the conductor. The probabilities for transmission from a probe into the conductor and into reservoir 1 or 2 are small because of the intervening

* S. Kaplan and C. Umbach, private communication.

tunneling barrier. Suppose the largest of these transmission probabilities is ϵ. The transmission probabilities of the conductor of Figure 4 can be expanded with respect to the small parameter ϵ. Transmission from port 1 to port 2 can proceed via paths which never cross the tunneling barrier, and thus $T_{12} = T_{12}^{(0)} + \cdots$ to lowest order. The upper index in parentheses indicates the order in ϵ. But transmission from port 1 to port 3, for example, is only possible by crossing a barrier, and thus $T_{13} = \epsilon T_{13}^{(1)} + \cdots$. Transmission from probe 3 to probe 4 requires that the barriers be traversed at least twice, and hence $T_{34} = \epsilon^2 T_{34}^{(2)} + \cdots$. Via current conservation, the reflection coefficients can be expressed in terms of the transmission probabilities. Evaluation of Equation (12) yields a resistance

$$\mathcal{R}_{12,34} = \left(\frac{h}{e^2}\right)\frac{1}{T}\frac{T_{31}^{(1)}T_{42}^{(1)} - T_{32}^{(1)}T_{41}^{(1)}}{(T_{31}^{(1)} + T_{32}^{(1)})(T_{41}^{(1)} + T_{42}^{(1)})}. \tag{26}$$

$T = T_{21}^{(0)} = T_{12}^{(0)}$ has the symmetry of the transmission probability of a two-terminal conductor given by Equation (15). The sums $T_{31} + T_{32}$ and $T_{41} + T_{42}$ are also symmetric with regard to flux reversal, since T_{34} is zero to order ϵ. Therefore, Equation (26) has precisely the symmetry required by the reciprocity theorem, Equation (3). Using Equation (12), it is now easy to calculate the resistances which are measured if current is fed and removed differently and the remaining "good and bad" contacts are used to measure the voltage. For the conductor of Figure 4, this yields six resistances which satisfy the sum rule, Equation (13). Equation (26) shows that the resistance, even when measured with point contacts, depends on the details of the coupling of the contacts to the conductor. *The resistance is not determined by the properties of the conductor alone (zero transmission probability through the contacts), but depends explicitly on how carriers can enter and leave the conductor through the probes.*

Instead of using Equation (7) we can derive Equation (26) in the following way: The voltage at probes 3 and 4 can be calculated by using Equation (17). To the lowest order in ϵ, the existence of one probe does not affect what is measured at the other. We thus find

$$\mu_3 = \frac{T_{31}\mu_1 + T_{32}\mu_2}{T_{31} + T_{32}} \tag{27}$$

and

$$\mu_4 = \frac{T_{41}\mu_1 + T_{42}\mu_2}{T_{41} + T_{42}}. \tag{28}$$

Here we have omitted, for simplicity of notation, the upper indices on the transmission probabilities indicating the order in ϵ. The measured potential difference is

$$\mu_3 - \mu_4 = \frac{T_{31}T_{42} - T_{32}T_{41}}{(T_{31} + T_{32})(T_{41} + T_{42})}(\mu_1 - \mu_2). \tag{29}$$

The net current through the conductor from probe 1 to probe 2 is to lowest order in ϵ unaffected by these probes. Thus the current is $I = (e/h)T(\mu_1 - \mu_2)$. Using this and Equation (29) yields the resistance given by Equation (26). Let us again emphasize the possibility of measuring negative resistances in a four-terminal setup. Both μ_3 and μ_4 are bounded by μ_1 and μ_2; i.e., $\mu_1 \geq \mu_3 \geq \mu_2$ and $\mu_1 \geq \mu_4 \geq \mu_2$, but μ_3 is not necessarily greater than μ_4. Thus, the only general bound we can give for the measured potential difference is $|\mu_3 - \mu_4| \leq \mu_1 - \mu_2$. Hence, the measured resistance $\mathcal{R}_{12,34}$ for the conductor of Figure 4 has upper and lower bounds given by the two-terminal resistance,

$$-\left(\frac{h}{e^2}\right)\frac{1}{T} \leq \mathcal{R}_{12,34} \leq \left(\frac{h}{e^2}\right)\frac{1}{T}. \tag{30}$$

We return to the subject of negative four-terminal resistances in Section 5.

• *The Landauer formula*

A very often quoted formula for the resistance of a one-dimensional conductor is the Landauer formula [16, 28, 29, 57]

$$\mathcal{R} = (h/e^2)(R/T). \tag{31}$$

How does this result relate to the resistance formulae discussed above? A four-terminal interpretation of Equation (31) has been put forth by Engquist and Anderson [32]. To arrive at Equation (31) they not only assume that the voltage probes are weakly coupled, as discussed above, but also assume that the probes couple to the conductor in a symmetric fashion with regard to right- and left-moving carriers. Furthermore, at the junction of the conductor with the probe, they match the currents and not the current amplitudes. In contrast, our treatment is fully quantum-mechanical. We also note that the situation envisioned by these authors differs from that of Figure 4 in that the voltage probes are connected to the perfect leads and the conductor is disordered only *between* the voltage probes. Elastic scattering is then characterized by a transmission and a reflection probability T and R of the disordered region. These simplifications and assumptions give rise to transmission probabilities $T_{12} = T_{21} = T$ to order ϵ^0, $T_{31} = T_{13} = T_{42} = T_{24} = 1 + R$, $T_{32} = T_{23} = T_{14} = T_{41} = T$ to order ϵ, and $T_{43} = T_{34} = T$ to order ϵ^2. Using this in Equation (29) yields

$$\mu_3 - \mu_4 = \tfrac{1}{4}[(1 + R)^2 - (1 - R)^2](\mu_1 - \mu_2) = R(\mu_1 - \mu_2). \tag{32}$$

Since the current is $I = (e/h)T(\mu_1 - \mu_2)$, this gives Equation (31). Thus, by using the assumptions of Engquist and Anderson, we can deduce the Landauer formula from Equation (12) or Equation (26). T has the symmetry of the transmission probability of a two-terminal conductor. Since $R = 1 - T$, the Landauer result is symmetric under flux

reversal. Instead of Equation (3), the Engquist and Anderson discussion yields $\mathcal{R}_{mn,kl}(H) = \mathcal{R}_{kl,mn}(H) = \mathcal{R}_{mn,kl}(-H)$; i.e., it is not necessary to exchange current and voltage leads when reversing the magnetic field. For a four-probe conductor, we typically have six differing resistances, whereas the Engquist and Anderson discussion yields only three. In addition to $\mathcal{R}_{12,34}$ given by Equation (31), using Equation (12) and the transmission probabilities as specified above, we find $\mathcal{R}_{14,23} = -(h/e^2)[R/T]$ and $\mathcal{R}_{13,42} = 0$. The sum of these three resistances according to Equation (13), is zero. (Note that in the latter configuration, the voltage difference is not measured along a piece of the conductor carrying a net current. Such voltage differences across Y-shaped leads are generally not zero and have indeed been measured [41]. For another experiment demonstrating such nonlocal effects, see [58].) In principle it could have been possible that for strictly one-dimensional conductors a higher symmetry than that predicted by Equation (3) applies. But Equations (12) and (26), which are valid independent of the number of channels, tell us otherwise. Note also that the symmetry assumed by Engquist and Anderson on the coupling of the voltage probe with the conductor ensures that the resistance, Equation (31), is always positive, in contrast to Equation (26). We return to the discussion of the Landauer formula from a different point of view in Section 5. The symmetry of the conductance formulae of Azbel [25] and Büttiker et al. [21] is discussed in Appendix B.

4. Rigidity of the reciprocity symmetry

The situation discussed until now is highly conceptual. We have discussed conductors with four leads which are connected to reservoirs so close to the conductor that it can be assumed that scattering within the conductor is only elastic. Clearly, the spatial separation of elastic and inelastic scattering is more a theorist's invention than an experimental reality. In the experiments, the probes lead away from the section of conductor which is under study. The probes are connected to macroscopic pads over distances which are large compared to the inelastic scattering length. Thus, inelastic scattering occurs in a rather uniform fashion throughout the conductor and the leads. Using the concepts developed here, we would like to understand why reciprocity is also observed in the presence of inelastic scattering. Furthermore, reciprocity is also observed regardless of how many probes are connected to the conductor. We have already pointed out that probes act like inelastic scatterers. *Thus the validity of the reciprocity relations both in the presence of inelastic scattering and in the presence of an arbitrary number of leads attached to the conductor is really the very same problem.*

Below we show that the relations of Equations (6) and (7) can be generalized and are valid for transmission probabilities which are the sum of an elastic coherent part (el) and an inelastic or incoherent part (in). Thus, in general,

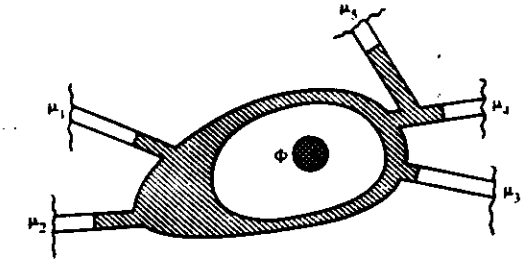

Five-probe conductor. The addition of a lead does not change the reciprocity symmetry and permits us to study conductors which are large compared to the phase-breaking length.

$$\hat{T}_{ij}(\Phi) = T_{el,ij}(\Phi) + T_{in,ij}(\Phi), \tag{33}$$

where the combined transmission probability $\hat{T}_{ij}$ has exactly the symmetry given by Equation (5). Similarly, the reflection coefficients are in general a sum of both an elastic and an inelastic part, and the symmetry of the total reflection probability is again given by Equation (5).

Consider now the conductor shown in Figure 5, where we have added a fifth probe connected to a potential μ_5. The currents in this conductor are determined by Equation (7), where $i = 1, \cdots, 5$. Here we want to show that by eliminating one of the chemical potentials, say μ_5, we once again obtain Equation (7), with $i = 1, \cdots, 4$ and T_{ij} replaced by $\hat{T}_{ij}$. This then shows that Equation (12) is still valid; the only difference is that the T are replaced by $\hat{T}$. If probe 5 is a voltage probe or an inelastic scatterer, we must require that $I_5 = 0$. This condition determines μ_5 as a function of the remaining chemical potentials,

$$\mu_5 = \frac{1}{(N_5 - R_{55})} \sum_{j=1}^{j=4} T_{5j}\mu_j. \tag{34}$$

Using Equation (34) to eliminate μ_5 in the equations for the currents at the other probes yields

$$I_i = \frac{e}{h}\left[(N_i - \hat{R}_{ii}) - \sum_{j=1}^{j=4} \hat{T}_{ij}\mu_j\right], \tag{35}$$

with

$$\hat{R}_{ii} = R_{ii} + \frac{T_{i5}T_{5i}}{N_5 - R_{55}}, \tag{36}$$

$$\hat{T}_{ij} = T_{ij} + \frac{T_{i5}T_{5j}}{N_5 - R_{55}}. \tag{37}$$

In Equations (36) and (37), the first term gives the reflection

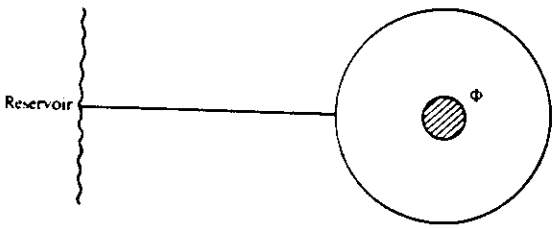

Normal loop penetrated by an Aharonov–Bohm flux supports a circulating equilibrium current despite the coupling to a phase-breaking dissipative reservoir. From [37], reprinted with permission.

(transmission) of carriers which have *not* entered reservoir 5, and the second term gives the reflection (transmission) of carriers which have entered reservoir 5. Since the reservoirs act as phase-breakers, the second term in Equations (36) and (37) can be viewed as the inelastic, incoherent part of the total reflection (transmission) probability. The first term in Equations (36) and (37), on the other hand, describes coherent reflection (transmission). Thus Equations (36) and (37) appear as simple generalizations of the relations found for a three-probe conductor [38–40].

Now it is easy to see that the symmetry of the new transmission and reflection probabilities $\hat{T}$ and $\hat{R}$ is the same as that of the original purely elastic transmission probabilities. Furthermore, by using Equation (7) for a five-probe conductor and eliminating μ_5, we obtain

$$N_i = \hat{R}_{ii} + \sum_{j=1}^{4} \hat{T}_{ij} \tag{38}$$

and

$$N_i = \hat{R}_{ii} + \sum_{j=1}^{4} \hat{T}_{ji}. \tag{39}$$

Equations (38) and (39) are a consequence of current conservation in a four-probe conductor. Therefore, the $\hat{T}$ and $\hat{R}$ satisfy the same symmetry conditions and current-conservation relations as the T and R. Hence, all results obtained for the T and R in Sections 2 and 3 of this paper are also valid for the $\hat{T}$ and $\hat{R}$.

Obviously, if we have a conductor with many leads $n > 4$, we can repeat the steps outlined above $n - 4$ times, until only the chemical potentials of the particular four-probe measurement under study occur. Equation (12) is then valid for a set of generalized transmission and reflection probabilities. Thus, these considerations show that the reciprocity symmetry is a very *rigid* feature of electrical conduction. Reciprocity applies regardless of the number of leads attached to the conductor and regardless of whether we deal with elastic or inelastic transmission.

5. Self-induced fields

Charge transport gives rise to magnetic and electric fields. In the presence of steady current flow, considered in this paper, current density and charge density are related to fields via

$$c\nabla \times B = j, \tag{40}$$

$$\nabla D = 4\pi e(\rho - \rho_0). \tag{41}$$

In this section we are chiefly concerned with the induced electric field, or with the associated electrostatic potential U:

$$\nabla^2 U + (4\pi e/e_L)(\rho - \rho_0) = 0. \tag{42}$$

The key intention is to explore the connection of the electrostatic potential $U(r)$, which is defined at every point in the conductor with the chemical potentials measured at the contacts, as discussed in the previous sections. Before discussing this, it is worthwhile to consider briefly the induced magnetic fields.

• *Magnetic field induced by persistent currents*

Consider the conductor in Figure 1 at equilibrium. All the reservoirs are at the same chemical potential, $\mu = \mu_1 = \mu_2 = \mu_3 = \mu_4$. According to Equation (7), this implies that the currents at all the contacts are zero, $I_1 = I_2 = I_3 = I_4 = 0$. However, this does not imply that the current density $j(r)$ is zero in the interior of the conductor. Simple model calculations suggest that there exists an equilibrium current pattern $j(r)$ in tiny and open conductors. Figure 6 shows an open conductor. A loop is connected to a reservoir via a single lead. The lead allows an exchange of carriers between the loop and the reservoir. As shown in [37], such a loop exhibits a persistent current which is a periodic function of the flux Φ threading the loop. The amplitude of the circular equilibrium current is nonzero as long as carriers can complete a full revolution before escaping from the loop into the reservoir. This simple model was introduced to discuss the effect of inelastic events on the circular currents found in *closed* loops in [18]. The simple model of Figure 6 demonstrates that circular equilibrium currents are not a property of closed systems only. Considering the lead connected to a reservoir as an inelastic scatterer, [37] arrives at the same conclusion as [59]: A modest number of inelastic events only reduces the amplitude of the circular currents but does not suppress such currents completely. Comparison [8, 10] of the inelastic effects introduced via a current lead coupled to a bath [37] with intrinsic inelastic effects in a closed loop [59] highlights the effect of coupling a measurement probe to a tiny conductor. For additional work on closed loops we refer to [60]. In the conductor of Figure 6, an equilibrium current pattern arises because elastic

scattering leads to a density of states which is sharply peaked near the eigenstates of the closed loop. In a more general geometry, such as the conductor in Figure 1, carriers are not confined to move on a circular path. However, it is known that quantum-mechanical interference leads to an enhanced probability for a carrier which initially is at point P to return to point P (see for example [15]). A net current arises if the probabilities for clockwise and anticlockwise motion along such a path are different. Since the net current through the contacts is zero, no joule heat is produced. Calculation of these currents requires knowledge of the wave functions at every point in the conductor. Moreover, since the currents are an equilibrium feature, they are not determined by the states at the Fermi energy alone but require knowledge of the wave functions at all energies. Typically, however, the main contribution to these currents arises from a narrow energy interval extending from the Fermi energy to an energy somewhat smaller. On a length scale, small compared to the phase-breaking length, we can thus expect to find a nonzero ensemble average $\langle [j(r)]^2 \rangle$. These currents induce a magnetic field according to Equation (40).

If the chemical potentials of the conductor of Figure 1 are different and a net current is induced, say from contact 1 to contact 2, then, as is well understood, an additional magnetic field $B(r; \mu_1 - \mu_2)$ is produced which is proportional to the difference of the chemical potentials. We do not discuss this further, but instead refer the reader to [42] and [61], which calculate such fields in the metallic diffusive regime.

• *Induced electric fields*

Induced electric fields in the presence of current flow past isolated impurities have been emphasized by Landauer [27, 28, 58, 62]. Local fields are of importance for the discussion of nonlinear effects [63, 64], and they play a central role in the von Klitzing effect [65]. Here we wish to stress the distinction between the local field $E(r)$, or the potential $U(r)$, and the chemical potentials μ_i discussed in the previous sections of this paper. The chemical potentials μ_i are thermodynamic potentials which characterize a bath. The potential $U(r)$, on the other hand, characterizes the distribution of unscreened charges in the conductor. In a macroscopic conductor, where each volume element also contains a large number of carriers, $U(r)$ also becomes a thermodynamic quantity, i.e., a local Fermi energy. In a macroscopic conductor, we can couple the volume element under consideration to a bath, and if the coupling is sufficiently "weak," the bath has a chemical potential $\mu(r) = eU(r)$, at least if $U(r)$ varies slowly compared to the screening length. In the coherent quantum transport regime we must be more cautious. It makes a difference whether a small conductor over a given length interval is closed, or has a junction to an extra lead, with a reservoir attached. In general, as we show, $\mu(r) \neq eU(r)$.

One-dimensional two-probe conductor

Consider a one-dimensional conductor consisting of a disordered region with perfect leads attached to each side. The perfect leads are in turn connected to reservoirs at chemical potentials $\mu_1 > \mu_2$. Now suppose that self-consistent screening applies for the equilibrium situation, i.e., for $\mu_1 = \mu_2$. Consider the additional charge density $\Delta\rho$ induced by the current flow. The density of states in the perfect leads, corresponding to states with positive velocity, is $dn/dE = 1/2\pi\hbar v$. We denote the wave function which describes carriers incident from reservoir 1 with chemical potential μ_1 by $\psi_1(x)$, and the wave function which describes carriers incident from the right by $\psi_2(x)$. The added charge is [37]

$$\Delta n = \frac{dn}{dE}(\mu_1 - \mu_2)|\psi_1(x)|^2, \tag{43}$$

where ψ_1 is normalized such that the incident beam has unit amplitude. Both the wave function and the density of states are taken at the Fermi energy. In a region where Δn is spatially independent, this excess density is screened. Since the total charge density in such a region is zero, the screening field raises or lowers the band bottom to achieve this [62]. The charge which is gained or lost by adjusting the band bottom is

$$\Delta n_{eq} = \frac{dn}{dE}(eU - \mu_2)(|\psi_1(x)|^2 + |\psi_2(x)|^2). \tag{44}$$

Note that Δn_{eq} is the local excess density which builds up if the chemical potential of both reservoirs is raised by $eU - \mu_2$ from $\mu_1 = \mu_2$. The net charge difference $\Delta\rho$, which remains unscreened and enters Equation (41), is thus $\Delta\rho = \Delta n - \Delta n_{eq}$. Inserting this into Equation (41) yields a differential equation for $U(x)$:

$$\lambda^2\nabla^2 eU(x) + [\mu_1|\psi_1|^2 + \mu_2|\psi_2|^2 - eU(x)(|\psi_1|^2 + |\psi_2|^2)] = 0, \tag{45}$$

where $\lambda = (\varepsilon_L/4\pi e^2)^{1/2}(dE/dn)^{1/2}$ is a screening length. The proper solution eU of Equation (45) has the value μ_1 in the left reservoir and drops to the chemical potential μ_2 in the reservoir to the right. Below, we resort, for simplicity, to drastic approximations. Suppose that the wave functions vary slowly on the scale λ, the screening length. In this case the first term in Equation (45), $\lambda^2\nabla^2 U$, can be neglected, and we obtain

$$eU(x) = \frac{|\psi_1(x)|^2\mu_1 + |\psi_2(x)|^2\mu_2}{|\psi_1(x)|^2 + |\psi_2(x)|^2}. \tag{46}$$

If the screening length is not short compared to the Fermi wavelength, we can still salvage Equation (46). If we are only interested in the long-range variation of $U(x)$, we can average the wave functions in Equation (45) over distances of the order of λ. Clearly, if such an averaging procedure is used, some information on the phase sensitivity of $U(x)$ is lost. Equation (46) was obtained by Entin-Wohlman et al.

[35], who argue that $eU(x)$ is what is actually measured at a chemical potential probe.

Applied to the perfect leads, Equation (46) reproduces, with an additional approximation, the Landauer result, Equation (31). To see this, consider a scatterer connected to perfect leads. The scatterer has a transmission probability $T = |t|^2$ and a reflection probability $R = |r|^2$. To the left we have $|\psi_1|^2 = 1 + R$, $|\psi_2|^2 = T$, and from Equation (46) we find

$$eU_1 = \tfrac{1}{2}[(1 + R)\mu_1 + T\mu_2]. \tag{47}$$

To the right we have $|\psi_1|^2 = T$, $|\psi_2|^2 = 1 + R$, and from Equation (46) we find

$$eU_2 = \tfrac{1}{2}[T\mu_1 + (1 + R)\mu_2]. \tag{48}$$

Since the total current driven through the conductor is $I = (e/h)T(\mu_1 - \mu_2)$, we immediately find $\mathcal{R} = (U_1 - U_2)/I = (h/e^2)(R/T)$.

In the derivation of the Landauer formula given above, we have related $|\psi|^2$ to the transmission and reflection probabilities. Since the reflected wave interferes with itself, the exact density of carriers is determined by $|\psi(x)|^2 = 1 + R + 2\mathrm{Re}(re^{-i\alpha x})$. Since the reflection amplitude r is proportional to $R^{1/2} \geq R$, it is actually the interference term which is dominant for weak elastic scattering ($R \ll 1$). If the exact expression for the charge densities is inserted into Equation (45), the result is a voltage which is oscillating even in a perfect lead. The suppression of such interference terms is one reason that Landauer's result is positive, whereas Equation (26), which allows for such interference terms, can give a negative resistance.

The voltage $U(x)$, as defined by Equation (46), does not match the chemical potentials of the reservoirs. (This can only be achieved by allowing the one-dimensional leads to spread out to accommodate a large density of states [16, 58, 66].) Imry [11] has pointed out that the difference in potential between a reservoir and a lead gives rise to a contact resistance, $\mathcal{R}_{\mathrm{con}} = (h/e^2)(V_1 - U_1)/I$, where $\mu_1 = eV_1$. Using Equation (47), the contact resistance is, according to this interpretation, universally equal to $h/2e^2$ for a one-channel conductor. However, due to the oscillatory nature of the voltage in the lead, we can expect such contact resistances to fluctuate from sample to sample and to exhibit a sensitivity to the phase of the wave function. If we consider the conductor of Figure 4 and use the results of Section 3, we find contact resistances which can fluctuate in a wide range. If we define the contact potential as $\mu_1 - \mu_3$ and use Equation (27), we find a contact resistance with a lower bound of zero and an upper bound of $(h/e^2)T^{-1}$.

Equation (46) can be used to determine the voltage U at two arbitrary points along the conductor [35]. Denote these points by x_1 and x_2. Then, by evaluating $\mathcal{R} = (U_1 - U_2)/I$ with the help of Equation (46), we find

$$\mathcal{R}(x_1, x_2) = \frac{h}{e^2}\frac{1}{T}\frac{|\psi_2(x_2)|^2|\psi_1(x_1)|^2 - |\psi_2(x_1)|^2|\psi_1(x_2)|^2}{[|\psi_1(x_1)|^2 + |\psi_2(x_1)|^2][|\psi_1(x_2)|^2 + |\psi_2(x_2)|^2]}. \tag{49}$$

Equation (49) is reminiscent of Equation (26). Like the Landauer formula, however, it does not contain any perturbations due to the leads. It links the electrical potential $U(x)$ to a "resistance." The "resistance" given by Equation (49) typically exhibits no symmetry at all with regard to flux reversal. If Equation (47) is applied to a one-dimensional ring [35, 67] and at least one of the points x_1 or x_2 lies in the disordered part of the conductor, the resistance given by Equation (49) can be expected to be neither antisymmetric nor symmetric with respect to flux reversal, despite the fact that the conductor is only connected to two reservoirs. This is demonstrated by a calculation in [67]. [Reference [67] makes an additional approximation and replaces the local equilibrium density of states with the density of states in the leads. This corresponds to setting the combined densities of the two wave functions multiplying U in Equation (45) equal to 2.] A similar calculation in [35] finds a purely antisymmetric resistance, due to the high symmetry of the conductor investigated and the symmetric location of the points x_1, x_2 chosen.

One-dimensional many-probe conductor

To better illustrate the difference between the voltage measured at a contact and U given by Equation (46), we consider for simplicity a *one-channel* conductor connected to three reservoirs, as shown in Figure 3. Let the density of states in all the leads be equal. Proceeding as above gives, for a three-probe conductor, a local voltage $U(r)$,

$$eU(r) = \frac{|\psi_1(r)|^2\mu_1 + |\psi_2(r)|^2\mu_2 + |\psi_3(r)|^2\mu_3}{|\psi_1(r)|^2 + |\psi_2(r)|^2 + |\psi_3(r)|^2}. \tag{50}$$

Here the index on the wave function indicates the reservoir from which the carriers are injected into the conductor. Equation (50) is valid for every branch of the conductor with $r = x$, $r = y$, or $r = z$ on the corresponding branch (see Figure 3). Connecting a lead to the conductor thus changes the potential throughout the conductor. Equation (48) has been evaluated in the perfect leads of a three-probe conductor in [38]. Let us briefly consider probe 3, acting as a voltage probe, and show that Equation (17) results. In this case, within the *perfect* lead of probe 3, we have $|\psi_1(x)|^2 = T_{31}$, $|\psi_2(x)|^2 = T_{32}$, and $|\psi_3(x)|^2 = 1 + R_{33}$. Inserting this into Equation (48) and using Equation (7) for $i = 3$ with $I_3 = 0$ yields $eU_3 = \mu_3$. This is an astonishing result in view of the approximations made to arrive at Equation (50). For a voltage lead which does not support a net current, it might be more adequate to consider just the long-range variation of U (and thus to neglect the interference terms in the absolute

values of the wave functions). Clearly, these results can easily be extended to a four-probe conductor with one-dimensional perfect leads. In this case, the voltage $U(r)$ is determined by four wave functions and four chemical potentials. Thus, for the many-probe conductor with one-dimensional leads, we have an (approximate) picture of the connection of the local potential with the chemical potentials of the measuring baths. We see that the reciprocity symmetry is connected to the fact that at a probe (a point of measurement), three (or four) wave functions determine the outcome of the measurement. In contrast, only two wave functions are used in Equations (46) and (49).

Potential fluctuations in the measurement lead

Equation (50) leads to a picture of the local potential $U(r)$ along a three-probe conductor, as shown in Figure 7. A net current flows from the bath with chemical potential μ_1 to the bath with chemical potential μ_2. The measurement probe, leading to a bath at a chemical potential μ_3 given by Equation (17), is connected to the conductor at point P. Equation (50) predicts a potential $U(r)$ which fluctuates along the probe depending on all three wave functions ψ_i. Fluctuations of $U(z)$ along the probe occur for several reasons. First, the probe itself is typically a disordered conductor. In this case the fluctuations are determined by the precise disorder configuration within a phase-breaking length. Even if the probe is an ideal perfect wire, a voltage variation occurs across the junction of the perfect probe with the conductor [38, 40]. Thus, in general, the chemical potential $\mu_3 = eV_3$ is not related in a simple way to the local potential $U_P = U(P)$. The fact that U_P and V_3 are not equal is important. It means that a *contact potential difference* $V_C = U_P - V_3$ exists between the local potential at P and the measured voltage. Typically, voltage drops arise due to current flow past an obstacle. But in the conductor depicted in Figure 7, there is *no net* current flow in the measurement lead. A situation similar to that shown in Figure 7 also follows from the work of Maekawa et al. [43] and Kane et al. [45]. They define a local electric field by enforcing current conservation on an expression for the nonlocal current–field relation.

The existence of such contact potentials means that a voltage measurement with a lead does not give us direct information on the local potential of the conductor at the point of attachment. Such contact potentials arise not only in the metallic diffusive limit. Even if voltages were measured by inserting a tunnel junction between the conductor and the lead, or if the tunneling microscope were used to measure the potential [68], such contact potentials would also be present. In the presence of a large barrier, the wave functions ψ_i are exponentially attenuated at the junction. The wave functions ψ_1 and ψ_2 have an exponentially small amplitude factor in the measurement lead; ψ_3, which is large in the probe, is exponentially small in the conductor. As shown by Equation (17), the measured

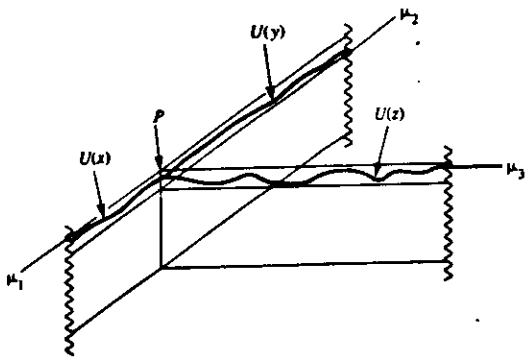

One-dimensional conductor with a voltage probe. Current flows from the bath at chemical potential μ_1 to the bath at chemical potential μ_2. A voltage probe is attached to the conductor at point P. The measured chemical potential is μ_3. The heavy line depicts the local potential U along the x, y, and z segments. Typically, the measured chemical potential differs from the electric potential U at the point P of attachment. Screening causes the band bottom (faint lines below μ_2) to follow $U(r)$.

voltage is determined by T_{31} and T_{32}, i.e., by the exponentially small wave functions ψ_1 and ψ_2 at the location of the bath. If the junction cannot be controlled on an atomic scale, the attenuation of ψ_1 and ψ_2 at the barrier varies exponentially from sample to sample. Hence the ratio T_{31}/T_{32} exhibits fluctuations that increase as the coupling between the lead and the conductor becomes weaker. Invoking tunnel junctions between the leads and the conductor can, therefore, be expected to increase the fluctuations in the contact potential and to lead to voltage fluctuations which are even bigger than those measured [41,42] in the metallic diffusive limit [40, 46, 49, 50]. Even metallic-diffusive voltage probes give rise to voltage fluctuations which increase with the length of the probe [40, 46].

Since the chemical potential of a measurement probe is not simply related to the voltage U at the point of attachment, measurement of negative resistance in the geometry of Figure 4 does not imply that the voltage U increases in the direction of the current flow. The contact potential V_C can be positive at probe 3 and negative at probe 4. If these contact potentials are large enough, we measure a negative resistance despite the fact that $U(r)$ drops monotonically along the conductor.

Voltages can be measured other than by the exchange of carriers with a probe; an alternative technique uses capacitive probes [57]. It is suggested that in the absence of particle exchange with the measurement probe we can

measure the local potential U_p. Thus, the appearance of contact potentials discussed previously is avoided. The key question which must be answered is this: Can we have enough Coulomb coupling between the conductor and a capacitor plate to make a measurement without significantly affecting the effective potential which the carriers see while moving along the conductor? A recent experiment which uses capacitive coupling to shift the phase of the Aharonov-Bohm oscillations [18–21] is described in [69].

Measurement-theoretical aspects

Equations (15) and (17) are also of interest for the theory of measurement [70]. We can look at these equations as describing the interaction between the measurement apparatus (the measurement probe with a bath attached at its end) and the system (the conductor). In contrast to the discussions of the measurement process, which treat a Hamiltonian for the combined system, the approach presented here describes the measurement as a scattering process and analyzes an S-matrix. The phase of the wave functions is broken by the reservoir at the end of the probe. This notion avoids a difficulty which measurement theory tries to explain: Why doesn't the measurement apparatus obey the superposition principle even though the total system is described by a Hamiltonian?

There is a fundamental difference in how we have treated the local potentials and the currents. The reciprocity symmetry is a consequence of microscopic reversibility. Current conservation and time-reversal invariance are what determine the symmetry of the transmission probabilities in Equations (6) and (7). In Equation (45) the time-reversed wave functions of ψ_1 and ψ_2 do not occur. The time-reversed wave function of ψ_1 describes carriers incident from both reservoirs which in the disordered region interfere, giving a beam of unit amplitude for the outgoing wave. The time-reversed wave functions are excluded, since carriers incident from different reservoirs are incoherent [18, 62].

Local potentials in a many-channel two-probe conductor

Consider a disordered region connected to two perfect leads. Assume, for simplicity, that the perfect leads are strips, with x the direction along the lead and y the direction perpendicular to the strip. Also assume that the perfect leads to the left and right are identical and support N quantum channels with a density of states $(dn_i/dE) = 1/2\pi\hbar v_i$. Here v_i is the velocity in channel i at the Fermi energy in the x direction. As in [21], we assume that the reservoir feeds channels incoherently with respect to one another. With these specifications the many-channel generalization of Equation (46) is

$$eU(x,y) = \frac{\sum_{i=1}^{i=N} \frac{1}{v_i} [|\psi_{1,i}(x,y)|^2 \mu_1 + |\psi_{2,i}(x,y)|^2 \mu_2]}{\sum_{i=1}^{i=N} \frac{1}{v_i} [|\psi_{1,i}(x,y)|^2 + |\psi_{2,i}(x,y)|^2]}. \quad (51)$$

Here $\psi_{1,i}$ is the wave function at the Fermi energy describing carriers incident in channel i from the left-hand reservoir. Similarly, $\psi_{2,i}$ describes carriers incident in channel i from the right-hand reservoir. As in the one-channel case, the amplitude of these wave functions is normalized such that the incident wave has amplitude 1. The voltage $U(x, y)$ obtained in this manner is a complicated fluctuating function of x and y. Let us briefly discuss the voltage $U(x, y)$ in one of the perfect leads. In the perfect leads we can represent the wave functions ψ as a superposition of eigenstates of the lead Hamiltonian. This Hamiltonian is separable and has eigenstates $e^{\pm ik_j x} f_j(y)$. Here $f_j(y)$ is the "transverse eigenfunction" of channel j and k_j is the wave vector along the lead. The wave functions in the left perfect conductor are

$$\psi_{1,i} = \sum_{j=1}^{j=N} f_j(y)[\delta_{ij} e^{ik_j x} + (v_i/v_j)^{1/2} r_{11,ji} e^{-ik_j x}] \quad (52)$$

for carriers incident from the left, and

$$\psi_{2,i} = \sum_{j=1}^{j=N} f_j(y)(v_i/v_j)^{1/2} t_{12,ji} e^{-ik_j x} \quad (53)$$

for carriers incident from the right. Here $r_{11,ji}$ is the probability amplitude for reflection into channel j of a carrier incident in channel i. $t_{12,ji}$ is the transmission probability for carriers incident in the right perfect conductor in channel j to reach channel i to the left. The density of carriers $|\psi_{1,i}|^2$ contains diagonal terms $f_i(y)f_j^*(y)$ proportional to the density of the incident wave (in channel i) and the density of the reflected waves. There are off-diagonal terms $f_i(y)f_j^*(y)e^{i(k_i-k_j)x}$ proportional to the reflection amplitudes in channels i and j. Furthermore, there are $2N$ terms which arise from multiplying the incident wave with the reflected waves. These latter terms are proportional to $f_i(y)f_j^*(y)e^{-ik_j x}$. Hence the voltage U in the perfect leads is nonuniform and exhibits long-range oscillations, since $k_i - k_j$ can be small (of the order of k_F/N). Therefore, since screening typically occurs over much shorter distances, the voltage $U(x, y)$ follows these long-range oscillations.

References [21], [25], and [34] do not allude to spatially nonuniform voltages in the leads, but attribute a spatially averaged voltage to each lead. In these works the densities $|\psi|^2$ are averaged with respect to x and y. Thus the densities are expressed in terms of transmission and reflection probabilities alone. The potential drop across the disordered region is obtained by introducing these averaged densities into Equation (51). The result for the conductance is given in Appendix B [Equation (B7)]. We emphasize that using the spatially averaged densities in Equation (51) is not equivalent to calculating a spatial average of the exact voltage; i.e., $\langle eU \rangle = \left\langle \frac{\quad}{\quad} \right\rangle \neq \frac{\langle \quad \rangle}{\langle \quad \rangle}$. Thus, the spatial average of Equation (53) is in general not equal to the potentials determined in [21, 25, 28, 29, 34]. To calculate the voltage drop across the disordered region, [21], [25], and

[34], following [28] and [29], treat the carrier densities classically.

To achieve a uniform voltage in a perfect lead, it is necessary to consider a lead that supports a number of channels which is large compared to $G/(e^2/h)$. In this case the amplitudes of the wave functions [Equation (53)] associated with the transmitted carriers are small. We can neglect the terms in Equation (51) proportional to μ_2 in the left perfect lead and can neglect the terms in Equation (51) proportional to μ_1 in the right perfect lead. Wide leads are needed if we want to construct a potential which smoothly joins the chemical potentials of the reservoirs.

6. Conclusions

The resistance formulae discussed in Sections 2–5 exhibit a certain beauty and elegance. Their agreement with the experimentally observed symmetries [27, 36] and their successful application [43–46, 49–50] makes one suspect that they will likely survive more realistic treatments of, for instance, the reservoirs. We have first derived expressions for quantum-mechanical coherent transmission. In physically relevant situations, we deal with coherent and incoherent transmission. Our expressions are also applicable in this case, and permit us to study the continuous transition from completely coherent to completely incoherent transmission [38, 39]. We have emphasized that resistances measured at contacts relate chemical potentials and currents. Furthermore, our discussion stresses that the measured resistance depends on the properties of the contacts, whether we deal with good contacts or with point contacts.

The discussion of the local electric potentials given in Section 5 seems much more susceptible to the detailed assumptions which we have made. Realistically, a reservoir feeds carriers into the conductor not in a continuous coherent fashion but with finite coherence length and with fluctuations in time. That has little effect on the total (time-averaged) current, and it is only currents which determine the resistances of Sections 2–5, but it is likely to alter the charge accumulated in some small spatial region. The detailed distribution of charge and voltage is, however, of interest and provides a physically appealing picture. We hope, therefore, that the problems exposed in Section 5 will stimulate further research in this direction.

Appendix A: Transmission probability expressions for the Casimir conductances

Reference [7] finds the following expressions for the conductances in Casimir's equation [(8), (9)] relating two currents in a four-pole conductor to the chemical potentials:

$$\alpha_{11} = (e^2/h)[(1 - R_{11})S - (T_{14} + T_{12})(T_{41} + T_{21})]/S, \quad \text{(A1)}$$

$$\alpha_{12} = (e^2/h)(T_{12}T_{34} - T_{14}T_{32})/S, \quad \text{(A2)}$$

$$\alpha_{21} = (e^2/h)(T_{21}T_{43} - T_{23}T_{41})/S, \quad \text{(A3)}$$

$$\alpha_{22} = (e^2/h)[(1 - R_{22})S - (T_{21} + T_{23})(T_{32} + T_{12})]/S, \quad \text{(A4)}$$

where

$$S = T_{12} + T_{14} + T_{32} + T_{34} = T_{21} + T_{41} + T_{23} + T_{43}. \quad \text{(A5)}$$

From Equation (5) it follows that the diagonal coefficients are symmetric in the flux, and the off-diagonal elements obey $\alpha_{12}(\Phi) = \alpha_{21}(-\Phi)$. The β conductances describing the situation where a current I_1 flows from terminal 1 to terminal 4 and a current I_2 flows from terminal 3 to terminal 2 are obtained by the substitution $3 \to 4$, $4 \to 2$, $2 \to 3$ in Equations (A1)–(A5). The γ conductances describing the situation where a current I_1 flows from terminal 1 to terminal 2 and a current I_2 flows from terminal 4 to terminal 3 are obtained by the substitution $3 \to 2$, $2 \to 4$, $4 \to 3$ in Equations (A1)–(A5).

Appendix B: Four-terminal interpretation of the conductance formulae of Azbel [25] and Büttiker et al. [21]

A four-terminal interpretation of the results of [21] and [25] is explicit in the work of Sivan and Imry [34]. Below we show that such an interpretation is compatible with the reciprocity theorem, Equation (1), in the absence of a magnetic field, but that it contradicts the reciprocity theorem, Equation (3), in the presence of a magnetic field. To this extent we picture, as in Figure 4, two contacts separated by a tunnel barrier from the perfect leads. We introduce the total transmission and reflection probabilities into channel i for carriers incident from the left,

$$R_i = \sum_{j=1}^{j=N} R_{21,ij}, \qquad T_i = \sum_{j=1}^{j=N} T_{21,ij}, \quad \text{(B1)}$$

and channel i for carriers incident from the right,

$$R_i' = \sum_{j=1}^{j=N} R_{12,ij}, \qquad T_i' = \sum_{j=1}^{j=N} T_{12,ij}. \quad \text{(B2)}$$

In these papers the measured voltage is determined by the piled-up densities. The density in channel i on the left is proportional to $v_i^{-1}T_i$ due to transmitted carriers from reservoir 1. It is now assumed that the piled-up densities determine the flow of current from the conductor to the measurement probe. The current from all of the N channels to reservoir 4 is taken to be proportional to

$$T_{41} = T_{14} = \epsilon \sum_{i=1}^{i=N} v_i^{-1}T_i, \quad \text{(B3)}$$

with a matrix element ϵ coupling *all* the channels of the conductor *equally* to those of the measurement lead. Note that in this discussion coupling of the conductor to the measurement leads is described by a single parameter ϵ. Similar considerations give

$$T_{32} = T_{23} = \epsilon \sum_{i=1}^{i=N} v_i^{-1}T_i', \quad \text{(B4)}$$

$$T_{31} = T_{13} = \epsilon \sum_{i=1}^{i=N} v_i^{-1}(1 + R_i), \quad \text{(B5)}$$

$$T_{42} = T_{24} = e \sum_{i=1}^{i=N} v_i^{-1}(1 + R_i'). \tag{B6}$$

Furthermore, $T_{34} = T_{43} = 0$ to order ϵ. To lowest order in ϵ, the transmission from reservoirs 1 to 2 is unaffected by the probes, $T = T_{21} = T_{12}$. T has the symmetry of the two-terminal transmission coefficient, Equation (16). Using these results in Equation (7) or Equation (8) yields

$$\mathcal{R}_{12,34} = \left(\frac{h}{e^2}\right)\frac{1}{T}\frac{\sum \frac{1}{v_i}(1 + R_i - T_i)}{2\sum \frac{1}{v_i}}. \tag{B7}$$

Equation (B7) is the main result of [21] and [25]. In the absence of a magnetic field, the transmission probabilities given above have the required reciprocity symmetry for the transmission probabilities associated with a four-terminal conductor. However, in the presence of a flux Φ, the transmission probabilities given above do not obey [Equation (5)], $T_{ij}(\Phi) = T_{ji}(-\Phi)$. From Equation (B3) we find

$$T_{41}(\Phi) - T_{14}(-\Phi) = e \sum_{i=1}^{i=N} v_i^{-1}[T_i(\Phi) - T_i(-\Phi)], \tag{B8}$$

which is in general not zero, since $T_i(\Phi) \neq T_i(-\Phi)$. As pointed out in Section 5, the results of Azbel [25] and Büttiker et al. [21] relate a spatially averaged local electric potential difference ΔU to a resistance, not a genuine chemical potential difference $\Delta\mu$. From this viewpoint it is not surprising that Equation (B8) is not symmetric under magnetic field reversal, as pointed out in [24]. The reciprocity symmetry (3) is a consequence of the relation between currents and chemical potentials, but says nothing about the relation of electric potentials and currents.

We conclude this appendix with an estimate of the magnetic field asymmetry [24] predicted by Equation (B7). We consider a piece of conductor of length l_ϕ (the phase-breaking length) and with an elastic scattering length l_e. The ensemble-averaged resistance is $\langle \mathcal{R}_\phi \rangle = \langle (h/e^2)T^{-1} \rangle = (h/e^2)(l_\phi/Nl_e)$, where N is the number of quantum channels. Using the argument of Lee [71] that the reflection coefficients fluctuate independently yields $\langle [\mathcal{R}_{12,34}(\Phi) - \mathcal{R}_{12,34}(-\Phi)]^2 \rangle \cong (h/e^2)^2(l_e/l_\phi)^2$. Since $l_e \ll l_\phi$, this is much smaller than the experimentally observed asymmetry [27, 41] which is of the order of $(h/e^2)^2\mathcal{R}_\phi^4$, independent of the separation of the voltage probes [41]. Equation (B7) predicts a small asymmetry because it is determined by spatially averaged voltages and because the physics of the contacts is neglected.

References and notes

1. G. F. C. Searle, "On Resistances with Current and Potential Terminals," *The Electrician* 66, 999–1002 (1911).
2. L. J. van der Pauw, "A Method of Measuring Specific Resistivity and Hall Effect of Discs of Arbitrary Shape," *Phillips Res. Repts.* 13, 1–9 (1958); four-probe measurements of the conductivity tensor in uniform conductors are discussed by J. D. Wasscher, "Note on Four-Point Resistivity Measurements on Anisotropic Conductors," *Phillips Res. Repts.* 16, 301–306 (1961).
3. L. Onsager, "Reciprocal Relations in Irreversible Processes. II.," *Phys. Rev. B* 38, 2265–2279 (1931).
4. H. B. G. Casimir, "On Onsager's Principle of Microscopic Reversibility," *Rev. Mod. Phys.* 17, 343–350 (1945).
5. R. Spal, "A New Method for Measuring the Magnetoconductivity Tensor of Anisotropic Crystals," *J. Appl. Phys.* 51, 4221–4225 (1980).
6. H. H. Sample, W. J. Bruno, S. B. Sample, and E. K. Sichel, "Reverse Field Reciprocity for Conducting Specimen in Magnetic Fields," *J. Appl. Phys.* 61, 1079–1084 (1987); E. K. Sichel, M. L. Knowles, and H. H. Sample, "Equipotential Distribution in the Quantum Hall Effect in GaAS–AlGaAs Heterostructures," *J. Phys. C: Solid State Phys.* 19, 5695–5713 (1986).
7. M. Büttiker, "Four-Terminal Phase Coherent Conductance," *Phys. Rev. Lett.* 57, 1761–1764 (1986).
8. M. Büttiker, "Quantum Oscillations in Normal Metal Loops," *Superconducting Quantum Interference Devices and Their Applications (SQUID'85)*, H. D. Hahlbohm and H. Lübbig, Eds., Walter de Gruyter, Berlin, 1985, pp. 429–560.
9. R. A. Webb, S. Washburn, C. P. Umbach, and R. B. Laibowitz, "In Search of Magnetic Flux Quantization in Normal Metal Rings," *Superconducting Quantum Interference Devices and Their Applications (SQUID'85)*, H. D. Hahlbohm and H. Lübbig, Eds., Walter de Gruyter, Berlin, 1985, pp. 561–584.
10. M. Büttiker, "Flux-Sensitive Effects in Normal Metal Loops," *New Techniques and Ideas in Quantum Measurement Theory*, D. M. Greenberger, Ed., *Ann. N.Y. Acad. Sci.* 480, 194–209 (1986).
11. Y. Imry, "Physics of Mesoscopic Systems," *Directions in Condensed Matter Physics*, G. Grinstein and G. Mazenko, Eds., World Scientific Press, Singapore, 1986, pp. 101–163.
12. S. Washburn and R. A. Webb, "Aharonov–Bohm Effect in Normal Metal Quantum Coherence and Transport," *Adv. Phys.* 35, 375–422 (1986).
13. P. A. Lee, A. D. Stone, and H. Fukuyama, "Universal Conductance Fluctuations in Metals: Effects of Finite Temperature, Interactions, and Magnetic Field," *Phys. Rev. B* 35, 1039–1070 (1987).
14. B. L. Al'tshuler and B. I. Shklovskii, "Repulsion of Energy Levels and Conductivity of Small Metal Samples," *Sov. Phys. JETP* 64, 127–135 (1986); B. L. Al'tshuler, V. E. Kravtsov, and I. V. Lerner, "Statistics of Mesoscopic System Fluctuations and Instability of One-Parameter Scaling," *Zh. Eksp. Teor. Fiz.* 91, 2276–2301 (1986) [*Sov. Phys. JETP* 64, 1352–1366 (1986)].
15. A. G. Aronov and Yu. V. Sharvin, "Magnetic Flux Effects in Disordered Conductors," *Rev. Mod. Phys.* 59, 755–779 (1987).
16. R. Landauer, "Transport in Open and Closed Systems," *Z. Phys. B* 68, 217–228 (1987).
17. C. P. Umbach, S. Washburn, R. B. Laibowitz, and R. A. Webb, "Magnetoresistance of Small, Quasi-One-Dimensional, Normal Metal Rings and Lines," *Phys. Rev. B* 30, 4048–4051 (1984).
18. M. Büttiker, Y. Imry, and R. Landauer, "Josephson Behavior in Small Normal One-Dimensional Rings," *Phys. Lett.* 96A, 365–367 (1983).
19. Y. Gefen, Y. Imry, and M. Ya. Azbel, "Quantum Oscillations and the Aharonov–Bohm Effect for Parallel Resistors," *Phys. Rev. Lett.* 52, 129–132 (1984).
20. M. Büttiker, Y. Imry, and M. Ya. Azbel, "Quantum Oscillations in One-Dimensional Normal Metal Rings," *Phys. Rev. A* 30, 1982–1989 (1984).
21. M. Büttiker, Y. Imry, R. Landauer, and S. Pinhas, "Generalized Many Channel Conductance Formula with Application to Small Rings," *Phys. Rev. B* 31, 6207–6215 (1985).
22. R. A. Webb, S. Washburn, C. Umbach, and R. A. Laibowitz, "Observation of h/e Aharonov–Bohm Oscillations in Normal-Metal Rings," *Phys. Rev. Lett.* 54, 2696–2699 (1985).
23. V. Chandrasekhar, M. J. Rooks, S. Wind, and D. E. Prober, "Observation of Aharonov–Bohm Electron Interference Effects with Period h/e and $h/2e$ in Individual Micron-Size, Normal-Metal Rings," *Phys. Rev. Lett.* 55, 1610–1613 (1985); S. Datta,

M. R. Melloch, S. Bandyopadhyay, R. Noren, M. Vaziri, M. Miller, and R. Reifenberger, "Novel Interference Effects Between Parallel Quantum Wells," *Phys. Rev. Lett.* **55**, 2344–2347 (1985).
24. M. Büttiker and Y. Imry, "Magnetic Field Asymmetry in the Multi-Channel Landauer Formula," *J. Phys. C* **18**, L467–L472 (1985).
25. M. Ya. Azbel, "Quantum *d*-Dimensional Landauer Formula," *J. Phys. C* **14**, L225–L472 (1981).
26. B. L. Al'tshuler and B. Z. Spivak, "Variation of the Random Potential and the Conductivity of Samples of Small Dimensions," *JETP Lett.* **42**, 447–450 (1985).
27. A. D. Benoit, S. Washburn, P. Umbach, R. B. Laibowitz, and R. A. Webb, "Asymmetry in the Magnetoconductance of Metal Wires and Loops," *Phys. Rev. Lett.* **57**, 1765–1768 (1986).
28. R. Landauer, "Spatial Variation of Currents and Fields Due to Localized Scatterers in Metallic Conduction," *IBM J. Res. Develop.* **1**, 223–231 (1957); R. Landauer, "Electrical Resistance of Disordered One-Dimensional Lattices," *Phil. Mag.* **21**, 863–867 (1970).
29. R. Landauer, "Transport as a Consequence of the Incident Carrier Flux," *Localization, Interaction, and Transport Phenomena*, G. Bergmann and Y. Bruynseraede, Eds., Springer-Verlag, Heidelberg, 1985, pp. 38–50.
30. P. W. Anderson, D. J. Thouless, E. Abrahams, and D. S. Fisher, "New Method for Scaling Theory of Localization," *Phys. Rev. B* **22**, 3519–3526 (1980).
31. D. C. Langreth and E. Abrahams, "Derivation of the Landauer Conductance Formula," *Phys. Rev. B* **24**, 2978–2984 (1981).
32. H.-L. Engquist and P. W. Anderson, "Definition and Measurement of the Electrical and Thermal Resistance," *Phys. Rev. B* **24**, 1151–1154 (1981).
33. D. S. Fisher and P. A. Lee, "Relation Between Conductivity and Transmission Matrix," *Phys. Rev. B* **23**, 6851–6854 (1981).
34. U. Sivan and Y. Imry, "Multichannel Landauer Formula for Thermoelectric Transport with Application to Thermopower Near the Mobility Edge," *Phys. Rev. B* **33**, 551–558 (1986).
35. O. Entin-Wohlman, C. Hartzstein, and Y. Imry, "Quantum Oscillations in the Magnetotransport of a Finite Two Dimensional Anderson Model," *Phys. Rev. B* **34**, 921–926 (1986).
36. L. L. Soethout, H. van Kempen, J. T. P. W. van der Maarseveen, P. A. Schroeder, and P. Wyder, "Current Voltage Reciprocity in the Magnetoresistance of Simple Metals," *J. Phys. F: Met. Phys.* **17**, L129–L134 (1987).
37. M. Büttiker, "Small Normal Loop Coupled to an Electron Reservoir," *Phys. Rev. B* **32**, 1846–1849 (1985).
38. M. Büttiker, "Role of Quantum Coherence in Series Resistors," *Phys. Rev. B* **33**, 3020–3026 (1986).
39. M. Büttiker, "Coherent and Sequential Tunneling in Series Barriers," *IBM J. Res. Develop.* **32**, 63–75 (1988).
40. M. Büttiker, "Voltage Fluctuations in Small Conductors," *Phys. Rev. B* **35**, 4123–4126 (1987).
41. A. D. Benoit, C. P. Umbach, R. B. Laibowitz, and R. A. Webb, "Length-Independent Voltage Fluctuations in Small Devices," *Phys. Rev. Lett.* **58**, 2343–2346 (1987).
42. W. J. Skocpol, P. M. Mankiewich, R. E. Howard, L. D. Jackel, D. M. Tennant, and A. D. Stone, "Non-Local Potential Measurements of Quantum Conductors," *Phys. Rev. Lett.* **58**, 2347–2350 (1987).
43. S. Maekawa, Y. Isawa, and H. Ebisawa, "Conductance Fluctuations in Small Metallic Samples," *J. Phys. Soc. Jpn.* **56**, 25–28 (1987).
44. C. L. Kane, R. A. Serota, and P. A. Lee, "Long Range Correlations in Disordered Metals," submitted to *Phys. Rev.*; manuscript available from C. L. Kane, Department of Physics, Massachusetts Institute of Technology, Cambridge, MA 02139.
45. C. L. Kane, P. A. Lee, and D. DiVincenzo, "Voltage Fluctuations in Multilead Devices," submitted to *Phys. Rev.*; manuscript available from C. L. Kane, Department of Physics, Massachusetts Institute of Technology, Cambridge, MA 02139.
46. S. Hershfield and V. Ambegaokar, "Resistance Fluctuations in a Four Probe Geometry with Infinite Leads," unpublished manuscript; available from S. Hershfield, LASSP, Cornell University, Ithaca, NY 14853.
47. P. A. Lee and D. S. Fisher, "Anderson Localization in Two Dimensions," *Phys. Rev. Lett.* **47**, 882–885 (1981).
48. A. D. Stone, "Magnetoresistance Fluctuations in Mesoscopic Rings and Wires," *Phys. Rev. Lett.* **54**, 2692–2695 (1985).
49. H. U. Baranger, A. D. Stone, and D. P. DiVincenzo, "Resistance Fluctuations in Multiprobe Microstructures: Length Dependence and Non-Locality," preprint; available from D. DiVincenzo, IBM Thomas J. Watson Research Center, P.O. Box 218, Yorktown Heights, NY 10598.
50. H. U. Baranger, D. P. DiVincenzo, and D. Stone, "Resistance Correlations in Multiprobe Microstructures," preprint; available from D. P. DiVincenzo, IBM Thomas J. Watson Research Center, P.O. Box 218, Yorktown Heights, NY 10598.
51. S. Strikhman and H. Thomas, "Remarks on Linear Magneto-Resistance and Magneto-Heat Conductivity," *Solid State Commun.* **3**, 147–150 (1965).
52. G. Timp, A. M. Chang, P. Mankiewich, R. Behringer, J. E. Cunningham, T. Y. Chang, and R. E. Howard, "Quantum Transport in an Electron-Wave Guide," *Phys. Rev. Lett.* **59**, 732–735 (1987).
53. B. L. Al'tshuler, "Fluctuations in the Extrinsic Conductivity of Disordered Conductors," *JETP Lett.* **41**, 648–651 (1985).
54. P. A. Lee and A. D. Stone, "Universal Fluctuations in Metals," *Phys. Rev. Lett.* **55**, 1622–1625 (1985).
55. Y. Imry, "Active Transmission Channels and Universal Conductance Fluctuations," *Europhys. Lett.* **1**, 249–256 (1986); J. P. Carton, J. L. Pichard, and N. Zanon, "Many-Channel Conductance of *d*-Dimensional Pure and Randomly Layered Materials," *J. Phys. C* **19**, 4041–4054 (1986).
56. F. P. Milliken, S. Washburn, C. P. Umbach, R. B. Laibowitz, and R. A. Webb, "Effect of Partial Phase Coherence on the Amplitude of the Aharonov–Bohm Oscillations in Metal Loops," *Phys. Rev. B* **36**, 4465–4468 (1987).
57. R. Landauer, "Spatial Variation of Currents and Fields Due to Localized Scatterers in Metallic Conduction," *IBM J. Res. Develop.* **32**, 306–316 (1988, this issue).
58. C. P. Umbach, P. Santhanam, C. Van Hasendonck, and R. A. Webb, "Nonlocal Electrical Properties in Mesoscopic Devices," *Appl. Phys. Lett.* **50**, 1289–1291 (1978).
59. R. Landauer and M. Büttiker, "Resistance of Small Metallic Loops," *Phys. Rev. Lett.* **54**, 2049–2052 (1985).
60. I. O. Kulik, "Flux Quantization in a Normal Metal," *JETP Lett.* **19**, 275–277 (1970); M. Büttiker and T. M. Klapwijk, "Flux Sensitivity of a Piecewise Normal and Superconducting Metal Loop," *Phys. Rev. B* **33**, 5114–5117 (1986); R. Landauer, "Zener Tunneling and Dissipation in Metallic Loops," *Phys. Rev. B* **33**, 6497–6499 (1986); R. Landauer, "Resistance of Metallic Loops," *Phys. Rev. Lett.* **58**, 2150 (1987); Y. Gefen and D. Thouless, "Zener Transitions and Energy Dissipation in Small Driven Systems," *Phys. Rev. Lett.* **59**, 1752–1755 (1987); G. Blatter and D. A. Browne, "Zener Tunneling and Localization in Small Conducting Rings," unpublished manuscript; available from G. Blatter, Brown Boveri Research Center, CH-5405 Baden, Switzerland; H. Cheung, Y. Gefen, and E. K. Riedel, "Isolated Rings of Mesoscopic Dimensions. Quantum Coherence and Persistent Currents," *IBM J. Res. Develop.* **32**, 359–371 (1988, this issue); a few historical references on persistent currents are given in M. Büttiker, *Phys. Scripta* **T14**, 82–88 (1986).
61. A. G. Aronov, A. Yu. Zyuzin, and B. Z. Spivak, "Low-Temperature Spatial Fluctuations of the Current in Disordered Conductors," *Pis'ma Zh. Teor. Fiz.* **43**, 431 (1986) [*JETP Lett.* **43**, 555–558 (1986)].
62. R. Landauer, "Residual Resistivity Dipoles," *Z. Phys. B* **21**, 247–254 (1975).
63. R. Landauer, "Nonlinearity: Historical and Technological View," *Nonlinearity in Condensed Matter*, A. R. Bishop, D. K. Campbell, P. Kumaravid, and S. E. Trullinger, Eds., Springer-Verlag, Heidelberg, 1987, pp. 2–22.
64. A. I. Larkin and D. E. Khmelnitskii, "Mesoscopic Fluctuations of Current–Voltage Characteristics," *Sov. Phys. JETP* **64**, 1075–

1077 (1987).
65. D. R. Yennie, "Integral Quantum Hall Effect for Nonspecialists," *Rev. Mod. Phys.* **59**, 781–824 (1987).
66. N. D. Lang, "The Resistance of a One-Atom Contact in the Scanning Tunneling Microscope," *Phys. Rev. B* **36**, 8173–8176 (1987).
67. M. Büttiker, in *Superconducting Quantum Interference Devices and Their Applications (SQUID'85)*, H. D. Hahlbohm and H. Lübbig, Eds., Walter de Gruyter, Berlin, 1985, p. 550.
68. P. Muralt, D. W. Pohl, and W. Denk, "Wide-Range, Low-Operating-Voltage, Bimorph STM: Application as Potentiometer," *IBM J. Res. Develop.* **30**, 443–450 (1986).
69. S. Washburn, H. Schmid, D. Kern, and R. A. Webb, "Normal-Metal Aharonov–Bohm Effect in the Presence of a Transverse Electric Field," *Phys. Rev. Lett.* **59**, 1791–1794 (1987).
70. K. Hepp, "Quantum Theory of Measurement and Macroscopic Observables," *Helv. Phys. Acta* **45**, 237–248 (1972).
71. P. A. Lee, "Universal Conductance Fluctuations in Disordered Metals," *Statphys.* **16**, H. Stanley, Ed., North-Holland Publishing Co., Amsterdam, 1986, pp. 169–174.

Received November 16, 1987; accepted for publication December 8, 1987

Markus Büttiker *IBM Thomas J. Watson Research Center, P.O. Box 218, Yorktown Heights, New York 10598.* Dr. Büttiker is a research staff member of the Physical Sciences Department at the Thomas J. Watson Research Center. He received a diploma in theoretical physics from the Federal Institute of Technology in Zurich, Switzerland, in 1974, and a Ph.D. from the University of Basel, Switzerland, in 1978. He joined IBM at the Thomas J. Watson Research Center in 1979. Dr. Büttiker's research interests include such diverse fields as instabilities in far-from-equilibrium systems, the statistical mechanics of solitons, noise-activated transport and nucleation phenomena, and charging effects in small tunnel junctions. In addition, Dr. Büttiker has been concerned with the time scales of quantum tunneling events. Recent work includes the prediction of quantum interference phenomena in small normal conductors. For this work Dr. Büttiker has received an Outstanding Technical Achievement Award.

Coherent and sequential tunneling in series barriers

by M. Büttiker

A simple approach which can describe both coherent tunneling and sequential tunneling is applied to resonant tunneling through a double-barrier structure. This approach models phase-randomizing events by connecting to the conductor a side branch leading away from the conductor to a reservoir. The reservoir does not draw or supply a net current, but permits inelastic events and phase randomization. A conductance formula is obtained which contains contributions due to both coherent and sequential tunneling. We discuss the limiting regimes of completely coherent tunneling and completely incoherent transmission, and discuss the continuous transition between the two. Over a wide range of inelastic scattering times tunneling is sequential. The effect of inelastic events on the peak-to-valley ratio and the density of states in the resonant well is investigated. We also present an analytic discussion of the maximum peak conductance e/h of an isolated resonance in a many-channel conductor.

1. Introduction

As is well known, the scattering of waves or carriers at a target which permits inelastic events in addition to elastic scattering exhibits a cross section consisting of two contributions: an elastic, coherent part and an inelastic, incoherent part [1, 2]. If for the purpose of calculating the conductance we view the conductor (or a device) as a target at which carriers are either reflected or permitted to traverse, we can similarly expect that the conductance also exhibits two contributions: a coherent contribution which arises from carriers traversing the sample suffering only elastic events, and an incoherent contribution due to carriers which suffered inelastic events while traversing the sample. Carriers which are scattered elastically emerge with a phase which has a definite relationship to the phase of the incident carriers. Carriers which are scattered inelastically emerge from the sample with a phase which is unrelated to that of the incident carriers. A discussion of conductance which views the sample as a target has long been advocated by Landauer [3, 4]. The incident currents are specified and the net current and the piled-up charges are obtained from the wavefunctions [3, 4]. This approach is typically restricted to the case of elastic scattering (coherent tunneling) only. Recently we have expanded this approach and have found an expression for the conductance which allows for both coherent and incoherent scattering processes [5]. The total transmission probability for a carrier to traverse the sample is

$$T_{tot} = T_c + T_i, \tag{1}$$

where T_c is the probability for a carrier to traverse the sample coherently and T_i is the transmission probability for carriers which have suffered an inelastic event. The coherent transmission probability cannot be calculated as if there were no inelastic events in the sample, since it is also affected by

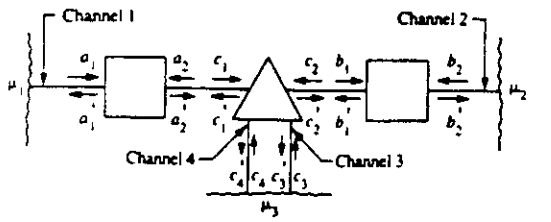

Double barrier (rectangles) with an inelastic scatterer in the well, modeled by an extra branch leading away from the conductor and connected to an extra reservoir 3. Reservoirs 1 and 2 serve as source and sink of carriers and energy. Reservoir 3 draws no net current but permits inelastic phase-randomizing events. A carrier which traverses the double barrier from reservoir 1 to reservoir 2 without entering reservoir 3 is said to tunnel coherently. A carrier which progresses from reservoir 1 to reservoir 2 via reservoir 3 is said to tunnel sequentially.

the presence of these processes. For the case of a single inelastic scatterer located in the sample, the incoherent transmission probability in Equation (1) is of the form [5]

$$T_i = \frac{S_b S_f}{S_b + S_f} \tag{2}$$

S_b is the transmission probability for a carrier emerging from the inelastic scatterer to traverse the sample backward against the direction of carrier flow. S_f is the transmission probability for a carrier emerging from the inelastic scatterer to traverse the sample forward in the direction of current flow. Equation (2) can be understood in the following way [4]: Only a fraction $S_f/(S_f + S_b)$ of the carriers reaching the inelastic scatterer will leave the sample in the forward direction. The probability for carriers incident on the sample to reach the inelastic scatterer is S_b, and the probability for incoherent transmission is thus S_b multiplied by the factor we have just discussed. A mathematical derivation of Equation (2) is given in [5] and in Appendix A of this paper.

It is the purpose of this paper to apply Equations (1) and (2) to a sequence of two barriers with a resonant well between them [6]. Resonant tunneling is of interest in double-barrier diodes [7–15], in tunneling through a barrier with impurity states [16–17], in strongly localized conductors [18–20], and also in scanning tunneling microscopy, where a localized state can be provided by a protruding adatom [21]. In particular we investigate the effect of inelastic events on tunneling. A carrier which traverses one of the barriers coherently but is scattered inelastically in the well and loses phase memory before eventually escaping from the well is said to tunnel sequentially [10]. A recent discussion of sequential tunneling which does not include a phase-randomizing agent found that coherent resonant tunneling and sequential tunneling lead to equivalent results for the current [14]. The analysis presented here does not support this conclusion. Coherent tunneling is contained in the first term of Equation (1), and sequential tunneling is given by the second term of Equation (1). Inelastic events which are needed to destroy phase coherence lead to a broadening and decrease of the resonant transmission [1, 2, 19] and, equivalently, to broadening of the density of states in the well. The decrease of the peak transmission with increasing inelastic scattering is accompanied by an increase of the off-resonant transmission. As a consequence the peak-to-valley ratio of the total transmission probability decreases with an increasing number of sequential processes.

To model inelastic events we use the approach of [5]. Consider Figure 1, which shows two barriers (indicated by squares) connected by pieces of perfect conductor (solid lines). The conductor is via a junction (the triangle in Figure 1) connected to a side branch. For simplicity the perfect conductors (denoted as channel 1 and channel 2 in Figure 1) are assumed to be one-dimensional, with two states only at the Fermi energy. The side branch, however, consists of two quantum channels (channels 3 and 4) and is, in turn, connected to a reservoir at a chemical potential μ_3. Reservoir 1, at a chemical potential μ_1, plays the role of a carrier source, and reservoir 2, at a chemical potential μ_2, acts as a sink. Reservoir 3, in contrast, draws or delivers no net current. The condition of zero net current in the side branch leading away from the conductor determines the chemical potential μ_3 as a function of μ_1 and μ_2 [see Equation (A11)]. Each of the reservoirs has the property that it absorbs carriers incident from the conductor, regardless of the energy and the phase of the carriers. Furthermore, each reservoir emits carriers into the adjacent conductor up to its chemical potential. These rules, therefore, specify the currents incident into the conductor [3, 4]. The triangle in Figure 1 represents a quantum-mechanical junction between the side branch and the conductor. A specific example is discussed and solved in Appendix B.

A carrier scattered from the conductor into the side branch propagates to reservoir 3, where the carrier suffers inelastic events. Eventually, to maintain zero net current, reservoir 3 emits a carrier toward the junction, where the carrier is either reflected back to the reservoir or is scattered into the conductor. S_f introduced in Equation (2) is the total probability for a carrier emitted by reservoir 3 to traverse into reservoir 2. Similarly, S_b is the total probability for a carrier emitted by reservoir 3 to end up in reservoir 1. Therefore, the carriers which traverse the sample sequentially are those that are scattered into reservoir 3 and re-emitted by reservoir 3. The junction (triangle) also allows for carriers incident in the conductor to be scattered not into

the side branch but again into the conductor. Therefore, a fraction of the carriers can traverse the sample from reservoir 1 to reservoir 2 without visiting reservoir 3, and these are the carriers which traverse the sample coherently.

Let us introduce the probability ϵ for a carrier approaching the junction to be scattered into the side branch (channels 3 and 4). For $\epsilon = 0$ the conductor and the side branch are completely disconnected. For $\epsilon = 1$ every carrier incident from the conductor on the junction is transferred into the side branch and reaches reservoir 3. Thus $\epsilon = 0$ is the case of completely coherent transmission, and $\epsilon = 1$ is the case of completely incoherent transmission. If ϵ differs from these limiting values, we have both coherent transmission and sequential transmission. Thus the parameter ϵ determines the amount of inelastic scattering. The approach discussed here and in [5] allows the study of the continuous transition from completely coherent to completely incoherent transmission. To achieve *complete* phase randomization, carriers need to be scattered with probability 1 into reservoir 3. If the junction is required to be symmetric with respect to right- and left-moving carriers, probability 1 can only be obtained if the side branch contains two channels. If the side branch contains only one channel and is symmetric with respect to right- and left-moving carriers, the maximum probability [5] which can be achieved for scattering into reservoir 3 is 1/2.

The method of introducing inelastic scattering or sequential processes described above is not limited to a single side branch. Conductors connected to many side branches are of interest as well [5, 22]. Another system is obtained if we eliminate two of the reservoirs in Figure 1 by forming the conductor into a loop. A normal loop, driven by a magnetic flux and with a single side branch to model the effect of inelastic events on coherent superconducting-like phenomena [23], is the subject of [24]. Another interesting feature of the approach proposed here is the following: The conductor shown in Figure 1 is a three-terminal device. Reservoir 1 can serve as a current source and reservoir 3 as a current sink. This situation bears a close resemblance to the experiment of Morkoç et al. [25], where current was drawn directly from the "well." As in the experiment [25], our approach also yields a resonant conductance in this case, even though a net current flows only through one barrier.

Below, we emphasize the two-terminal conductance [26] $\mathcal{G} = \mathcal{R}^{-1} = (e^2/h)T_{res}$ considering channels 1 and 2 as the conductor. Thus we are not directly addressing the negative differential conductance phenomena which were first discussed by Tsu and Esaki [7] and which have generated much interest lately [8–15, 25]. Instead, we assume that we can control the Fermi energy and that it is the dependence of the conductance on the Fermi energy which matters. This paper is also limited to the case where kT is small compared to the width of the resonance (see, however, Appendix A). Most of the calculations leading to the results presented below are relegated to four appendices. We focus on one-dimensional conductors, except in Appendix C, where we discuss the peak conductance due to an isolated resonant state in a many-channel conductor.

2. Completely coherent versus completely incoherent transmission

In this section we discuss the extreme limits in which one of the terms in Equation (1) vanishes. In the completely coherent limit $T_i = 0$, the coherent transmission probability through two barriers in series exhibits resonances near the energies of the quasi-eigenstates of the well,

$$T_c = T_{res} \frac{\frac{1}{4}\Gamma_e^2}{(E - E_r)^2 + \frac{1}{4}\Gamma_e^2}, \tag{3}$$

with a peak value at resonance

$$T_{res} = \frac{4T_1T_2}{(T_1 + T_2)^2}. \tag{4}$$

The peak value is 1 if the transmission probabilities of the two barriers are equal, and is smaller than 1 and given by $T_{res} \approx 4T_1/T_2$ in the case that $T_1 \ll T_2$. In Equation (3),

$$\Gamma_e = \Gamma_1 + \Gamma_2 \tag{5}$$

is the total elastic width; Γ_1 and Γ_2 are the partial elastic widths of the resonant level. $1/\tau_e = \Gamma_e/\hbar$ is the decay rate of the resonant state. The transmission through a double-barrier structure is analyzed in Appendix B. This calculation, which invokes some simplifying assumptions not relevant for our subsequent discussion, yields for the partial elastic widths the WKB expressions

$$\Gamma_1 = \hbar\nu T_1, \qquad \Gamma_2 = \hbar\nu T_2. \tag{6}$$

Here ν is an attempt frequency, and in the case of a square well is given by $\nu = 2v/v$, where w is the width of the well and v is the velocity of a carrier in the well at the resonant energy E_r. At energies E away from E_r, transmission is still coherent but typically many orders of magnitude smaller than T_{res}, and, approximately,

$$T_c = T_{off} \approx \tfrac{1}{4}T_1T_2. \tag{7}$$

Therefore, the peak-to-valley ratio T_{res}/T_{off} is exponentially large if the transmission probabilities are exponentially small. Such huge peak-to-valley ratios have not been observed experimentally; inelastic scattering, discussed below, is one reason for this discrepancy. But there are other reasons also, e.g., the averaging over an energy range due to a three-dimensional incident distribution [10], deviations from an ideal planar structure, and elastic scattering due to impurities [15].

Let us now turn away from the limit of completely coherent transmission and consider the limit of completely

incoherent transmission, i.e., $T_c = 0$. In this case *every* carrier reaching the inelastic scatterer loses phase. In this limit a carrier cannot travel from one side of the resonant well to the other without being scattered inelastically. This process is a special limit of the sequential tunneling process and is labeled *completely incoherent*. In general, a sequential tunneling process permits many oscillations in the well with frequency ν before the carrier loses phase memory. We invoke a scatterer (triangle in Figure 1) which re-emits carriers with equal probability to the left and right into the conductor. In the limit of complete phase randomization, the probability of a carrier emerging from the inelastic scatterer to traverse the sample backward is given by $S_b = T_1$, and similarly the probability of a carrier being scattered in the forward direction is $S_f = T_2$. Therefore, in the completely incoherent limit Equation (2) yields [5]

$$T_{tot} = T_i = \frac{T_1 T_2}{T_1 + T_2} = \left[\frac{1}{T_1} + \frac{1}{T_2}\right]^{-1}. \tag{8}$$

A single barrier with transmission probability T_j in an otherwise perfect wire gives rise to a two-terminal resistance $\mathcal{R}_j = (h/e^2)T_j^{-1}$. Therefore, Equation (8), using $\mathcal{R} = (h/e^2)T_{tot}^{-1} = (h/e^2)T_i^{-1}$, yields the series addition of resistors, $\mathcal{R} = \mathcal{R}_1 + \mathcal{R}_2$. If inelastic scattering is so strong that every carrier loses phase memory while traversing the well, the resistance of the structure contains no detailed information about the geometrical arrangements of the scatterers (separation of the barriers) but is the sum of the resistances due to the individual scatterers. Note that the transmission in the incoherent limit, Equation (8), is not the same as the off-resonant coherent transmission, Equation (8). If the transmission probabilities are small, the completely incoherent transmission probability, Equation (8), far exceeds the off-resonant coherent transmission probability, Equation (7). On the other hand, the transmission at resonance T_m, Equation (3), exceeds the purely sequential transmission probability, Equation (8). It is now clear what happens when we start from a situation where only coherent processes are allowed and introduce inelastic events. Both the transmission at resonance [peak value, Equation (4)] and the off-resonance transmission [minimum value, Equation (7)] must, with increasing inelastic scattering, eventually approach the completely incoherent limit, Equation (8). Therefore, the peak value must in general decrease with an increasing amount of inelastic scattering, and the off-resonant transmission must in general increase with increasing inelastic scattering.

The transition from the completely coherent limit to the completely incoherent limit occurs through the sequential tunneling regime in which carriers can execute many oscillations in the well before losing phase memory. The distinction of three regimes, the *coherent* limit, the *sequential* tunneling regime, and the *completely incoherent* limit, is made because resonant tunneling has two frequency scales [27] which, when compared with the inelastic scattering rate $\Gamma_i/\hbar$, yield three physically distinct regimes: The time scales [2] associated with a resonance are the elastic decay rate $\Gamma_e/\hbar$ given by Equations (5) and (6) and the attempt frequency $\nu = v/2w$. We show that for $\Gamma_i \ll \Gamma_e$ we are in a regime where the main part of the current is carried by coherent processes, in the regime $\Gamma_e \ll \Gamma_i \ll h\nu$ current is carried by sequential tunneling processes, and if $h\nu \ll \Gamma_i$ we are in the completely incoherent limit. Below we discuss this in more detail.

3. Crossover from coherent to sequential transmission

To study the crossover from coherent resonant tunneling to coherent sequential tunneling it is possible to apply the formulae of Breit and Wigner [1, 2]. The applicability of these formulae to tunneling through disordered conductors in the presence of inelastic scattering is mentioned by Azbel et al. [18]. However, the results presented in [18] are not compatible with the Breit and Wigner approach. Subsequently results compatible with the Breit and Wigner formulae were obtained for a symmetrical double barrier by Stone and Lee [19]. They used an imaginary (optical) potential to describe inelastic scattering. This does not allow the determination of the forward and backward scattering probabilities. Reference [19] makes the plausible assumption (for a symmetric barrier) that $S_b = S_f = S$, and consequently $T_i = S/2$. The approach of [5] introduced in Section 1 allows us to determine the forward and backward scattering rates S_b and S_f. These probabilities are also determined by the Breit and Wigner formulae, which are mentioned in textbooks [2] but seem to have found little attention in solid-state physics. A discussion of these formulae is presented in Appendix C.

The key point of Breit and Wigner [1, 2] is the notion that if there is elastic resonant transmission from channel 1 to channel 2,

$$T_e = T_{21} = \frac{\Gamma_1 \Gamma_2}{(E - E_r)^2 + \frac{1}{4}\Gamma^2}, \tag{9}$$

then the weakly coupled inelastic channels (channels 3 and 4 in Figure 1) are also characterized by resonant transmission and couple to the elastic transmission with partial widths Γ_3 and Γ_4. The backward scattering probability becomes

$$S_b = \frac{\Gamma_1 \Gamma_i}{(E - E_r)^2 + \frac{1}{4}\Gamma^2}, \tag{10}$$

and the forward scattering probability becomes

$$S_f = \frac{\Gamma_2 \Gamma_i}{(E - E_r)^2 + \frac{1}{4}\Gamma^2}, \tag{11}$$

where $\Gamma_i = \Gamma_3 + \Gamma_4$ is the total inelastic width. According to Breit and Wigner, the width Γ in Equations (9)–(11) is the sum of all the partial rates,

$$\Gamma = \sum_{j=1}^{j=4} \Gamma_j = \Gamma_e + \Gamma_i. \tag{12}$$

Γ_1 and Γ_2 are specified by Equation (6). For the model studied in Appendix B, the inelastic widths are

$$\Gamma_3 = \Gamma_4 = \hbar\nu\epsilon. \tag{13}$$

Here ϵ is the probability for a carrier in the conductor, approaching the junction, to be scattered into the side branch [see Figure 1 and Equation (B8)]. By using Equations (10), (11), and (2), we find for the sequential transmission probability

$$T_i = T_{res} \frac{\frac{1}{4}\Gamma_e\Gamma_i}{(E - E_r)^2 + \frac{1}{4}\Gamma^2}. \tag{14}$$

Here we have used the fact that $T_{res} = 4\Gamma_1\Gamma_2/\Gamma_e^2$. The total transmission probability near a resonance is thus

$$T_{tot} = T_{res} \frac{\frac{1}{4}\Gamma_e\Gamma}{(E - E_r)^2 + \frac{1}{4}\Gamma^2}. \tag{15}$$

Therefore, the peak value of the total transmission probability at resonance is $T_{res}\Gamma_e/\Gamma$. Thus the inclusion of inelastic or sequential events leads to a decrease of the peak value and broadens the resonance. It is interesting to compare the fraction of the current carried by the carriers traversing the structure coherently, $T_c/T_{tot} = \Gamma_e/\Gamma$, with the fraction of the current carried by the carriers traversing the sample sequentially, $T_i/T_{tot} = \Gamma_i/\Gamma$. To evaluate these fractions we have used Equations (1), (2), (9), and (10). We see that if the total elastic width and the total inelastic width are equal, the currents due to coherent tunneling and due to sequential tunneling are equal. The smaller the elastic width, the smaller is the amount of inelastic scattering [19] needed to make the sequential tunneling current dominant.

In the crossover region $\Gamma_e \simeq \Gamma_i$ we have not only a decrease of the peak value of the transmission with inelastic scattering, but also an increase of the off-resonance transmission probability. The model calculation in Appendix B yields an off-resonance (minimal) transmission probability

$$T_{tot,off} \propto \frac{1}{4}\frac{\Gamma}{\Gamma_e} T_1 T_2. \tag{16}$$

Using Equations (15) and (16) yields a peak-to-valley ratio of the order

$$\frac{T_{tot,res}}{T_{tot,off}} \propto \left(\frac{\Gamma_e}{\Gamma}\right)^2 \frac{1}{(T_1 + T_2)^2} \approx \frac{(\hbar\nu)^2}{\Gamma^2}, \tag{17}$$

where we have used Equation (5). Thus the peak-to-valley ratio of the transmission probability decreases rapidly as sequential tunneling processes become important.

We mention here an additional result which is derived in Appendix D. The density of states in the resonant well also depends on the degree of sequential tunneling. For the density of states in the well we find in the crossover region

$$\left[\frac{dN}{dE}\right] = \frac{1}{\pi} \frac{\frac{1}{2}\Gamma}{(E - E_r)^2 + \frac{1}{4}\Gamma^2}. \tag{18}$$

Note that the density of states in the well is determined by the total width Γ, Equation (12). Thus, as the number of sequential tunneling processes increases, the density of states in the well becomes less sharply peaked at the resonant energy and broadens. Reference [14], in attempting to show that resonant tunneling and sequential tunneling are equivalent, uses a density of states which is independent of the degree of inelastic scattering.

The Breit and Wigner formalism can only handle the crossover from the coherent to the sequential tunneling regime. If the inelastic scattering rate exceeds the elastic width by orders of magnitude, one must go beyond this formalism.

4. Coherence corrections of the completely incoherent transmission

In the limit in which every carrier traversing the well is scattered inelastically, the coherent transmission probability T_c vanishes and $S_b = T_1$ and $S_f = T_2$. The total transmission probability is given by Equation (8). The completely incoherent transmission is independent of the separation w of the barriers. Consider now the situation in which a tiny fraction of all the carriers can execute one or more full revolutions in the well before losing phase memory. We can then expect a small correction of Equation (8) by a term which depends on the phase $\phi = kw$ accumulated during well traversal. This correction term is, therefore, sensitive to the geometrical arrangement of the barriers. Below we consider the case where the carriers in the well can execute at most one revolution before losing phase memory.

Suppose that the carriers have a small probability $1 - \epsilon$, with ϵ close to 1 to traverse the well without being scattered into reservoir 3. Interestingly, to the lowest order in $1 - \epsilon$, it is the forward and backward scattering probabilities which contain these interference terms, not the coherent transmission probability. The coherent transmission probability T_c is easily obtained in this limit. The probability amplitude for traversal of the structure of Figure 1 from channel 1 to channel 2 is $t_{21} = t_1\sqrt{1 - \epsilon}\, t_2$, and hence

$$T_c = T_{21} = |t_{21}|^2 = (1 - \epsilon)T_1T_2. \tag{19}$$

Carriers which traverse coherently from channel 1 to channel 2 and in addition execute a full revolution in the well have to traverse the well at least three times and are of order $(1 - \epsilon)^2$.

Now consider the sequential tunneling process and let us focus on the backward scattering probability S_b. Consider the carriers which are injected by the inelastic scatterer into the conductor with a negative velocity. A fraction of these leave the well through the left barrier with amplitude t_1 and give rise to a backscattering probability $S_b = T_1$ to lowest order. Most carriers are reflected back into the well if R_1 is close to

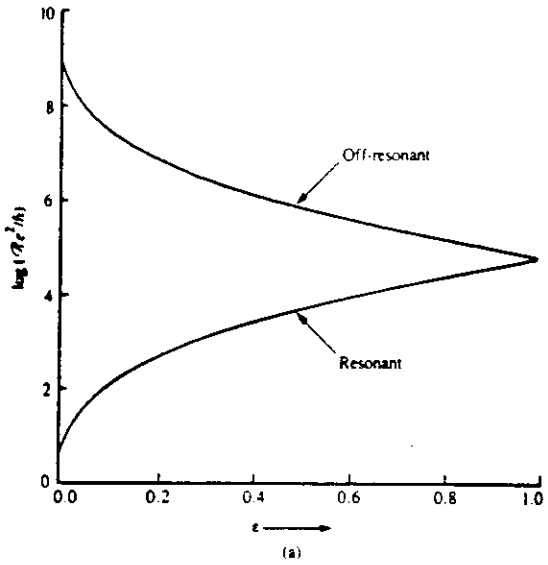

(a) Maximum resistance and minimum resistance corresponding to off-resonant and resonant transmission of a double-barrier structure as a function of ϵ. The parameter ϵ is the probability for carriers incident on the junction to be scattered into the extra reservoir. The two barriers forming the well have transmission probability $T_1 = 0.05$ and $T_2 = 0.01$. (b) Ratio of coherent current and sequential current as a function of ϵ for the double-barrier structure with parameters as in Figure 2(a).

1, and a tiny fraction of these carriers traverses the well back and forth, completing a full revolution. The probability amplitude for a carrier starting in the well and completing a full revolution is $A = (\sqrt{1-\epsilon}\, R_1^{1/2})(\sqrt{1-\epsilon}\, R_2^{1/2})e^{i(2\phi+\Delta\phi)}$. Here $\sqrt{1-\epsilon}$ is the absolute value of the probability amplitude for a carrier to traverse the well without losing phase (without being scattered into reservoir 3 of Figure 1), and $R_2^{1/2}$ and $R_1^{1/2}$ are the absolute probability amplitudes for reflection at the right and left barrier. $\phi = kw$ with w the width of the well is the phase accumulated during well traversal, and $\Delta\phi$ is the phase accumulated during the two reflection processes. The superposition of the carriers escaping directly from the well with amplitude t_1 on those that escape after one revolution with probability amplitude $t_1 A$ gives rise to a combined amplitude $t_1 + t_1 A$, and hence to an interference correction proportional to $2T_1 \mathrm{Re}\,[A]$, with

$$\mathrm{Re}\,[A] = (1-\epsilon)R_1^{1/2}R_2^{1/2}\cos(2\phi + \Delta\phi). \tag{20}$$

Consideration of *all* the processes that contribute to the backward-scattering probability to order $1-\epsilon$ gives (see also Appendix B)

$$S_b = T_1[1 - (1-\epsilon)(T_2 + 2R_1^{1/2}R_2^{1/2}\cos(\Phi))]. \tag{21}$$

Here $\Phi = 2\phi + \Delta\phi$ is the total phase. In contrast to T_c, the backward-scattering probability S_b is sensitive to the separation of the two barriers. Similarly, for the forward-scattering probability we find

$$S_f = T_2[1 - (1-\epsilon)(T_1 + 2R_1^{1/2}R_2^{1/2}\cos(\Phi))]. \tag{22}$$

Using Equations (19) - (22) to evaluate Equations (1) and (2) yields

$$T_{tot} = \frac{T_1T_2}{T_1+T_2}[1 + 2(1-\epsilon)(T_1T_2 - R_1^{1/2}R_2^{1/2}\cos(\Phi))]. \tag{23}$$

For $\epsilon = 1$, Equation (23) gives exactly the result of Equation (8) for completely incoherent transmission. Equation (23) is valid independent of the magnitude of the transmission probabilities T_1 and T_2. If these are taken to be small compared to unity and if we use in addition Equation (B22), which expresses ϵ in terms of the inelastic scattering time τ_i and the well frequency $\nu = v/2w$, Equation (23) becomes

$$T_{tot} = \frac{T_1T_2}{T_1+T_2}[1 - 2e^{-1/2\nu\tau_i}\cos(\Phi)]. \tag{24}$$

Thus, in the case of strong inelastic scattering $2\nu\tau_i < 1$, we obtain corrections to the completely incoherent transmission which are sensitive to the geometrical arrangement of the scatterers. If the Fermi energy is such that $\Phi = (2n+1)\pi$, we have maximum transmission, and for $\Phi = 2\pi n$ we have minimal transmission.

Due to interference effects, the number of states in the well per unit energy (see Appendix D) is also modified. In the case of complete phase randomization, the number of states per unit energy is $dN/dE = 2w(dn/dE)$. A calculation yields

$$dN/dE = 2w(dn/dE) \times [1 + (1/2)(1-\epsilon)(R_1 + R_2 - 2R_1^{1/2}R_2^{1/2}\cos(\Phi))], \tag{25}$$

which in the limit of small transmission probabilities becomes

$$dN/dE = 2w(dn/dE)[1 + 2e^{-1/2\nu\tau_i}\sin^2(\Phi/2)]. \tag{26}$$

The enhanced transmission at $\Phi = (2n + 1)\pi$ coincides with an enhanced density of states and the minimal transmission at $\Phi = 2n\pi$ is accompanied by a reduced density of states.

5. Transition from completely coherent to completely incoherent transmission

In Section 2 we discussed the limiting behavior of completely coherent and completely incoherent transmission. In Sections 3 and 4 we investigated the departure from these simple limits. In this section we address the transition from one limiting behavior to the other for the entire domain of inelastic scattering. A simple model calculation is presented in Appendix B, and here we summarize these results by discussing Figures 2 and 3.

Figure 2(a) shows the two-terminal resistance $R/(h/e^2) = T_{tot}^{-1}$, with T_{tot} given by Equations (1) and (2) evaluated in Appendix B for a two-barrier structure with $T_1 = 0.05$ and $T_2 = 0.01$ as a function of the coupling parameter ϵ. The upper curve shows the maximum resistance (minimum or off-resonant transmission) and the lower curve shows the minimum resistance (peak transmission). $\epsilon = 0$ is the purely coherent limit, and the minimum (maximum) resistance is determined by Equations (3) and (7), respectively. $\epsilon = 1$ is the purely incoherent limit, and the resistance is determined with the help of Equation (8). For small ϵ the minimum resistance is given by Equation (15) (Breit and Wigner limit) and the maximum resistance is determined by Equation (16). An increasing number of sequential tunneling processes (increasing ϵ) leads to a decreasing ratio of the minimum and maximum resistance (transmission) caused both by a decrease in the maximum transmission probability and by a rise in the minimum transmission probability. Thus sequential tunneling leads to lower peak values in the transmission, but increases the off-resonant transmission. For ϵ close to 1, only small corrections remain from the completely incoherent transmission. These corrections are due to a small fraction of carriers which can undergo a complete revolution before leaving the well, as discussed in Section 4.

Figure 2(b) shows the ratio of the coherent current to the total current, T_c/T_{tot}, and the ratio of the current due to incoherent (sequential) processes to the total current, T_i/T_{tot}. For small transmission probabilities, a small amount of inelastic scattering $2\epsilon = 1/\nu\tau_i > (T_1 + T_2) = 1/\nu\tau_e$ makes the sequential current dominant.

The density of states in the well gives a good indication of the degree to which coherence effects play a role. In Figure 3 the density of states in the well (calculated in Appendix C) is shown as a function of $E - E_r$ for three different scattering rates. For small scattering rates Equation (16) applies. With increasing inelastic scattering, the variation in the density of states is less pronounced. For $\epsilon = 1$, i.e., when carriers are scattered every time they reach the junction in Figure 1, the density of states in the well is without structure.

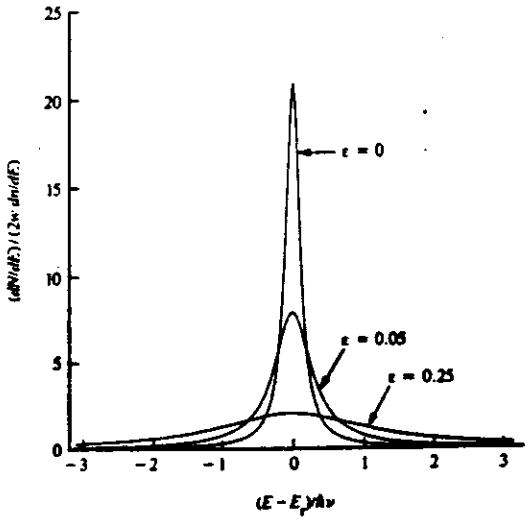

Number of states per unit energy in the resonant well for three different degrees of inelastic scattering as a function of energy. E_r is the resonant energy and ν is the well frequency; (dn/dE) is the density of states in the perfect conductors and w is the well width.

Phase randomization is a consequence of inelastic events. To describe such processes it is necessary to explicitly take into account the phase-randomizing agent. To describe sequential tunneling in terms of a density of states corresponding to the completely coherent case, as in [14], is not correct. In order to have sequential tunneling we must have a phase-randomizing scatterer, and this in turn affects the density of states.

Admittedly, in this paper we have focused on a one-dimensional (one quantum channel) conduction problem, and inelastic scattering might have a more drastic effect in such small systems. The approach introduced here can, however, be extended to treat more complex situations, as indicated in Appendix C.

Note added in proof

References [14] and [34] consider a large applied voltage V which exceeds the width Γ of the resonance. References [14] and [34] find an integrated current which is independent of the inelastic width Γ_i, when the resonance is centered in the applied bias range. We emphasize that Equation (15) has a limited range of validity. For an applied voltage large compared to the elastic width Γ_e but small compared to $h\nu$, the current decreases with increasing elastic width Γ_i with a slope

$$-\frac{\partial}{\partial \Gamma_i} \log I \cong \frac{1}{eV} \geq \frac{1}{h\nu}. \tag{27}$$

Equation (27) is valid for a small inelastic width. The peak-to-valley ratio is smaller than that given by Equation (17) and is proportional to $\hbar^2 v^2/\Gamma V$.

Acknowledgment

I thank R. Landauer for valuable comments, and am also grateful for discussions with N. D. Lang, P. Marcus, E. Mendez, P. Price, and H. Thomas.

Appendix A: Coherent and sequential parts of conductance

Consider the conductor [5] in Figure 1. To derive Equations (1) and (2) we have to calculate the net current which flows due to a difference in the chemical potentials μ_1 and μ_2. The perfect conductors between the reservoir and the scatterers are assumed to be one-dimensional; i.e., there are two states at the Fermi energy, one with positive velocity (from the reservoir toward the conductor) and one with negative velocity. Let us consider the case of a low temperature such that the energy spread kT can be neglected. The reservoir j feeds all channels connected to it equally [29] and up to the chemical potential μ_j. Let us introduce a reference potential μ_0 which is smaller than or equal to the lowest of the three chemical potentials μ_1, μ_2, μ_3. Below the reference potential μ_0 all states are completely filled and we need to consider only the energy range above μ_0. The current emitted by the reservoir j into an adjacent channel in the energy range $\mu_j - \mu_0$ is

$$I_{in} = ev(dn/dE)(\mu_j - \mu_0). \tag{A1}$$

Here v is the Fermi velocity and dn/dE is the density of states (for one spin direction). In one dimension $dn/dE = (dn/dk)(dk/dE) = 1/2\pi\hbar v$, since $dn/dk = 1/2\pi$. Thus the reservoir injects into each channel connected to it a current

$$I_{in} = (e/2\pi\hbar)(\mu_j - \mu_0). \tag{A2}$$

To obtain the net currents we must specify the probabilities of carriers for transmission and reflection at the conductor of Figure 1. Let T_{kl} be the probability for a carrier incident in channel l to traverse the structure into channel k to reach a different reservoir. The probabilities for a carrier emitted by a reservoir to be scattered back into the same reservoir are denoted by R_{kk}. In the absence of a magnetic field the probabilities are symmetric, $T_{kl} = T_{lk}$, $R_{kl} = R_{lk}$. Furthermore, because of current observation,

$$R_{11} + T_{12} + T_{13} + T_{14} = 1, \tag{A3a}$$

$$T_{21} + R_{22} + T_{23} + T_{24} = 1, \tag{A3b}$$

$$T_{31} + T_{32} + R_{33} + R_{34} = 1, \tag{A3c}$$

$$T_{41} + T_{42} + R_{43} + R_{44} = 1. \tag{A3d}$$

Consider now the net current flowing in channel 1. In channel 1, reservoir 1 contributes a net current $(e/2\pi\hbar)(1 - R_{11})(\mu_1 - \mu_0)$. The incident current given by Equation (A2) is diminished by reflection at the sample. Current injected by reservoir 2 gives rise to a current $-(e/2\pi\hbar)T_{12}(\mu_2 - \mu_0)$ in channel 1. Current injected by reservoir 3 into channels 3 and 4 gives rise to a current $-(e/2\pi\hbar)(T_{13} + T_{14})(\mu_3 - \mu_0)$ in channel 1. Collecting all contributions yields a net current in channel 1,

$$I_1 = \frac{e}{2\pi\hbar}[(1 - R_{11})\mu_1 - T_{12}\mu_2 - S_b\mu_3]. \tag{A4}$$

Here we have introduced the total transmission probability

$$S_b = T_{13} + T_{14} \tag{A5}$$

for a carrier incident in channel 3 or 4 to be scattered into channel 1. The reference chemical potential does not occur in Equation (A4) since the currents proportional to μ_0 add to zero because of Equation (A3a). Similar considerations yield a current in channel 2 given by

$$I_2 = \frac{e}{2\pi\hbar}[(1 - R_{22})\mu_2 - T_{21}\mu_1 - S_f\mu_3], \tag{A6}$$

where

$$S_f = T_{23} + T_{24} \tag{A7}$$

is the total probability for carriers incident in channels 3 and 4 to be scattered into channel 2. Finally, the currents in channels 3 and 4 are found to be

$$I_3 = \frac{e}{2\pi\hbar}[(1 - R_{33} - R_{34})\mu_3 - T_{31}\mu_1 - T_{32}\mu_2], \tag{A8}$$

$$I_4 = \frac{e}{2\pi\hbar}[(1 - R_{44} - R_{43})\mu_3 - T_{41}\mu_1 - T_{42}\mu_2]. \tag{A9}$$

The net current flow in the extra branch consisting of channels 3 and 4 has to be zero. Using Equations (A3) and the definition equations (A5) and (A7), we find

$$0 = I_3 + I_4 = \frac{e}{2\pi\hbar}[(S_f + S_b)\mu_3 - S_b\mu_1 - S_f\mu_2], \tag{A10}$$

and hence the chemical potential μ_3 is given by [5]

$$\mu_3 = \frac{S_b\mu_1 + S_f\mu_2}{S_b + S_f}. \tag{A11}$$

Equation (A11) is a result which is important beyond the context of this paper. The extra branch leading away from the conductor and connected to the reservoir also can describe a voltage probe, and μ_3 is the chemical potential which is measured at this probe [28]. Equation (A11) generalizes earlier concepts of "potentiometers" used in [29–31] because it invokes no assumptions on the symmetry of the coupling between the lead and the conductor and because the junction in Figure 1 is treated fully quantum-mechanically; i.e., amplitudes are matched, and not intensities.

Here we use Equation (A11) to eliminate μ_3 from Equation (A4) or Equation (A6) to determine the net current flow along the conductor. Current conservation requires $I = I_1 = -I_2$. Using Equation (A3) and the symmetry $T_{ij} = T_{ji}$ yields, after a little algebra,

$$I = \frac{e}{2\pi\hbar}\left(T_c + \frac{S_b S_f}{S_b + S_f}\right)(\mu_1 - \mu_2). \tag{A12}$$

Here $T_c = T_{12} = T_{21}$ is the coherent transmission probability. These carriers never reach reservoir 3. Thus the total transmission probability has two terms, as indicated in Equations (1) and (2). The two-terminal conductance with the voltages (chemical potentials) measured at reservoirs 1 and 2 becomes

$$\mathcal{G} = I/V = eI/(\mu_1 - \mu_2) = (e^2/h)T_{tot}$$

$$= (e^2/h)\left(T_c + \frac{S_b S_f}{S_b + S_f}\right). \tag{A13}$$

An extension of this approach for conductors with many states at the Fermi energy is discussed in [28].

For completeness, and to avoid potential misunderstanding, the expression for the conductance for the case of a sizable spread kT is added here. Assuming that reservoir j emits carriers with a Fermi distribution

$$f(E - \mu_j) = [\exp(E - \mu_j)/kT + 1]^{-1}, \tag{A14}$$

a repetition of the steps explained above yields $\mathcal{G} = \mathcal{G}_c + \mathcal{G}_i$, with

$$\mathcal{G}_c = (e^2/h)\int dE(-df/dE)T_c(E) \tag{A15}$$

and

$$\mathcal{G}_i = (e^2/h)\frac{\int dE(-df/dE)S_b(E)\int dE(-df/dE)S_f(E)}{\int dE(-df/dE)[S_b(E) + S_f(E)]}, \tag{A16}$$

where df/dE is the derivative of the equilibrium Fermi function $f(E - E_F)$.

Appendix B: Solution of specific example

Below we present a calculation which specifies the basic ingredients of our approach, the transmission probabilities T_{ij} and the reflection probabilities R_{ij}. The barriers to the right and left of the junction (see Figure 1) are specified by 2×2 s-matrices which determine the outgoing waves in terms of the incident waves. (Alternatively, we can also specify transfer matrices.) The elements of the 2×2 s-matrix are the reflection amplitudes r_1, r_1' and the transmission amplitudes $t_1 = t_1'$ for the scatterer to the left and r_2, r_2', t_2 for the scatterer to the right. Here the quantities without a prime give the reflection and transmission amplitudes for carriers incident from the left and the quantities with a prime give the reflection and transmission amplitudes for carriers incident from the right. These amplitudes are conveniently expressed in the form

$$t_j = T_j^{1/2}e^{i\phi_j} \tag{B1}$$

and

$$r_j = iR_j^{1/2}e^{i(\phi_j + \phi_{a,j})}, \tag{B2}$$

$$r_j' = iR_j^{1/2}e^{i(\phi_j - \phi_{a,j})}, \tag{B3}$$

where T_j and R_j are the transmission and reflection probability of the barrier, respectively; ϕ_j is the phase accumulated during barrier traversal; $\phi_j + \phi_{a,j}$ is the phase change associated with reflection for carriers incident from the left-hand side, and $\phi_j - \phi_{a,j}$ is the phase change associated with reflection for carriers incident from the right-hand side. The phase ϕ accumulated by traversing the piece of perfect wire between the two barriers can also be included in the amplitudes given above. Below we assume that the junction (triangle in Figure 1) connects precisely to the center of the well. The following substitutions in Equations (B1) – (B3) account for the phase increments for traversal from the barrier to the center of the well: $\phi_1 \to \phi_1 + \phi/2$, $\phi_{a,1} \to \phi_{a,1} - \phi/2$, $\phi_2 \to \phi_2 + \phi/2$, $\phi_{a,2} \to \phi_{a,2} + \phi/2$. Multiplication of the two transfer matrices associated with the two scatterers yields a combined transmission probability through the double well structure given by

$$T_{12} = \frac{|t_1 t_2|^2}{|1 - r_1' r_2|^2}. \tag{B4}$$

By using Equations (B1) – (B3) and the substitutions just discussed, Equation (B4) becomes [3]

$$T_{12} = \frac{T_1 T_2}{1 + R_1 R_2 + 2R_1^{1/2}R_2^{1/2}\cos(\Phi)}, \tag{B5}$$

where

$$\Phi = 2\phi + \phi_1 + \phi_2 + \phi_{a,2} - \phi_{a,1}. \tag{B6}$$

Equations (B5) and (B6) are exact. The phase accumulated in the well is

$$\phi = kw = w(2mE)^{1/2}/\hbar, \tag{B7}$$

where w is the distance between the barriers and E is the energy of the incident carriers. To simplify the analysis, we assume now that it is only the energy dependence of the phase accumulated in the well which matters, and that the energy dependence of all the other amplitudes and phases in Equations (B5) and (B6) can be neglected. Thus $\Phi(E) = 2\phi(E) + \Delta\phi$, with ϕ determined by Equation (B7) and $\Delta\phi$ an energy-independent phase. Note that we are only concerned with transmission in a narrow energy interval. If only the phase ϕ accumulates during well-traversal counts, then the condition for resonance of the transmission probability [Equation (B5)] is $\Phi = 2\phi(E) + \Delta\phi = \pi(2n + 1)$, where n is an integer. This condition determines the phase $\phi = \phi_{r,n}$ accumulated at resonance, and determines through Equation (B7) the resonant energy $E_{r,n}$. In the limit of

impenetrable barriers, $R_1 = R_2 = 1$, we have $\Delta\phi = \pi$, and the resonance condition $\Phi = 2\phi(E) + \Delta\phi = \pi(2n + 1)$ yields the ladder of eigenstates of a square well, $E_n = (\hbar^2\pi^2/2m)(n/w)^2$. Due to the simplifying assumption made above, the transmission probability, Equation (B5), exhibits a whole ladder of resonant states. Below we investigate the behavior of the transmission probability near one of these resonant levels. Expansion of the denominator away from $\phi = \phi_{r,n}$ for small transmission probabilities $T_1 \ll 1$, $T_2 \ll 1$, yields Equations (3) – (6). The transmission is minimal for $\Phi = 2\pi n$, and this value is taken as a measure for the off-resonant transmission probability. For small transmission probabilities the denominator of Equation (B5) is $(1 + R_1^{1/2}R_2^{1/2})^2 \approx 4$, and hence the off-resonant transmission is proportional to $\frac{1}{4}T_1T_2$ as stated in Equation (7).

Let us now specify the properties of the junction in Figure 1. The junction connects the conductor (channels 1 and 2) to the extra branch (channels 3 and 4). The amplitudes of the incoming waves in these channels (see Figure 1) are denoted by c_i and the amplitudes of the outgoing waves are denoted by c_i'. These amplitudes are related by a 4×4 scattering matrix s_{kl} such that $c_k' = \sum s_{kl}c_l$. A simple choice is [5]

$$s = \begin{pmatrix} 0 & \sqrt{1-\epsilon} & \sqrt{\epsilon} & 0 \\ \sqrt{1-\epsilon} & 0 & 0 & \sqrt{\epsilon} \\ \sqrt{\epsilon} & 0 & 0 & -\sqrt{1-\epsilon} \\ 0 & \sqrt{\epsilon} & -\sqrt{1-\epsilon} & 0 \end{pmatrix}. \quad \text{(B8)}$$

The parameter ϵ plays the role of a coupling parameter and is later related to the inelastic scattering rate. For $\epsilon = 0$, the junction completely decouples the extra branch (channels 3 and 4) from the conductor. For $\epsilon = 1$, carriers incident in channel 1 are transmitted into channel 3 with probability 1 and carriers incident in channel 2 are transmitted into channel 4 with probability 1. Therefore, in this limit all the carriers in the conductor approaching the junction reach reservoir 3. Some detailed results presented below do depend on the particular choice of the splitter, Equation (B8). We cannot, in general, expect results which are independent of the specific phase-randomizing mechanism. In general, all the matrix elements in Equation (B8) can be different from zero. Moreover, the matrix elements can be energy-dependent. As mentioned in [5], this can give rise to peaks in the conductance whose origin is not resonant transmission.

To obtain the overall transmission probabilities T_{ij}, R_{ij} for the structure shown in Figure 1, we need to determine four wave functions ψ_j. The wave function ψ_j has amplitude 1 in channel j describing incident carriers with a unit flux, and has amplitude r_{ij} describing carriers reflected into channel i and amplitude t_{ij} describing carriers transmitted into channel j. From these amplitudes the transmission and reflection probabilities T_{ij} and R_{ij} are obtained. A calculation yields the following results:

$$R_{11} = [R_1 + (1-\epsilon)^2R_2 + 2R_1^{1/2}R_2^{1/2}(1-\epsilon)\cos(\Phi)]/|Z|^2, \quad \text{(B9)}$$

$$R_{22} = [R_2 + (1-\epsilon)^2R_1 + 2R_1^{1/2}R_2^{1/2}(1-\epsilon)\cos(\Phi)]/|Z|^2, \quad \text{(B10)}$$

$$R_{33} = \epsilon^2R_1/|Z|^2, \quad \text{(B11)}$$

$$R_{44} = \epsilon^2R_2/|Z|^2, \quad \text{(B12)}$$

$$R_{43} = R_{34} = [1 + R_1R_2 + 2R_1^{1/2}R_2^{1/2}\cos(\Phi)]/|Z|^2, \quad \text{(B13)}$$

$$T_{21} = T_{12} = (1-\epsilon)T_1T_2/|Z|^2, \quad \text{(B14)}$$

$$T_{31} = T_{13} = \epsilon T_1/|Z|^2, \quad \text{(B15)}$$

$$T_{32} = T_{23} = \epsilon(1-\epsilon)T_2R_1/|Z|^2, \quad \text{(B16)}$$

$$T_{41} = T_{14} = \epsilon(1-\epsilon)T_1R_2/|Z|^2, \quad \text{(B17)}$$

$$T_{42} = T_{24} = \epsilon T_2/|Z|^2, \quad \text{(B18)}$$

where

$$|Z|^2 = 1 + (1-\epsilon)^2R_1R_2 + 2(1-\epsilon)R_1^{1/2}R_2^{1/2}\cos(\Phi). \quad \text{(B19)}$$

If we allow for complex ϕ (complex energy), the amplitude $Z = 1 + (1-\epsilon)R_1^{1/2}R_2^{1/2}e^{i\Phi}$ vanishes at the energy $E = E_r - i(\Gamma_e + \Gamma_i)/2$. Here the elastic width is given by

$$\Gamma_e = -\hbar\nu\log(R_1R_2), \quad \text{(B20)}$$

and the "inelastic" width by

$$\Gamma_i = -2\hbar\nu\log(1-\epsilon). \quad \text{(B21)}$$

For $\epsilon = 0$, when channels 3 and 4 are decoupled from the conductor we find the results discussed at the beginning of this Appendix; i.e., the results for T_{12} given by Equations (B5) and (B14) are the same, and $R_{11} = R_{22} = 1 - T_{12}$. The Breit and Wigner formulae [1, 2] (see also Appendix C) are obtained from Equations (B9) – (B18) in the limit $O(\epsilon) = O(T_1) = O(T_2) \ll 1$, with the partial widths given by Equations (6) and (13). The total elastic and inelastic widths are consistent with Equations (B20) and (B21) in the limit of small transmission probability and small ϵ. The results of Section 4, the limit of ϵ close to 1, are obtained by expanding Equations (B14) – (B18) to first order in $(1-\epsilon)$. Equation (B21) allows an interpretation of the parameter ϵ in terms of an inelastic scattering time; with $\Gamma_i = \hbar/\tau_i$ we obtain from Equation (B21)

$$\epsilon = 1 - e^{-1/2\nu\tau_i}. \quad \text{(B22)}$$

From Equations (B15) – (B18) we obtain for the forward and backward scattering rates

$$S_b = \epsilon T_1[1 + (1-\epsilon)R_2]/|Z|^2, \quad \text{(B23)}$$

$$S_f = \epsilon T_2[1 + (1-\epsilon)R_1]/|Z|^2. \quad \text{(B24)}$$

Together with $T_c = T_{12}$, with T_{12} given by Equation (B14), Equations (B23) and (B24) determine the total transmission probability T_{tot}, Equation (1), for arbitrary coupling ϵ. Figures 2(a) and 2(b) are generated with the help of these results.

Appendix C: The Breit and Wigner formulae

The Breit and Wigner formulae determine the scattering matrix in the presence of a resonance. They are usually derived in the context of nuclear reactions [1, 2] and this perhaps accounts for the fact that they seem not to be appreciated in solid-state physics. Consider a barrier connected to two perfect wires [4, 29]. In the perfect wires the longitudinal motion is assumed to be separable from the transverse motion. Thus motion in narrow perfect wires can be characterized by the quantized motion in the transverse direction, giving rise to a set of discrete energies E_j. Kinetic longitudinal energy can be added to the transverse energy to give the Fermi energy: $E_F = \hbar k_j^2/2m + E_j$. Here we have used a free-particle term to characterize the kinetic energy of the longitudinal motion, but this is not essential. Thus each channel j is associated with two states at the Fermi level with longitudinal velocities $v_j = \pm\sqrt{(2/m)(E_F - E_j)}$. We have N input channels and N output channels. The set of transverse energies in the perfect wire to the left of the barrier can be equal to or different from the set of transverse energies to the right of the barrier. Similarly, for conductors with side branches, we assign a set of channels to each branch of the conductor [5, 22, 28]. For the conductor of Figure 1, $N = 4$. The conducting sample mixes these channels; i.e., a wave incident in channel j leads in general to outgoing waves in all the channels. We have used here the notion of channels in a perfect conductor [29] as an example. The Breit and Wigner formulae presented below apply quite independently of the particular properties of the channels, i.e., whether we deal with plane waves, Bloch waves, or spherical waves. Let us denote the amplitude of the incident current in channel j by a_j and the outgoing current amplitude in channel j by a_j'. The relation between the incoming waves and the outgoing waves is given by an s-matrix $a_i' = \sum_{j=1}^{j=N} s_{ij} a_j$. Current conservation requires the matrix s to be unitary, and time reversal (in the absence of a magnetic field) requires in addition that this matrix be symmetric, $s_{ij} = s_{ji}$. Suppose now that the barrier contains a state with a long lifetime $\hbar/\Gamma$ at an energy $E = E_r - i\Gamma/2$. The key point of Breit and Wigner is the following: All matrix elements of the s-matrix which relate to the decay of the resonance must themselves be resonant and have a denominator of the form $E - E_r + i\Gamma/2$. Below we assume that all the channels of the s-matrix discussed above couple to the resonant state. If this is not the case, our considerations apply to a properly defined and reduced portion of the s-matrix. The s-matrix takes an especially simple form if it is expressed on the basis of the "eigenchannels" which are related to the channels discussed above by an orthogonal transformation O. Consider for simplicity a sample (barrier) connected to only two perfect wires. The eigenchannels are defined in the following way: Away from the resonant energy, transmission through the sample is very small and can be neglected. Thus, away from resonance, carriers incident on the sample are (in this approximation) totally reflected. In general, carriers incident in channel j are reflected with nonvanishing probabilities into all the channels of the perfect conductor. The eigenchannels are chosen such that the reflection away from resonance is diagonal. There is an orthogonal transformation O_l which transforms the channels of the left perfect conductor and an orthogonal transformation O_r which transforms the channels of the right perfect conductor. On the basis of eigenchannels the s-matrix away from resonance is given by $s_{mn} = \delta_{mn} e^{i(\delta_m + \phi_m)}$, where δ_{mn} is the Kronecker symbol and δ_m are the phases acquired in the reflection process. On the basis of the eigenchannels, and in the presence of resonant transmission, the matrix elements of the s-matrix are of the form

$$s_{mn} = \left[\delta_{mn} - i\frac{\Gamma M_{mn}}{E - E_r + i\Gamma/2}\right] e^{i(\delta_m + \phi_n)}, \tag{C1}$$

where the matrix elements M_{mn} remain to be determined. The s-matrix is symmetric, and hence $M_{mn} = M_{nm}$. Furthermore, since s is unitary, differing rows of the s-matrix must be orthogonal to one another. The orthogonality of rows m and n gives

$$\frac{M_{mn}^*}{E - E_r - i\Gamma/2} - \frac{M_{mn}}{E - E_r + i\Gamma/2} = \frac{i\Gamma \sum_{j=1}^{j=N} M_{mj} M_{nj}^*}{(E - E_r)^2 + \frac{1}{4}\Gamma^2}. \tag{C2}$$

As shown in [2], Equation (C2) implies first that M_{mn} is real and second that M_{mn} is a matrix which is equal to its own square. Since M is symmetric, it can be diagonalized, and since the matrix is unimodular, its eigenvalues are either 0 or 1. If there is no accidental degeneracy of resonant levels in the sample, all eigenvalues of the M-matrix are equal to 0 except for one eigenvalue, which is equal to 1. As shown in [2], in this case

$$M_{mn} = \sqrt{\Gamma_m \Gamma_n}/\Gamma, \tag{C3}$$

where the Γ_m are called the *partial widths* of the channels and $\Gamma = \sum_{j=1}^{j=N} \Gamma_j$ is the total width of the resonant level. Thus the set of phases δ_n, $n = 1, \cdots, N$, and the N partial widths determine the matrix elements of the s-matrix. The matrix [Equation (C1)] specified by Equation (C3) is unitary. The constraint $\sum_{n=1}^{n=N} \delta_n = \delta$, where $\sin\delta = \Gamma/2[(E - E_r)^2 + (\Gamma/2)^2]^{1/2}$, makes s_{mn} a special unitary matrix. Using Equations (C3) and (C1) yields a probability

$$S_{mn} = |s_{mn}|^2 = \frac{\Gamma_m \Gamma_n}{(E - E_r)^2 + \frac{1}{4}\Gamma^2} \tag{C4}$$

for $m \neq n$ and

$$S_{nn} = |s_{mn}|^2 = \frac{(E - E_r)^2 + \frac{1}{4}(\Gamma - \Gamma_n)^2}{(E - E_r)^2 + \frac{1}{4}\Gamma^2} \quad \text{(C5)}$$

for $n = m$. Thus the Breit and Wigner formulae, Equations (C4) and (C5), determine the transmission probabilities and the reflection probabilities of a resonant scatterer coupled to N channels in terms of the partial widths of these channels. For the particular example analyzed in Appendix B, we find that in the Breit and Wigner limit, Equations (B11), (B12), and (B14) – (B18) are of the form given by Equation (C4), and Equations (B9), (B10), and (B13) are of the form given by Equation (C5). In this example the transformation to eigenchannels affects only channels 3 and 4.

As an additional application of these results, let us consider the case of a single resonant well in a barrier connected to the left and right to perfect wires (see [16] and [17]). The perfect wire to the left has N_l quantum channels, and the perfect wire to the right has N_r quantum channels. The total number of channels is $N = N_l + N_r$. The decay into the eigenchannels on the left-hand side of the barrier gives rise to the partial widths $\Gamma_{l,i}$ and the decay into the eigenchannels on the right-hand side gives rise to the partial widths $\Gamma_{r,i}$. The probability for transmission from channel j (on the l.h.s.) to channel i (on the r.h.s.) is, according to Equation (C4), $T_{ij} = \Gamma_{r,i}\Gamma_{l,j}/[(E - E_r)^2 + \frac{1}{4}\Gamma^2]$. Here $\Gamma = \Gamma_r + \Gamma_l$ is the total width and $\Gamma_r = \sum_{i=1}^{i=N_r} \Gamma_{r,i}$ is the total partial width associated with decay of the resonant state into the r.h.s. perfect conductor, and $\Gamma_l = \sum_{j=1}^{j=N_l} \Gamma_{l,j}$ is the total width associated with the decay into the l.h.s. perfect conductor. The conductance [29, 32]

$$G = \left(\frac{e^2}{h}\right) \mathrm{tr}(t^* t) = \left(\frac{e^2}{h}\right) \sum_{i=1,j=1}^{i=N_r, j=N_l} T_{ij}$$

is easily evaluated and given by

$$G = \left(\frac{e^2}{h}\right) \frac{\Gamma_r \Gamma_l}{(E - E_r)^2 + \frac{1}{4}(\Gamma_r + \Gamma_l)^2}. \quad \text{(C6)}$$

Here we have evaluated the conductance on the basis of eigenchannels, which is allowed since $\mathrm{tr}(t^* t)$ is invariant under the orthogonal transformations O_r and O_l discussed above. Thus, application of the Breit and Wigner formulae immediately yields the key result of Kalmeyer and Laughlin [17]. In the presence of a single resonant state the conductance is bounded by e^2/h. The maximum value is obtained if $\Gamma_r = \Gamma_l$. A single resonant state, described in the Breit and Wigner formalism by requiring that the M-matrix have only one eigenvalue equal to 1, can at best provide one *effective conduction channel* [33].

Appendix D: Local density of states

In this section we discuss the density of states in the well and the effect of inelastic scattering on the density of states. Let x be the coordinate along the conductor, with $x = 0$ marking the location of the junction. The number of carriers in the segment of the conductor between x and $x + dx$ and in an energy interval E, $E + \Delta E$ due to carriers incident in channel j is [24, 31]

$$dN(x) = (dn/dE)\Delta E\, |\psi_j(E, x)|^2 dx. \quad \text{(D1)}$$

Here $(dn/dE) = 1/2\pi\hbar v$ is the density of states in channel j. The wave function is normalized such that the incident wave has amplitude 1. In the conductor of Figure 1 we have a total of four wave functions, each describing carriers incident in one of the four channels. Thus, in the sample of Figure 1, assuming that the density of states of all the channels is the same, the number of carriers in an interval from x to $x + dx$ is given by

$$dN(x) = (dn/dE)\Delta E \sum_{j=1}^{j=4} |\psi_j(E, x)|^2 dx. \quad \text{(D2)}$$

Let us now apply Equation (D2) to find the total number of carriers in the resonant well. This requires that we integrate the right-hand side of Equation (D2) over the width of the well. Dividing this by ΔE yields the number of states in the well per unit energy,

$$dN/dE = (dn/dE) \sum_{k=1}^{k=4} \int_{x=-w/2}^{x=w/2} dx\, |\psi_k(E, x)|^2. \quad \text{(D3)}$$

For a well which is wide compared to the Fermi wavelength, the integration limits are determined by the turning points. We are not interested in density variations on the scale of a Fermi wavelength and, therefore, it is sufficient to use a density which has been averaged over a small volume several times larger than the scale set by the Fermi wavelength [3, 24, 29, 31]. In the well the wave function is a superposition of plane waves. The averaged square of the wave function to the left (and right) of the splitter is determined by a pair of amplitudes, a_2, a_2', b_1, b_1', respectively. For instance, the averaged wave functions to the left of the splitter are given by $(|\psi_j(x)|^2) = |a_2(j)|^2 + |a_2'(j)|^2 = |c_1(j)|^2 + |c_1'(j)|^2$. Here the $( )$ indicate the spatial average. Because the a and c coefficients (see Figure 1) in this equation differ only by phase factors, either set can be used. For brevity we do not present this calculation in detail but only give the final result,

$$\begin{aligned} dN/dE = {} & (dn/dE)(w/2)(1/|Z|^2) \\ & \times [(2 - \epsilon)(T_1 + T_2) + (1 - \epsilon)(2 - \epsilon)(R_1 T_2 + R_2 T_1) \\ & + 2\epsilon + \epsilon(2 - \epsilon)(R_1 + R_2) + 2\epsilon(1 - \epsilon)R_1 R_2]. \end{aligned} \quad \text{(D4)}$$

The number of states per unit energy, Equation (D4), is shown in Figure 3. Equation (B7) is used to obtain the energy dependence. In the Breit and Wigner limit, Equation (D4) yields Equation (17). In the limit $\epsilon = 1$ corresponding to complete phase randomization, the density of states in the well is the same as that in the perfect leads connecting to the reservoirs; i.e., Equation (D4) yields $dN/dE = (dn/dE)2w$. Clearly, for a narrow well with a width of the order of the

Fermi wavelength, the approximations used above to find the number of states in the well are not adequate. The key point of our discussion, already made in [24], is that inelastic scattering affects the density of states.

References and notes

1. G. Breit and E. Wigner, *Phys. Rev.* **49**, 519 (1936).
2. L. D. Landau and E. M. Lifshitz, *Quantum Mechanics (Non-Relativistic Theory)*, Pergamon Press, Oxford, 1977. See p. 603 *ff.*
3. R. Landauer, *IBM J. Res. Develop.* **1**, 223 (1957); R. Landauer, *Philos. Mag.* **21**, 863 (1970).
4. R. Landauer, "Electrical Transport in Open and Closed Systems," *Z. Phys. B* **68**, 217 – 228 (1987).
5. M. Büttiker, *Phys. Rev. B* **33**, 3020 (1986).
6. E. O. Kane, *Tunneling Phenomena in Solids*, E. Burnstein and D. Lundquist, Eds., Plenum Press, New York, 1969.
7. R. Tsu and L. Esaki, *Appl. Phys. Lett.* **22**, 562 (1973); L. L. Chang, L. Esaki, and R. Tsu, *Appl. Phys. Lett.* **24**, 593 (1974).
8. T. C. L. Sollner, W. D. Goodhue, P. E. Tannenwald, C. D. Parker, and D. D. Peck, *Appl. Phys. Lett.* **43**, 588 (1983).
9. R. Ricco and M. Ya. Azbel, *Phys. Rev. B* **29**, 1970 (1984).
10. S. Luryi, *Appl. Phys. Lett.* **47**, 490 (1985).
11. P. J. Price, *Superlattices and Microstructures* **2**, 593 (1986).
12. F. Capasso, K. Mohammed, and A. Y. Cho, *IEEE J. Quant. Electron* **QE-22**, 1853 (1986).
13. E. Mendez, L. Esaki, and W. I. Wang, *Phys. Rev. B* **33**, 2893 (1986).
14. T. Weil and B. Vinter, *Appl. Phys. Lett.* **50**, 1281 (1987).
15. P. J. Price, *Phys. Rev. B* **33**, 1314 (1987).
16. H. Knauer, J. Richter, and P. Seidel, *Phys. Status Sol. (a)* **44**, 303 (1977); A. Hartstein and R. H. Koch, *Phys. Rev. B* **35**, 6442 (1987).
17. V. Kalmeyer and R. B. Laughlin, *Phys. Rev. B* **35**, 9805 (1987).
18. M. Ya. Azbel, A. Hartstein, and D. P. DiVincenzo, *Phys. Rev. Lett.* **52**, 1641 (1984).
19. A. D. Stone and P. A. Lee, *Phys. Rev. Lett.* **54**, 1196 (1985).
20. A. B. Fowler, G. L. Timp, J. J. Wainer, and R. A. Webb, *Phys. Rev. Lett.* **57**, 138 (1986).
21. N. D. Lang, *Phys. Rev. Lett.* **58**, 45 (1986); "The Resistance of a One-Atom Contact in the Scanning Tunneling Microscope," preprint.
22. M. Büttiker, *Phys. Rev. Lett.* **57**, 1761 (1986).
23. M. Büttiker, Y. Imry, and R. Landauer, *Phys. Lett.* **96A**, 365 (1983).
24. M. Büttiker, *Phys. Rev. B* **32**, 1846 (1985); *Ann. N.Y. Acad. Sci.* **480**, 194 (1986).
25. H. Morkoç, J. Chen, U. K. Reddy, T. Henderson, and S. Luryi, *Appl. Phys. Lett.* **49**, 70 (1986).
26. The results of [5] are expressed in terms of the Landauer formula $R_{2t} = (h/e^2)(1 - T_{nn})/T_{nn}$. This differs from the two-terminal conductance used here by a "contact resistance" h/e^2. See Y. Imry in *Directions of Condensed Matter Physics*, (Memorial Volume in Honor of Shang-keng Ma), G. Grinstein and G. Mazenko, Eds., World Scientific Press, Singapore, 1986, and [4].
27. We assume here that inelastic scattering in the well is the dominant effect. If the inelastic scattering time is short compared to the single-barrier traversal time [see M. Büttiker and R. Landauer, *Phys. Rev. Lett.* **49**, 1739 (1982); C. R. Leavens and G. C. Ares, *Solid State Commun.* **62**, 1101 –1105 (1987)], inelastic effects during barrier traversal must be taken into account.
28. M. Büttiker, *Phys. Rev. B* **35**, 4123 (1987).
29. M. Büttiker, Y. Imry, R. Landauer, and S. Pinhas, *Phys. Rev. B* **31**, 6207 (1985).
30. H. L. Engquist and P. W. Anderson, *Phys. Rev. B* **24**, 1151 (1981).
31. O. Entin-Wohlman, C. Hartzstein, and Y. Imry, *Phys. Rev. B* **34**, 921 (1986).
32. D. S. Fisher and P. A. Lee, *Phys. Rev. B* **23**, 6851 (1981).
33. Y. Imry, *Europhys. Lett.* **1**, 249 (1986).
34. J. Jonson and A. Grincwajg, "The Effect of Inelastic Scattering on Resonant and Sequential Tunneling in Double Barrier Heterostructures," preprint; available from authors, Institute of Theoretical Physics, Chalmers University of Technology, Goteborg, Sweden.

Received September 11, 1987; accepted for publication September 20, 1987

Markus Büttiker *IBM Thomas J. Watson Research Center, P.O. Box 218, Yorktown Heights, New York 10598.* Dr. Büttiker is a research staff member of the Physical Sciences Department at the Thomas J. Watson Research Center. He is currently conducting research in coherent transport phenomena in ultrasmall metallic structures. He received a Diploma in theoretical physics from the Federal Institute of Technology in Zurich, Switzerland, in 1974, and a Ph.D from the University of Basel, Switzerland, in 1978. He joined IBM at the Thomas J. Watson Research Center in 1979. Dr. Büttiker's research interests include such diverse fields as current instabilities in semiconductors, the statistical mechanics of solitons, and thermal activation and nucleation phenomena.

NANOSTRUCTURE PHYSICS AND FABRICATION

Proceedings of the International Symposium

College Station, Texas *March 13–15, 1989*

Edited by

Mark A. Reed

Central Research Laboratories
Texas Instruments Incorporated
Dallas, Texas

Wiley P. Kirk

Department of Physics
Texas A&M University
College Station, Texas

ACADEMIC PRESS, INC.
Harcourt Brace Jovanovich, Publishers

Boston San Diego New York
Berkeley London Sydney
Tokyo Toronto

WHEN IS THE HALL RESISTANCE QUANTIZED?

M. Büttiker

IBM Research Division,
IBM Thomas J. Watson Research Center
P. O. Box 218, Yorktown Heights, New York 10598

I. INTRODUCTION

In this paper, we apply to the quantum Hall effect (1) some elements of a theory which expresses electric conduction in terms of global transport coefficients (2). This approach relates transmission probabilities directly to global longitudinal resistances and global Hall resistances. It is an extension and modification of earlier work (3) with the key distinction that current and voltage probes are treated on the same physical principles. As a consequence this approach (2) explicitly reflects the fundamental symmetries of electrical conduction (4-6). This approach (2,6) has recently been used to address a wide range of problems: voltage fluctuations in small metallic conductors (7), transport in ballistic conductors (8), low field anomalies of the Hall effect (9-14), the effect of phase randomizing events on the series addition of resistances including resonant tunneling (15), and electron focusing (5). The application to the quantum Hall effect of this approach (2,6) was noted independently by Beenakker and van Houten (10), Peeters (11) and the author (16). Remarkably the generalized resistance expressions found in (2,6) are valid over the entire range of fields. Furthermore, in contrast to other recent work (17,18, 19) on the quantum Hall effect, the discussion based on (2) does not invoke any a priori assumptions about what is measured at a voltage contact. This approach permits the study of the Hall effect in highly non-uniform samples and highlights the role of current and voltage contacts. Under special circumstances the theory (16) predicts simultaneously *quantized* Hall resistances and *quantized* longitudinal resistances at values which are not given by the number of bulk Landau levels

ISBN 0-12-585000-X

below the Fermi energy. Such anomalous plateaus have been observed in experiments by Washburn et al. (20) and Haug et al. (21). The approach predicts that contacts are important, whenever there exists a non-equilibrium population of current carrying states (16). A striking demonstration of this effect has been given by van Wees et al. (22). Experiments by Komiyama et al. (23) also require a proper treatment of the contacts and point to extremely long equilibration lenghts. Van Wees et al. (24) have demonstrated the suppression of the Shubnikov-de Haas oscillations if current is injected or detected with a point contact. Very small samples, as observed by Chang et al. (25), exhibit fluctuations both in the longitudinal resistances and the Hall resistances (26). The longitudinal resistance can even be negative (25,27). The approach advanced here invokes transport along edge states (28,29). A direct test of transport along edge states is provided by the analysis of the Aharonov-Bohm effect (30). Motion along edge states leads to the prediction (16,18) that the Aharonov-Bohm effect is *suppressed* in the quantum Hall regime for ring structures which are wide compared to a cyclotron radius, and this has indeed been observed by Ford et al., Timp et al., van Loodsrecht et al., and van Wees et al. (31). Aharononv-Bohm like oscillations require backscattering either in the bulk (18) or at the contacts (19). The suppression of the Aharonov-Bohm effect is important, since some of the pioneering papers do invoke the sensitivity of a two-dimensional electron gas to an Aharonov-Bohm flux (28,32) to explain the quantum Hall effect. Below, we address the question posed in the title of this paper by discussing a few representative simple examples. We are concerned with situations where electron motion can be completely described by edge states with localized interactions between them. More complex situations at arbitrary fields can be analyzed computationally as is nicely demonstrated by the work of Ravenhall et al. (12) and Kirczenow(13). Finally, we address some older experiments, which by measuring voltages at interior contacts, have led to the conclusion that current transport cannot be along edge states. We point to a differing interpretation of these experiments.

II. GLOBAL RESISTANCES

Fig. 1a shows an electric conductor consisting only of resistive elements and connected to a number of terminals at chemical potentials μ_i, i = 1,2,3,4... The terminals are sources and sinks of carriers and energy and are assumed to have a density of states so large that the current density can always be assumed to be zero. The terminals are at equilibrium. The currents incident from the terminals on the conductor are related to the voltages $V_i = \mu_i/e$ by the conductances (33),

$$I_i = \sum_{j \neq i} G_{ij} V_j \tag{1}$$

The G_{ij} in Eq. (1) are global conductances; they describe conduction from one terminal to the other. A quantum transport theory is obtained by spacing the terminals so closely that electron motion from one terminal to the other is phase-coherent. The conductor scatters carriers only elastically. Inelastic, phase-randomizing and energy dissipating events occur only in the reservoirs. We can then follow (3) and view the conductor as a target which permits transmission and reflection of carriers. Ref. 2 finds for the currents I_i incident on the conductor,

$$I_i = \frac{e}{h}[(M_i - R_{ii})\mu_i - \sum_{j \neq i} T_{ij}\mu_j], \tag{2}$$

where M_i are the number of channels in reservoir i and R_{ii} and T_{ij} are the total probabilities for reflection at terminal i and the total probability for transmission from probe j to probe i. Comparison of Eq. (2) and Eq. (1) taking into account that each row (and colum) of the matrix defined by Eq. (2) adds to zero, yields $G_{ij} = (e^2/h)T_{ij}$. In a configuration where reservoirs m and n are used as a source and sink and contacts k and l are voltage probes, the resistance is $\mathcal{R}_{mn,kl} = (\mu_k - \mu_l)/eI$. Here $I = I_m = -I_n$ is the current impressed on the sample. At the voltage contacts, there is zero net current flow, $I_k = I_l = 0$. These conditions on the currents determine the resistance (2,6)

$$\mathcal{R}_{mn,kl} = (h/e^2)(T_{km}T_{ln} - T_{kn}T_{lm})/D. \tag{3}$$

D is a subdeterminant of rank three of the matrix formed by the coefficients in Eq. (2), which multiply the chemical potentials. All subdetrminants of rank three of this matrix are equal and independent of the indices m,n,k, and l. Microreversibility, implies $T_{ij}(B) = T_{ji}(-B)$, $R_{ii}(B) = R_{ii}(-B)$. Using this in Eq. (3) gives rise to the reciprocity of four-terminal resistances, $\mathcal{R}_{kl,mn}(B) = \mathcal{R}_{mn,kl}(-B)$. We cite here only two recent experimental demonstrations of this symmetry (4,5), which is a manifestation of the Onsager-Casimir symmetry of the transport coefficients of Eqs. (1) and (2), and refer the reader to (6) for additional references. Ref. 6 discusses conductors with more than four terminals and shows that a mapping exists such that a generalization of Eq. (3) applies. If the terminals cannot be assumed to be closely spaced, fictitious contacts can be used to bring incoherence into the conduction process (14,15) or alternatively inelastic scattering has to be incorporated in the calculation of the global conductances from the outset (7). A derivation of Eqs. (1-3)

Stone and Szafer (34).

III. THE QUANTUM HALL EFFECT

Let us next consider how the quantum Hall effect is established. For the scope of this paper, it will be sufficient to assume that electron motion occurs in a potential eU(x,y) which varies slowly compared to the cyclotron radius. The states at the Fermi energy E_F are then determined by the solution of the equation

$$E_F = \hbar\omega_c(n + 1/2) + eU(x,y) \tag{4}$$

where n is a positive integer and x,y is a path in two-dimensional space. We emphasize, that it is the equilibrium potential eU which matters, i.e. the potential in the absence of a net current flow ($\mu_1 = \mu_2 = \mu_3 = \mu_4$). Eq. (4) admits two types of solutions: There are open paths which necessarily originate and terminate at a contact. In addition, there are closed paths. We refer to the open paths as "edge" states since typically the open states form close to the boundary of the sample. In Fig. 1 the open paths are indicated by faint solid lines. At zero temperature and in the absence of tunneling between open states and the closed paths it is only the open paths (edge states) which contribute to electric conduction. It is the connection of the contacts via edge states (open paths) which determines the measured resistance. Each edge state provides a path along which carriers can traverse the conductor without backscattering (16). If

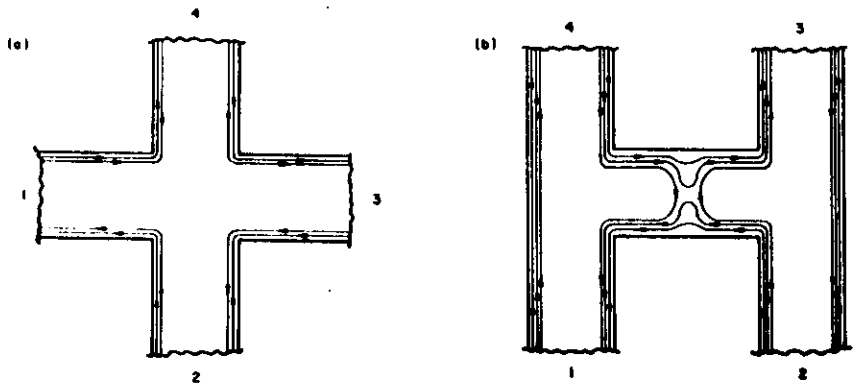

Fig. 1. (a) Conductor with Hall probes. (b) Conductor with barrier reflecting K edge states.

each of the incident edge states carries a unit current (is full), all outgoing edge states carry also a unit current (are full). Given N edge states, the total transmission probabilities in the conductor of Fig. 1a are $T_{41} = N$, $T_{34} = N$, $T_{23} = N$, and $T_{12} = N$. All other T_{ij} are zero. The total reflection probabilities in the absence of internal reflection are $R_{ii} = M_i - N$. The Hall resistance $\mathcal{R}_{13,42}$ is determined by $T_{41}T_{23} - T_{43}T_{21}$, which is equal to N^2. Evaluation of the subdeterminant yields $D = N^3$. All Hall resistances of the conductor of Fig. 1a are quantized and yield $\pm h/e^2N$. The "longitudinal" resistances (for example $\mathcal{R}_{12,43}$) are zero. Note, that the resistance is determined by states at the Fermi energy only.

IV. ANOMALOUSLY QUANTIZED FOUR-TERMINAL RESISTANCES

There are many arguments which can be put forth to explain the quantum Hall effect. To test such arguments, they should be applied to make predictions for situations which are not ideal (35). The discussion given above can easily be applied to the case where various current and voltage probes are interconnected with the result that the two-terminal resistance is $\mathcal{R}_{12,12} = (h/e^2)(p/q)$ with p and q integers as found experimentally by Fang and Stiles (35). Below we analyze situations where the connection of edge states to various contacts is changed in a well controlled fashion. Fig. 1b shows a conductor where a gate creates a barrier to carrier flow. For a certain range of barrier height K edge states are reflected. Application of Eq. (3) predicts Hall resistances (16)

$$\mathcal{R}_{13,42} = \left(\frac{h}{e^2}\right)\frac{1}{(N - K)} \tag{5}$$

$$\mathcal{R}_{42,13}(B) = \mathcal{R}_{13,42}(-B) = -\left(\frac{h}{e^2}\right)\frac{N - 2K}{N(N - K)} \tag{6}$$

and *quantized* longitudinal resistances (16) which are symmetric in the field,

$$\mathcal{R}_{12,43}(B) = \mathcal{R}_{12,43}(-B) = \mathcal{R}_{43,12}(B) = \left(\frac{h}{e^2}\right)\frac{K}{N(N - K)}. \tag{7}$$

All other four-terminal resistance measurements on the conductor of Fig. 1b are zero. The plateaus predicted by Eqs. (5-7) have been observed in strikingly clear experiments by Washburn et al. (20) and Haug et al. (21). Interestingly, van Houten et al. (36) found Eq. (7) to be a good approximation to the low field four-terminal magneto-resistance of a constriction, if there is some equilibration

vation of Eqs. (5-7) assumes equilibration only in the reservoir.

So far we have assumed that carriers which reach a contact from the interior of the sample can escape into the reservoir with probability 1. This is called a contact without internal reflection (16). Correspondingly, if carriers approaching a contact have a probability of less than 1 to escape into the reservoir, we have a contact with *internal* reflection. A current source contact with internal reflection populates edge states in a non-equilibrium fashion, similar to the barrier discussed above. If contacts with no internal reflection and contacts with internal reflection *alternate* along the perimeter of the sample all Hall resistances are still quantized (proportional to 1/N) and all longitudinal resistances are zero (16). But if two contacts with internal reflection are adjacent there is at least one Hall measurement which depends on the detailed scattering properties of the contacts. A clear demonstration of this has come with the work of van Wees et al. (22). They consider two contacts spaced closely compared to an equilibration length. The width of the contacts can be varied and thus a barrier is created at the contacts which permits only a limited number of edge states to transmit. Fig. 2a shows a particular situation, where N-K edge states transmit at contact 1 and N-L edge states transmit at contact 2. The Hall resistance $\mathcal{R}_{13,42}$ is determined by the number N of bulk edge states, since carrier flow is from contact 1 to contact 4 and contact 4 provides equilibration. But if carrier flow is from contact 2 to contact 4 the Hall resistance is

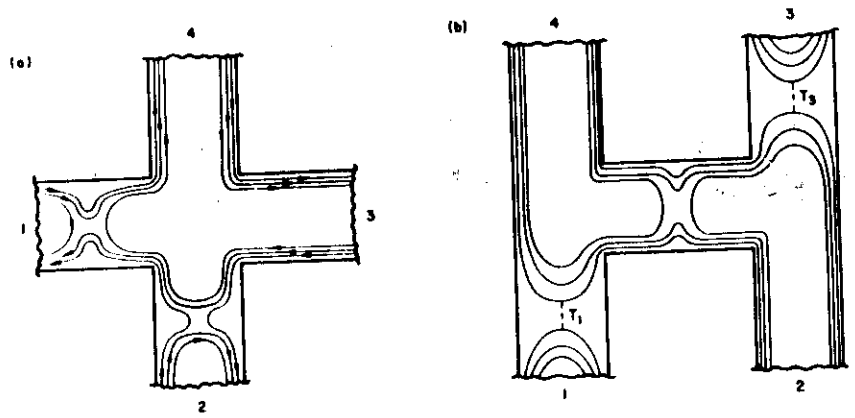

Fig. 2. (a) Conductor with two contacts with internal reflection. (b) Conductor with barrier and two weakly coupled contacts.

where M=min(K,L). It is the contact which provides less reflection, i. e. which exhibits the larger conductance which determines the outcome of the measurement (5,22).

Let us briefly return to the conductor of Fig. 1b. Clearly, the anomalous quantization found in the conductor of Fig. 1b also hinges on the properties of the contacts (at least as long as the contacts are within an equilibration length of the barrier). To show this, consider the conductor in Fig. 2b where two of the contacts are separated by barriers from the main conducting channel. If this barrier forms a smooth saddle, the contacts interact only with the outermost edge state. Let the probability for transmission from this contact to the outermost edge be $T_1 < 1$ at contact 1 and $T_3 < 1$ at contact 3. The Hall resistances are anti-symmetric in the field and given by $(h/e^2)1/(N - K)$ independent of T_1 and T_2. *All longitudinal resistances are zero (!)* in contrast to the example discussed above. That this is so is seen by inspection of Fig. 2b. It is only the outermost edge state which is measured and this state penetrates the barrier. These simple examples show the significance of the properties of contacts. This of course is only true as long as the contacts are close enough to the barrier to sense the differing population of the edge states. If the contacts are further than an equilibration length away from the barrier then the outcome of the measurement is independent of the properties of the contacts and given by Eqs. (5-7). Komiyama et al. (23) have performed experiments on conductors with contacts which exhibit internal reflection. (The contacts in these experiments are probably much more complex then the simple examples discussed here). These experiments are interesting in many ways: they demonstrate that an equilibration of the population of edge states does not occur even over distances of *several hundred* μm. Furthermore, they drastically demonstrate the highly non-local nature of conductance in the quantum Hall regime. The absence of longitudinal resistance in Fig. 2b is closely related to a recent experiment by van Wees et al. (24) which demonstrates the suppression of the Shubnikov-de Haas oscillations by selectively populating or detecting edge states with a point contact.

V. INTERIOR CONTACT

The approach advanced here which emphasizes the transport along edge states, which is supported by the experiments described above, has been objected to in the past on seemingly clear experimental evidence (37-40). Cage (40) writes "There is considerable confusion about this question, due mainly to

goes on to defend a classical current distribution pattern based on the notion of local electric conductivities σ_{xx} and σ_{xy}. A number of experiments have been performed with contacts in the interior of the conductor, as shown schematically in Fig. 3a. Even for fields at which the Hall resistance is quantized, the voltage measured with reference to an interior contact exhibits large fluctuations as the field is increased through the plateau. It is argued that since carrier motion in high magnetic fields is along equipotential lines, the measurement of a voltage which differs from that of the current source or current sink in the interior of the sample indicates current flow in the bulk of the sample. Below we point out that the voltage measured at an interior contact can exhibit large swings without an appreciable change in the current flow pattern.

The conductor of Fig. 3a has three reservoirs and it is, therefore, sufficient to consider Eq. (2) for i=1, 2, and 3. In the presence of zero net current flow into reservoir 3 the chemical potential is (14)

$$\mu_3 = \frac{T_{31}\mu_1 + T_{32}\mu_2}{T_{31} + T_{32}}. \qquad (9)$$

The measured chemical potential is determined by the probabilities of carriers entering contacts 1 and 2 to reach contact 3. The bottleneck for this processes is the transmission from the edge states to the contact. Motion along the edge

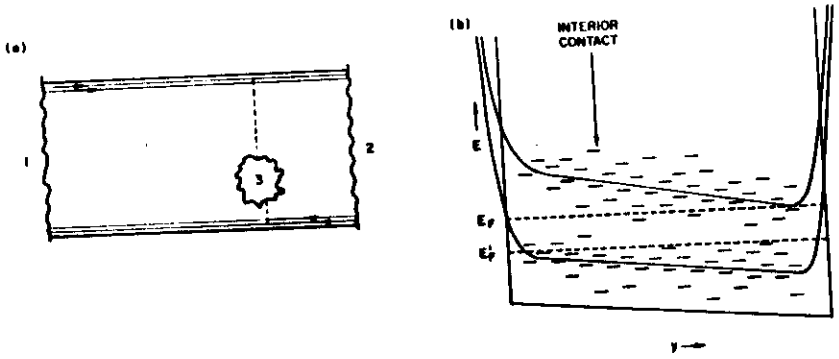

Fig. 3. (a) Conductor with interior contact. (b) Typical energy spectrum of the conductor. The arrow indicates the position of the contact.

form the edge states to the contact can occur via quantum tunneling and at higher temperatures via Mott hopping through impurity states. We can thus assume that the transmission probabilities T_{31} and T_{32} are extremely small. The current exchanged between the edge states and the measurement reservoir is negligible compared to the current flowing along the edges. Despite the minuscule current which flows from the upper edge to the lower edge the measured chemical potential exhibits very large fluctuations. Indeed if $T_{32} << T_{31} << N$, the measurement yields a potential $\mu_3 \sim \mu_1$ and if $T_{31} << T_{32} << N$, the chemical potential is $\mu_3 \sim \mu_2$. Large swings in the chemical potential of interior contacts are indeed experimentally observed and in macroscopic conductors are likely due to small but large scale non-uniformities of the sample which for some fields make a Mott hopping path to one edge more likely than to the other. Fig. 3b shows the spectrum of the conductor in the vicinity of the interior contact. The interior contact is taken to be closer to the lower edge and in Fig. 3b its position is indicated by an arrow. If the Fermi energy is slightly above the bulk Landau level N (onset of the N Hall resistance plateau) carrier flow to the upper edge is more likely since there are more impurity states available. The measured chemical potential is slightly less but close to μ_1. As the magnetic field is increased (the Fermi energy lowered) the density of impurity states between the contact and the lower edge increases and this path becomes favorable. Hence the potential at the interior contact approaches that of the lower edge and is closer to μ_2. In large samples it is only the average impurity distribution which counts. In smaller samples we can expect the sample specific impurity distribution to become important and to produce very irregular chemical potential fluctuations (7). If additional exterior contacts are added to the conductor in Fig. 3b, our model gives, in complete agreement with experiment, that a two terminal measurement, using an interior contact and an arbitrary exterior contact (without internal reflection or arbitrary contacts but spaced further apart than an equilibration length) does not depend on the exterior contact. That is because motion along the edge occurs without resistance. If open edge states were to reach the interior contact the resistance would be of the order of h/e^2 and not as experimentally observed in the mega ohm range.

Transport along edge states combined with a formula which expresses resistances in terms of global transport coefficients (2,6) leads to an appealing and simple picture of the quantum Hall effect and is applicable to a variety of highly non-uniform sample geometries. Recent experiments by Chang and Cunningham (41) indicate that an extension of this approach to the fractional quantum Hall effect should also be possible.

REFERENCES

1. K. von Klitzing, G. Dorda and M. Pepper, Phys. Rev. Lett. **45**, 494 (1980).
2. M. Büttiker, Phys. Rev. Lett. **57**, 1761 (1986).
3. J. Frenkel, Phys. Rev. **36**, 1604 (1930); R. Landauer, IBM J. Res. Dev. **1**, 223 (1957); Z. Phys. **B21**, 247 (1975); ibid. **68**, 217 (1987); H. L. Engquist and P. W. Anderson, Phys. Rev. **B24**, 1151 (1981); M. Büttiker, Y. Imry, R. Landauer, S. Pinhas, Phys. Rev. **B31**, 6207 (1985).
4. A. D. Benoit, S. Washburn, C. P. Umbach, R. B. Laibowitz, and R. A. Webb, Phys. Rev. Lett. **57**, 1765 (1986).
5. H. van Houten, C. W. J. Beenakker, J. G. Williamson, M. E. I. Broekaaart, and P. H. M. van Loosdrecht, B. J. van Wees and J. E. Mooij, C. T. Foxon and J. J. Harris, (unpublished); C. W. J. Beenakker, H. van Houten, and B. J. van Wees, Supperlattices and Microstructures **5**, 127 (1989).
6. M. Büttiker, IBM J. Res. Develop. **32**, 317 (1988).
7. M. Büttiker, Phys. Rev. B **35**, 4123 (1987); H. U. Baranger, A. D. Stone and D. P. DiVincenzo, Phys. Rev. B **37**, 6521 (1988); S. Maekawa, Y. Isawa, and H. Ebisawa, J. Phys. Soc. Jpn. **56**, 25 (1987); C. L. Kane, P. A. Lee, and D. P. DiVincenzo, Phys. Rev. B **38**, 2995 (1988); S. Herschfield and V. Ambegoakar, Phys. Rev. **B38**, 7909 (1988). S. Datta and M. J. McLennan, (unpublished).
8. G. Timp, A. M. Chang, P. Mankiewhich, R. Behringer, J. E. Cunningham, T. Y. Chang, and R. E. Howard, Phys. Rev. Lett. **59**, 732 (1989); Y. Takagaki, K. Gamo, S. Namba, S. Ishida, S. Takaoka, K. Murase, K. Ishibashi and Y. Aoyagi, Solid State Communic. **68**, 1051 (1988); Y. Avishai and Y. B. Band, (preprint).
9. M. L. Roukes, A. Scherer, S. J. Allen, Jr., H. G. Craighead, R. M. Ruthen, E. D. Beebe, and J. P. Harbison, Phys. Rev. Lett. **59**, 3011 (1987); A. M. Chang and T. Y. Chang, (unpublished); C.J. B. Ford, S. Washburn, M. Büttiker, C. M. Knoedler and J. M. Hong, (unpublished).
10. C. W. J. Beenakker and H. van Houten, Phys. Rev. Lett. **60**, 2406 (1988).
11. F. M. Peeters, Phys. Rev. Lett. **61**, 589 (1988).
12. D. G. Ravenhall, H. W. Wyld and R. L. Schult, Phys. Rev. Lett. **62**, 1780 (1989).
13. G. Kirczenow, Phys. Rev. Lett. **62**, 1920 (1989).
14. H. Baranger and A. D. Stone, (unpublished).
15. M. Büttiker, Phys. Rev. **B33**, 3020 (1986); IBM J. Res. Develop. **32**, 63 (1988); D. Sokolovski, Phys. Lett. **A123**, 381 (1988); C.W. J. Beenakker and H. van Houten, (unpublished).
16. M. Büttiker, Phys. Rev. **B38**, 9375 (1988).
17. P. Streda, J. Kucera and A. H. MacDonald, Phys. Rev. Lett. **59**, 1973 (1987); see also Ref. 21.
18. J. K. Jain, Phys. Rev. Lett. **60**, 2074 (1988); J. K. Jain and S. A. Kievelson, Phys. Rev. Lett. **60**, 1542 (1988).
19. U. Sivan, Y. Imry, and C. Hartzstein, Phys. Rev. **B39**, 1242 (1989).
20. S. Washburn, A. B. Fowler, H. Schmid, and D. Kern, Phys. Rev. Lett. **61**, 2801 (1988).
21. R. J. Haug, A. H. MacDonald, P. Streda, and K. von Klitzing, Phys. Rev. Lett. **61**, 2797 (1988); R. J. Haug, J. Kucera, P. Streda and K. von Klitzing, (unpublished).
22. B. J. van Wees, E. M. M. Willems and C. J. P. M. Harmans, C. W. J. Bennakker, H. van Houten and J. G. Williamson, C. T. Foxon and J. J. Harris, Phys. Rev. Lett. **62**, 1181 (1989).
23. S. Komiyama, H. Hirai, S. Sasa and S. Hiyamizu, (unpublished); S. Komiyama, H. Hirai, S. Sasa and F. Fuji, (unpublished).

24. B. J. van Wees, E. M. M. Willems, L. P. Kouwenhoven, C. J. P. M. Harmans, J. G. Williamson, C. T. Foxon, and J. J. Harris, (unpublished).
25. A. M. Chang G. Timp, J. E. Cunningham, P. M. Mankiewich, R. E. Behringer and R. E. Howard, Soli State Commun. **76**, 769 (1988).
26. M. Büttiker, Phys. Rev. Lett. **62**,229 (1989).
27. M. Büttiker, Phys. Rev. **B38**, 12724 (1988).
28. B. I. Halperin, Phys. Rev. **B25**, 2185 (1982).;
29. A. H. MacDonald and P. Streda, Phys. Rev. **B29**, 1616 (1984).
30. M. Büttiker, Y. Imry and R. Landauer, Phys. Lett. **A96**, 365 (1983); Y. Gefen, Y. Imry, M. Ya. Azbel, Phys. Rev. Lett. **52**, 129 (1984); M. Büttiker, Y. Imry and M. Ya. Azbel, Phys. Rev. **A30**, 1982 (1984); U. Sivan and Y. Imry, Phys Rev. Lett. **61**, 1001 (1988).
31. C. J. B. Ford, T. J. Thornton, R. Newbury, M. Pepper, H. Ahmed, D. C. Peacock, D. A. Ritchie, J. E. F. Frost, and G. A. C. Jones, Appl. Phys. Lett. **54**, 21 (1989); G. Timp, P. Mankiewich, P. de Vegvar, R. Behringer, J. E. Cunningham, R. E. Howard, H. U. Baranger, and J. Jain, Phys. Rev. **B39**, 6227 (1989); P. H. M. van Loosdrecht, C. W. J. Beenakker, H. van Houten, J. G. Williamson, B. J. van Wees, J. E. Mooij, C. T. Foxon, and J. J. Harris, Phys. Rev. **B38**, 162 (1988); B. J. van Wees, L. P. Kouwenhoven, C. J. P. M. Harmans, J. G. Williamson, C. E. Timmering, M. E. I. Broekaart, C. T. Foxon, and J. J. Harris, (unpublished).
32. R. B. Laughlin, Phys. Rev. **B23**, 5632 (1981).
33. G. F. C. Searle, *The Electrician*, **66**, 999 (1911).
34. A. Baranger and A. D. Stone, (unpublished). A. D. Stone and A. Szafer, IBM J. Res. Develop. **32**, 384 (1988).
35. F. F. Fang and P. J. Stiles, Phys. Rev. **B29**, 3749 (1984); D. A. Syphers and P. J. Stiles, Phys. Rev. **B32**, 6620 (1985).
36. H. van Houten, C. W. J. Beenakker, and P. H. M. van Loosdrecht, T. J. Thornton, H. Ahmed, and M. Pepper, C. T. Foxon, and J. J. Harris, Phys. Rev. **B37**, 8534 (1988).
37. G. Ebert, K. von Klitzing and G. Weimann, J. Phys. **C18**, L257 (1985).
38. E. K. Sichel, H. H. Sample and J. P. Salerno, Phys. Rev. **B32**, 6975 (1985).
39. H. Z. Zheng, D. C. Tsui and A. M. Chang, Phys. Rev. **B32**, 5506 (1985).
40. M. E. Cage, in *The Quantum Hall Effect*, edited by R. E. Prange, and S. M. Girvin, Springer Verlag, New York, 1987. page 56.
41. A. M. Chang and J. E. Cunnigham, (unpublished).